Design and implementation of a microstrip filter biosensor for healthcare applications

A thesis submitted to the Faculty of Science, Agriculture and Engineering

for the Degree of Doctor of Philosophy

By

Hayder Q. M. Ashelaish

School of Mechanical & Systems Engineering

Newcastle University

May 2019

Abstract

The aim of this research was to develop high-frequency biosensors by a combination of traditional microstrip filters and microfluidics.

Lowpass and bandpass microstrip filters were designed for operational frequencies less than 3 GHz. Analytical modelling was used to initially determine microstrip filter geometry and then 3D electromagnetic simulation software utilised to examine their performance. Once the design was optimised, devices were fabricated using traditional PCB manufacturing approaches and clean room evaporation techniques. The fabricated filters were compared with the simulation results. The characteristic filter features at 0.66 GHz, 0.80 GHz, and 1.60 GHz demonstrated good agreement to within 90% of the simulated models. Microfluidic reservoirs were then attached to the microstrip filters prior to biological testing.

The targeted biomolecules for detection were prostate specific antigen (PSA). A vector network analyser was used to measure the S-parameters of the filters at each stage of functionalisation and immobilisation. Biosensor performance was assessed by measurement of the resonant amplitude and frequency shifts at the characteristic operational frequencies as a function of concentration of the immobilised PSA. The efficacy test of the produced biosensors demonstrated label-free detection down to a minimum analyte concentration of 6.125 ng/ml, this corresponding to an amplitude change of 9 dB and a frequency shift of 10 MHz in the characteristic feature of the S_{11} signal.

This work has demonstrated the applicability of both lowpass and bandpass microstrip filters, with an operational frequency range less than 3 GHz and with suitably integrated microfluidics, to perform as biosensors. This is the first experimental assessment report of this type of radio frequency-based biosensor showing the real-time detection of PSA biomarkers.

Dedication

To my family

Marwa, Leanne and our little boy Thulfiqar

Acknowledgement

First of all, I am indebted to my supervisor Dr. John Hedley who provided insight and expertise that greatly assisted the research. John's participation and advises that supported me and helped me get results of better quality.

My appreciation also goes to the technicians in the electronic and multi-laboratory workshops for their help. I am also grateful to my friends and colleagues for their friendship and support; it was a pleasure to study with you.

Finally, I owe a limitless thanks to my family for their love, kindness and patient throughout the voyage of PhD pursuit. Their unwavering care allowed me to finish this study. I am indebted to my family for reviving the joy in my life.

Table of Contents

List of figures

List of abbreviations and symbols

1p	Bandpass microstrip filter characterised by Chebyshev response
2p	Lowpass microstrip filter characterised by Chebyshev response
3p	Lowpass microstrip filter characterised by Butterworth response
4q	Lowpass microstrip filter characterised by Chebyshev response
5q	V-shaped bandpass microstrip filter characterised by Chebyshev response
6q	Reduced size bandpass microstrip filter characterised by Chebyshev response
7q	Reduced size lowpass microstrip filter characterised by Chebyshev response
BW	Bandwidth
C	Capacitor
CPW	coplanar waveguide
dB	Decibel
FR-4	Dielectric substrate made of fire-retardant epoxy
g	numerical value of element in standard table
h	Dielectric substrate height
IDC	Interdigital comb capacitor
IgG	Anti-immunoglobulin G
L	Inductor
l	Microstrip length
LOD	Limit of detection
PDMS	Polydimethylsiloxane
PSA	Prostate Specific Antigen
R	Resistor
RT/duroid	Dielectric substrate made of woven-glass reinforced laminate
s	spaces between microstrips of bandpass microstrip filter
SIR	Stepped impedance resonators
SRR	Split ring resonator
VNA	Vector Network Analyser
w	Microstrip width
Y	Admittance
Z	Impedance
ε_r	relative permittivity
λ	wave length

Chapter 1. Introduction

1.1. Introduction

Rapid and non-invasive sensing and prognosis of diseases is an outstanding obligation. However, cancer traditional diagnosis by contemporary methods is complex and require a long time for processing and analysing. Furthermore, a high cost of diagnosis, difficult sample collection and surgery inside dedicated facilities are other concerns.

Prostate cancer diagnosis and level of prostate illness require a comprehensive and complicated urological examination. The patient suffers more because of biopsy to collect samples. Besides, further medical works cause distress and anxiety to the patient [1].

However, PSA biomarkers of prostate illness can be found in urine, blood and body tissues, PSA is generated by both normal and malignant cells of the prostate gland, and they travel through the bloodstream. Prostate Specific Antigen (PSA) biomarkers can be congregated from blood without biopsy and can be used in biosensors. The utilisation of biosensor for PSA detection can prevent traditional medical test difficulties. Therefore, Biosensing technology represents a promising solution to enhance healthcare applications due to ease of use and cost-effective production.

1.2. Biosensing technology

Great development emerged recently in sensing technology and sensors equipment. Consequently, the growth of biosensing knowledge is reaching good approaches. New devices can provide healthcare and home diagnosis via on-site sampling and examination. Early diagnosis promotes healthcare efforts and prevents further damages. Furthermore, monitoring the progression of diagnosed and treated cases. Unprecedented devices are under developing concurrently with massive development in electronics and fabrication technologies. As a result, electronical, mechanical and optical biosensors have been realised, but they are still in the investigation phase [2]. However, there are four main types of biosensors, these are; optical, mechanical, electrical and radio frequency based.

Optical biosensors offer high sensitivity, although these instruments tend to be lab-based. Mechanical or mass-based biosensors express high sensitivity in a small form factor. However, it is marred by the added complexity of microfluidics integration, signal recovery and system uncertainty. Electrical impedance biosensors proposed the most straightforward and cheapest technology platform at the expense of reduced sensitivity. Nonetheless, most of impedance detection methods include nano metal particles of labelling processes. Consequently, it promotes samples invasive tests. For point of care diagnostics, technology should be simple to

use, cheap to manufacture and provides clinically appropriate ranges of sensitivity levels. Therefore, microwave chip-based biosensors offering good compromise among these competing factors [3]. Potential radio frequency biosensor provides label-free, rapid and real-time identification [4]. Besides, microwave can penetrate cells and influence by their liquid content. Penetrating property provides non-invasive analysis tool due to the non-ionizing nature of microwave [5]. Therefore, longer preservation time for samples. Additionally, radio frequency biosensors can provide early prognostic of cancer which can prompt the treatment [6], eliminates further risks and reduce cost. Radio frequency technology is applied in cancer therapy. Therefore, it is safe as a bio-sensing tool [7]. Furthermore, radio frequency-based biosensors can be used in drug discovery and food control. Regarding prostate cancer, early detection of abnormal and fluctuating levels of prostate-specific antigen (PSA) might indicate diseases in their earliest stage, consequently leading to enhance treatment in an initial time.

Radiofrequency planar biosensors are individually cheap which provides low manufacturing cost. Hence, cost-effective diagnosis tool, compact and can be disposable for hygiene purposes. Furthermore, Microstrip based biosensors are small in size, therefore, requires a limited power supply and provides low consumption. Microstrip filter represents a perfect tool that can be used as a biosensor component due to it is physical and electrical properties [8-26].

1.3. Problems, motivation and aim

In terms of biosensing application, many different biosensors and few radio frequency-based biosensors have emerged lately. However, this subject is still under investigations. In addition, using frequencies higher than 30 GHz added more complexity and cost to the radio frequency biosensors research. Despite the reasonable efforts, many areas need to be investigated, such as lowpass microstrip filter based biosensor, lower frequencies range (1-3) GHz, microfluidic integrity and different biomolecules and cells, as shown in chapter 2. On the other hand, simple geometry of microstrip filter and lower operational frequency can promote the commercialisation of the microstrip based biosensor, these criteria are shown in chapter 5, and the applicability of the proposed biosensor is shown in chapter 6 of this work.

Reasons behind the motivation of using microstrip filter as a biosensor in this thesis are health problems and possible solutions mentioned above. Moreover, it represents a new type of biosensing technology. Microstrip has two essential features, it has flat top surface and quasi-mode of travelling waves, wherein waves are travel partially in the air outside microstrip. Microfluidic can be attached to the top surface of the microstrip filter. Therefore, electromagnetic fields can travel through microfluidic and the medium under test. Moreover,

lower operational frequency and low-cost of the proposed microstrip filters makes it a suitable means for implementing a portable and easy to use sensing device.

This research aims to design and fabricate novel radio frequency-based biosensor. The proposed microstrip filter based biosensor can detect, recognise and quantify the concentration of biological analytes. This transduction signal device of radio frequency-based biosensor is a viable tool in healthcare applications. For example, the identification and monitoring of cancerous cells and diseases, it is also applicable for use in environmental observations as well as for Biohazard and epidemiological infection detection. The submitted biosensor can be used as an early diagnosis and monitoring tool for diseases. The main focus of the thesis is to show the feasibility of 3 GHz radio frequency biosensing. Therefore, this thesis attempts to address new radio frequency-based biosensor by examining lowpass and bandpass microstrip filters as an (RF) biosensors towards specific analyte selection.

1.4. Task, procedure and objective

Design of microstrip filters is first accomplished by numerical calculation, and then the modelling of designed microstrip filters is done using a 3D electromagnetic simulation tool. The modelled designs of the microstrip filters were then fabricated according to design criteria. Then an electrical characterisation of the fabricated devices was carried out using a vector network analyser (VNA) to analyse and to characterise the fabricated microstrip filters. Subsequently, the integration of biosensor was done, and its performance is examined against a clinical analyte by VNA measurements. Moreover, analyte selectivity of PSA and biochemical regeneration of several nano concentrations are achieved, and biochemical control is applied to biosensors.

Two types of microstrip filters are designed. The designed microstrip filters are modelled by 3D full-wave electromagnetic simulators and characterised by vector network analysers. Microstrip filters integration with microfluidic and microchambers is achieved with the aim of producing the complete system of the biosensor. Furthermore, two new reduced size microstrip filters are accomplished with the sole intention of achieving a miniaturised biosensor. The assembled biosensors are then prepared for detection purposes by following the biochemical immobilisation protocol. These procedures made them functionalised to capture any immobilised PSA analytes. Reproducibility, regeneration and control of biosensor are examined. Experimental results derived from several tests confirmed the biosensing function of a fabricated biosensor. These results showed the feasibility of specific application of a microstrip-based biosensor and as such the objectives of the work are achieved. A schematic

diagram is shown in figure (1-1) that illustrates the procedure for the design and implementation of microstrip filters and biosensor assembly.

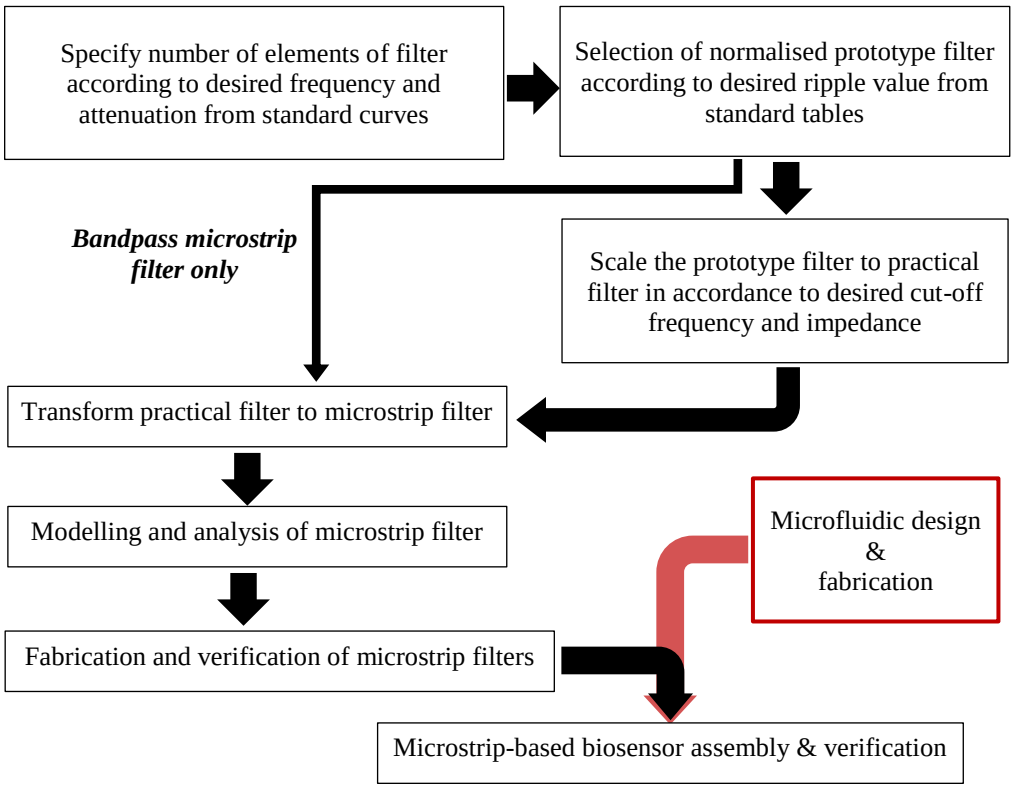

Figure 1-1. Schematic diagram illustrating the design and implementation of microstrip filters and biosensor assembly.

1.5. Contributions

The original contribution of the entire current study is the establishment of a new radio frequency-based biosensor using the existing technology of lowpass and bandpass microstrip filters with operating frequency less than 3 GHz and PSA analyte detection. This contribution is shown from the concept and design criteria in chapter 3. Previously published works employed split ring resonator (SRR) which consists of two split rings only and a coplanar waveguide which connected directly to the ground from the strip's sides. The modelling, fabrication and all through the biosensor realisation is discussed in chapter 4 and 5, biomedical test, detection and functionality are in chapter 6.

Contributions will be further explained in chapter 7 of conclusion, referring to the achieved goal and further possible developments.

In addition to presenting new biosensor, this microstrip based biosensor was utilised to detect PSA analyte in different concentrations; this is the first time a radio frequency-based

biosensor detects PSA. Another contribution of this work is the developing of a new method to join microfluidic to microstrip filter, and this joining procedure is adequate and practical.

1.6. Outline of the thesis

The framework of this thesis describes the concept of radio frequency biosensing as a biosensor, and it is possible for healthcare applications. Details of microstrip filter models and operating parameters, as well as detailed designs, are stated in chapter three. Numerical analysis of the microstrip filters is performed in chapter four. Chapter five comprises the details of microstrip filters fabrication. Subsequently, the evaluation and analysis of microstrip filters and corresponding integrated biosensors are stated. Biochemical experimental tests, biosensor functionality and selectivity assessment are expressed in chapter six, additionally, expressed the detection of a minimum analyte concentration. Chapter seven addressed the conclusion and future work depending on results from previous chapters.

1.7. Summary of Introduction chapter

This chapter exhibited the motivation behind the idea of using a microstrip filter as a sensor for healthcare applications. Refereeing to problems in biosensing research and medical issues to offer solutions related to the proposed biosensor. Besides, this chapter stated the aim of this work, as the design and fabrication of a microstrip filter based biosensor. Information about the significant contribution of this thesis is covered in this chapter as the use of radio frequency microstrip filter of lower than 3 GHz frequency as a biosensor. In this chapter, the method of design, modelling and fabrication towards biosensor assembly and testing was expressed. The outline of the thesis was also included in this chapter, after this introduction, the thesis will cover specific topics in detail in the following chapters;

Chapter 3 concerned with the design process of the microstrip filters according to desired factors, wherein filter parameters are submitted, and the final design realised. Leading to chapter 4 which covered modelling and numerical analysis of the designed microstrip filters, and it will be followed by chapter 5 which talks about the fabrication and characterisation of microstrip filters and the produced biosensor. An established biosensor is verified in chapter 6 by biomedical experiment to test its biosensing functionality against the targeted analyte. Finally, conclusions and future work are linked to all chapters and presented in chapter 7.

Chapter 2. Literature review

2.1. Introduction

Recently, there is a growing trend towards the application of electrical, mechanical, optical and microwave technologies in biosensing for healthcare purposes. Biosensors research performed characterisation processes to different biomolecules, glucose and biological tissues which encouraged this trend.

Biosensors can be used in diseases detection, monitoring and control because they react to biochemical functionalisation and immobilisation processes. Basic biosensing processes classified into two main categories; label assisted and label-free. Label assisted is based on labelling materials to develop and enhance detection mechanism. Label-free transduces signals from direct reaction of the analyte with sensing element of the biosensor.

Regarding biosensors research, there are several challenges to overcome such as electronics and microfluidic integration, biological sample preparation and high complexity of some systems. On the other hand, they have advantages such as rapid diagnosis, a small volume of sample, portable, disposable, easy to use, cost-effective, small size and real-time measurement.

2.2. Biosensors types

There are different categories of biosensors depending on their transducers, the main types stated in the following sections.

2.2.1. Microcantilever biosensors

Mechanical resonators concept is mass-based biosensing [27], vibrations of a mechanical microcantilever due to mass difference resultant from the binding of bioparticles. Therefore, measuring mass change through frequency differences and transduce it to readable data.

Interaction with targeted molecules deflects the cantilever; strain gauge changes its time-dependent resistance. Followed responses comparison leads to a recognition process [28-30]. A piezo-resistive cantilever is an enhanced mechanical biosensing device. Mechanical biosensors are used to investigate viruses, cancer cells and protein-membrane [31-35].

2.2.2. Electrical impedance biosensors

Electrical impedimetric biosensing is based on the concept of electrical impedance [36, 37]. An impedance of biological samples can be measured between two electrodes. External sinusoidal potential and current in the low-frequency band, are applied in electrical impedimetric biosensing. Detection and analysis performed by measuring electrochemical impedance change. Electrical impedance biosensors employed alternative voltage, and the applied

frequency is within the range of kilo to Megahertz. Responses evaluated through impedance variation produced by biological materials. Impedance change is due to a change of biological sample under test. They are mostly deployed to measure glucose levels [38], tumour revealing [39-41] and cholesterol levels. Nevertheless, most of them are labelled biosensors [42-48].

2.2.3. Optical biosensors

Optical biosensors [49, 50] are working in accordance to the concept of applied optical field. Light fields interact with targeted biological samples or reflect from biochemically treated surfaces [51]. Therefore, quantifying radiation change resultant due to absorption and reflection of light. Light can be produced or absorbed by reacting materials or their products.

Furthermore, measuring produced light from the luminescent process. For example, surface plasmon resonance (SPR) based biosensor. SPR based biosensor measures angle shift of reflected light from biochemical reactions surfaces [52-57].

2.3. Radiofrequency biosensors

Radio-frequency spectroscopy [58, 59] is applied to detect, characterise and analyse biomolecules. Microwave biosensing uses various forms of active and passive microwave transmission networks, the elements of the scattering matrix used as a detection indicator.
Measuring frequency shifts and amplitude attenuations reveals information about material under test. Several configurations of biosensors architectures are developed as well as various biochemical protocols were practised. Previous work included an intricate design of microwave transmission line resonators, some of them cooperated capacitive planar components. Moreover, others used a time consuming and complicated biochemical protocols. Furthermore, few researchers used labels to enhance the detection of a signal change.

Recently, regarding healthcare promotion, several biosensors based on a microwave transmission line networks and microfluidic channels are reported. They are interested in investigating the detection of analytes, individual cells, biological tissues, cancer cells biomarkers and glucose concentration levels [60-64].

2.4. Recent efforts in radiofrequency biosensors

Work in this area mostly focused on the examination of cells and biomolecules. Devices used split ring resonator and coplanar waveguide but not lowpass microstrip filter. Therefore, electromagnetic waves offer an investigation tool to analyse the variance of the electrical properties between normal and abnormal cells. Moreover, glucose levels analysis by coplanar microwave waveguides has considerable interest. Next context provided a brief description and review to most valuable previous research in this field.

2.4.1. Biomolecules and analytes biosensors

Descending summary is given to cells detection and their dielectric properties analysis by transmission network-based biosensors.

C. F. Liu et al. introduced new microwave biosensor based on nearfield hairpin electromagnetic resonator [65] and targeted the detection of B16F10 melanoma cells in solution.

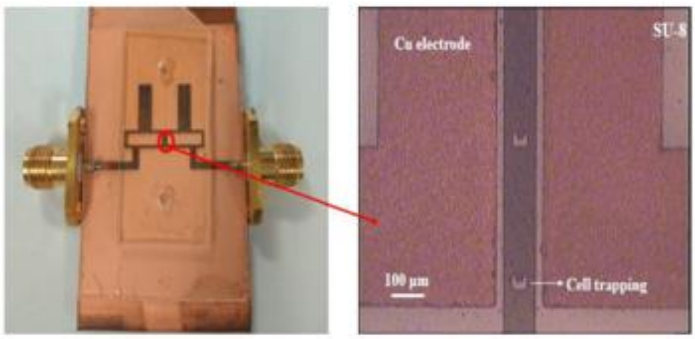

Figure 2-1. Biosensor structure by C. F. Liu et al. [65]

The proposed biosensor consists of stepped impedance resonators (SIR) in the form of hairpin microstrip on a quartz substrate; biosensor structure showed in figure (2-1). Device's length is equal to the half wavelength, a transmission line integrated with polydimethylsiloxane (PDMS) microfluidic in order to carry samples under test. Biosensor response is in linear proportionality with some tested cells. Proposed biosensor has a potential application in cell discrimination.

V. Nerguizian et al. introduced a microwave system to measure complex permittivity for different cancer cells [66]. The measurement system consists of two ports rectangular resonant cavity with a capillary tube inside it to hold the sample solution. Perturbation in resonance frequency denotes measure scale. Single cell permittivity calculated from measuring an analyte in solution by Hanai formula [67]. Response change measured by transmitted wave parameter S_{21}. Applied power is 0 dBm over frequency range 2-4.5 GHz.

A radiofrequency analysis studied by Jae-hoon Ji et al. [68]. They presented a new dependent microwave biosensing system. Device-based on two ports coplanar waveguide architecture as illustrated in figure (2-2) to detect monomeric biomaterials.

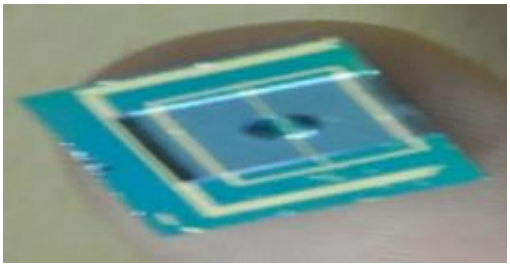

Figure 2-2. Biosensor by Jae-hoon Ji et al. [68]

Radio frequency signals used to detect glucose, glucose levels and albumin. Scattering parameters represent the measurement scale. Device detection is limited to 1.8 mg/dl, biosensing device's substrate made of Silicon Si and silicon oxide SiO2 layer. Electron-beam evaporation of photolithography used to fabricate top electrode from Ti and Au with a ratio equal to 1/15 nm. The device consists of two separated electrode beams, the gap between them is 2 µm in its closest point. Electrodes are compatible with targeted samples. Polydimethylsiloxane (PDMS) microchamber deposited on the surface at the meeting point of the electrodes. Applied power of vector network analyser is -20 dBm and frequency up to 4.5 GHz. They managed to evaluate the impedance and extracted capacitance of samples under test as a function of concentration. Although, human serum, a relaxed frequency of capacitance measurements showed value change only.

A theoretical approach towards split ring resonator (SRR) based biosensor made by M. Wellenzohna and M. Brandla [69]. The biosensor is modelled and simulated by finite element method and optimised to work in a high-frequency range close to 3 GHz. They designed two ports device consists of FR-4 substrate and three metal layers on top. Metals are gold, nickel and copper. A reflected coefficient of scattering matrix is used to indicate the changes of proposed biosensing functionality. A hydrogel used as material under test. Resultant change expressed as a frequency shift.

Intracellular Dielectric Spectroscopy is reported by J. Leroy et al. [70]. They presented a high radio frequency biosensor. They used scattering parameters and impedance spectroscopy as a characterisation function for their biosensor. Dielectrophoresis forces are utilised to trap particles. Applied frequency range is up to 6 GHz. The biosensor is based on bandpass filter made of thick gold electrodes (15µm) and microfluidics as shown in figure (2-3). They attempted to trap biomolecules inside the selected sensitive region and detect them by measuring capacitive change. Capacitive change induced by electromagnetic frequency change. Primary analysis is accomplished to calculate cell permittivity. Though, identify a specific type of cells within different cells solution is not clear.

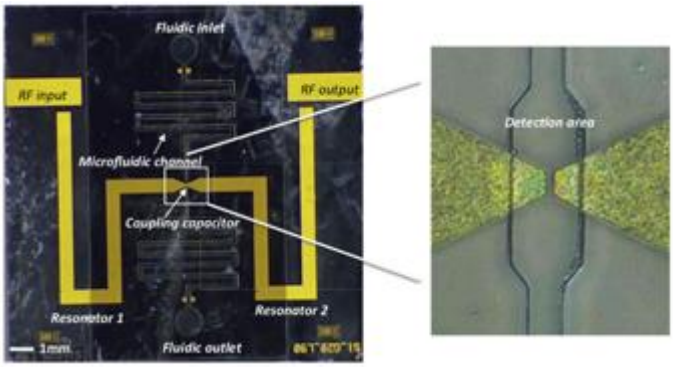

Figure 2-3. Microfluidic biosensor by J. Leroy et al. [70]

Split ring resonator (SRR) is examined by K. Jaruwongrungsee et al. in the field of biosensing [71]. Their study reported new radio frequency biosensor based on metamaterial structure of a microstrip coupled split ring resonator (SRR). The device consists of a metallic loop of gold on RT/duroid substrate and a dielectric gap. Regarding biosensor production, a prepared device integrated with a microfluidic chamber as shown in figure (2-4).

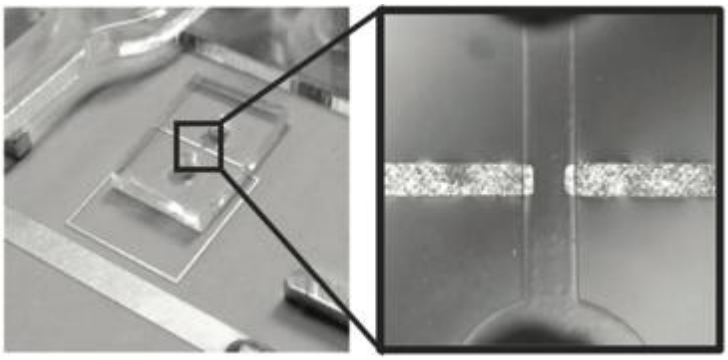

Figure 2-4. Integrated biosensor by K. Jaruwongrungsee et al. [71]

SRR made by PCB fabrication method and microfluidic chamber made from polydimethylsiloxane (PDMS). Material under test is anti-immunoglobulin G (IgG). Scattering matrix is used as biosensor response function within frequency range 1.1-2.3 GHz. More specifically, scattering parameter S_{21} is the change indicator. S_{21} indicates IgG presence as a shift in resonance frequency. Real-time and label-free measurements conducted. The change occurred in amplitude and frequency after loaded samples.

Radio frequency device made of a microwave coplanar transmission network [72]. Applied for cancer cells (HepG2) dielectric classification is conducted by Yu-Fu Chen et al. Research introduced a microwave biosensor based on a transmission line network consists of coplanar waveguide, illustrated in figure (2-5). Hepatoma G2 cancerous cells are characterised dielectrically by this biosensor. Scattering parameter S_{21} is the measuring parameter.

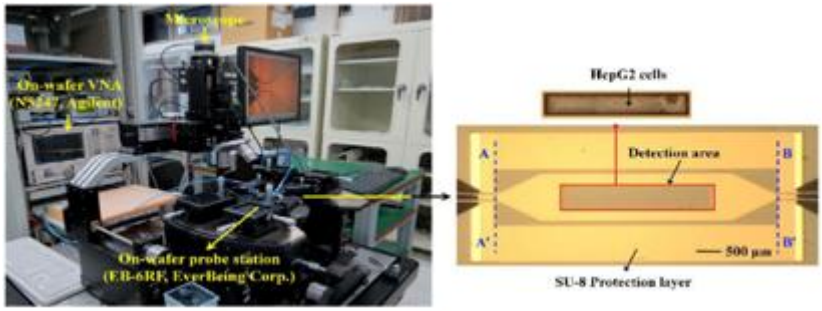

Figure 2-5. Biosensing experimental configuration by Yu-Fu Chen et al. [72]

The frequency bandwidth is 1-40 GHz. Wave attenuation and cell dielectric constant are measured, a transmission line made on a quartz substrate by semiconductor fabrication techniques. Microchamber made by a deposition of SU8 layer of thickness equal to 55μm on a best sensitive area. Researcher and his group concluded that propagating wave is attenuated by polarised charged biomolecules. Transmitted parameter S_{21} is disturbed by cells density. Therefore, biosensor detectability stimulated. They reached a lower detection limit equal to 20 cell/μl. Several concentrations tested. Also, they developed a mathematical model to calculate parasitic disturbances and remove their effects from collected data. Although biomedical protocol needed a long time of preparation, the biosensor can be reused after a wash by water only.

L.Y. Zhang et al. illustrated the use of microwave in colorectal tumour cells investigations. They measured permittivity of Bio-cells [73], coplanar waveguide made on fused silica substrate with gold electrodes used. Polymer microchamber prepared to hold samples during the test. They managed to differentiate among different levels of disease stages depending on electrical properties of bio-cells. They utilised the idea that bio-cells walls are penetrable by radio frequency waves at microwave frequency. Therefore, probing the possibility of these biological cells and analyse them. Researchers concluded that biological cells properties depend on their inner contents. Authors used a similar transmission line design by Delmay et al. previously mentioned. It constructed of interdigital comb capacitor (IDC) with the coplanar waveguide (CPW). Lean on comb capacitor change resultant from electrical distress by presented biological samples load. DC voltage applied to a biased network diode of an integrated circuit. Biosensing process made on bio-cells without been in solution. Biological cells are folded by formaldehyde and deposited directly on the surface of a biosensor. Although, number of seeded cells controlled by culture process. Biochemical preparation is not rapid and difficult to confirm positions of cells without the use of a microscope. This research found a relationship between

abnormal cells properties and radio frequency signal change. Moreover, detect and analyse of a few cells is possible.

A published study [74] involved RF based biosensors for the analyte detection by H. Lee et al. developed an RF biosensor based on SRR resonator and microstrip line network. The device exhibited a frequency shift around 5 MHz due to analyte. In this study, H. J. Lee et al. used planar split ring resonator to fabricate biosensor based on two ports microwave line, illustrated in figure (2-6). Electronic structure of biosensor consists of a high impedance transmission line. Transmission line function is to excite the golden resonance supported transducer by magnetic fields. Magnetic fields are varying with time due to a passing current. The device fabricated by printed circuit board technology.

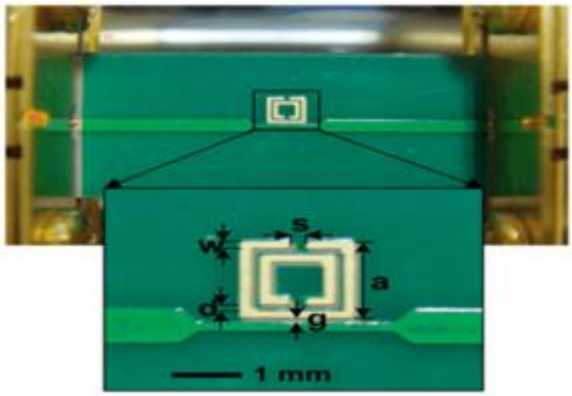

Figure 2-6. SPR resonator used as a biosensor by H. J. Lee et al. [74]

Biosensor's surface composed of copper, nickel and gold. Device covered by mask layer except for biosensing region. Material under test is anti- cortisol. Protein G. Fluorescent stains make linking of immobilisation on the gold surface are added to obtain an optical observation of the reactions of materials under test. Measurements indicated by scattering parameters. Particularly, scattering parameter S_{21} of the transmitted wave. Responses exhibited a quantifiable change in amplitude value and shifted frequency. Limited of detection (LOD) of their biosensor is a concentration of 100pg/ml. Moreover, different concentrations 0.1-100 ng/ml tested over frequency up to 13 GHz.

In the same context, Dalmay et al. proposed a new biosensor to investigate the identification and refinement of biological cells and their electrical properties [75]. The proposed biosensor consists of coupled bandpass microstrip filter as shown in figure (2-7).

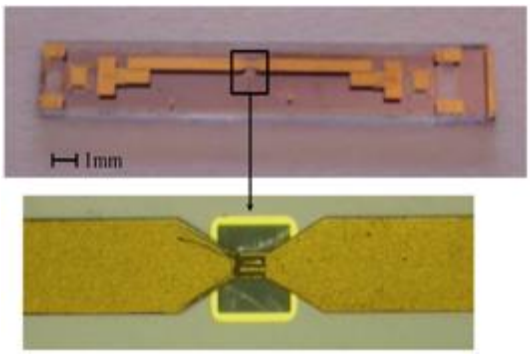

Figure 2-7. Bandpass microstrip filter designed for biosensor of Dalmay et al. [75]

The designed filter had deep ripples to help biosensing principles and run in 13 GHz. A biosensor can achieve label-free biosensing. They showed one individual cell detection is possible. Gigahertz frequencies enabled such approach of cell examining. Henceforward, microwave can penetrate cell membranes and interact with the inner materials of cells depending on the phenomena of different electrical properties between normal and abnormal human cells, specifically, permittivity and conductivity of these cells. Proposed biosensor managed to recognise different biological cells. They applied the same concept of scattering parameters change due to loaded biomolecules samples. They connected response of change to inherent properties of biological cells. Vector network analyser is used to analyse transmitted and reflected signals S_{11} and S_{12} respectively. For detection purpose, targeted human cells positioned on the surface of biosensor without using any solid or liquid holding medium. Therefore, the measurement performed as samples is on-chip and in the air. This technique helped to avoid measurements noises due to holding medium. On other hands, this method needs a long time (several days) to complete. Moreover, it has some complex biochemical preparations parts. Moreover, individual cell type recognition needs more clarification and explanation.

Dalmay et al. distributed another study on biosensing [76]. They used the same concept of previously reported work to study the dielectric properties of human cells. Their micro-size biosensor, made of a band stop coplanar transmission line, constructed on a fused silica substrate and inter-digited capacitor. They examined intrinsic relative permittivity at different radio frequency bands. Thus, electromagnetic waves can penetrate inside cells. Cellular inner medium investigated to determine cells electromagnetic characteristics, frequencies from 15 to 35 GHz used in the differentiation process. Evaluation method and indicators are scattering parameters. They concluded that the real part of cell permittivity depends on frequency domain related to each cell. Micro biomolecule load will induct frequency shift due to change in its capacitance value. Samples loaded utilising a polymeric matrix, sucrose gel used as a medium

for tested materials. They decided that samples location is not crucial in the detection process due to equally distributed fields' line. Many cells have an essential rule to determine biosensor responses. Nevertheless, produced biosensor managed to detect small conductivity of cells and identify them despite the complex biochemical protocol. Although deposited dead cells caused a problem to the measurement.

Another published study by C. Dalmay et al. demonstrated cells analysis by impedance spectroscopy of microwave [77]. Two poles coplanar waveguide of 5µm thickness golden microstrips fabricated on a fused silica substrate. Silica utilised due to its low loss at the operational frequency and transparency. Thick SU8 used to build microchamber to hold samples during the test. Measurement is indicated by scattering parameter of reflection S_{11} over a frequency range up to 16 GHz. Presence of targeted cells caused frequency shift equal to 100 MHz. Also, a 0.5 dB attenuation in S_{11} recorded at 14.4 GHz. They concluded an impedance difference amid measured cells ranks. They considered cell permittivity as an indicator of the degree of cell differentiation.

K. Grenier et al. reported radio frequency biosensor based on a band stop microstrip filter to investigate human cultured cells [78]. Frequency shift equal to 0.39 GHz resulted between living and dead cells. Radiofrequency biosensor presented and characterised. The biosensor consists of two-ports coplanar waveguide assembled with a microfluidic channel as shown in figure (2-8).

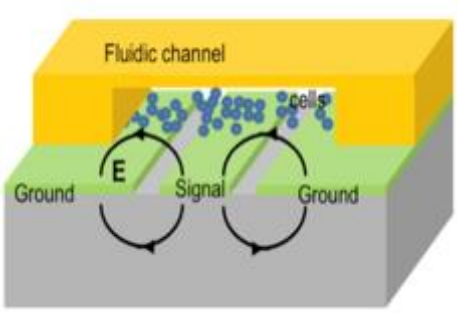

Figure 2-8. A schematic shape of the proposed biosensor by K. Grenier et al. [78]

Sensing functionality tested against samples of HUVEC human cells, and different solutions of 3µL volume samples applied. Samples detected and characterised by the biosensor. Hence, cells suspensions caused transmitted signal phase to change. Scattering matrix used to perform the measurements over frequency range 400 MHz-35GHz. Besides, scattering parameters utilised to determine the complex permittivity of biological samples.

Frequency-dependent complex permittivity measurements of biological solutions conducted by S. Seo et al. [79]. Throughout utilising coplanar waveguide transmission line on

a glass substrate. SU8 polymer reservoir added to hold samples under test. Top metals of the planar transmission line are gold and copper, as shown in figure (2-9). Measurements frequency range is 1-32 GHz, scattering matrix elements used as the sign indication factors. A volume of samples equal to few microliters injected. Tested samples are liquids and biomolecules. Research performed dielectric characterisation of biomolecules and concluded that permittivity of samples decreased with frequency.

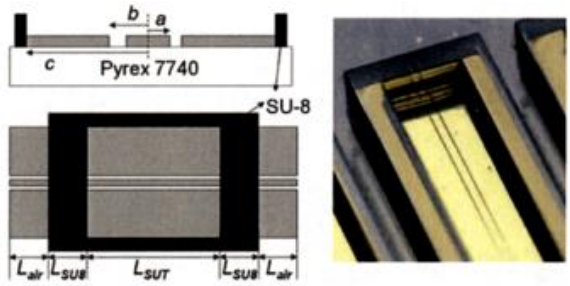

Figure 2-9. Schematic and image of a utilised device by S. Seo et al. [79]

J. H. Chien et al. [80] presented a biosensor paper. They developed new microwave biosensor based on lowpass microstrip filter and gold nanoparticles (AuNPs) and aimed at immunoassay bio-sensing. Biosensor made on a glass substrate, titanium and copper represent microstrip metal layers. A radio frequency probe did measurements over the bandwidth of frequency. Scattering parameters are the measurement indicator. Specifically, scattering parameter S_{21} showed a quantifiable change. S_{21} change is proportional with AuNPs increment. They conducted label detection and tested different concentrations of protein analyte throughout frequency range up to 30 GHz. Gold nanoparticles employed as bioconjugates in biomolecules immobilisation process due to their biocompatibility. Gold nanoparticles support high-frequency response. Therefore, fabricated biosensor had limited response to a bio-layers formation and needed signal amplification. AuNPs enhance biosensor ability. They amplify undetectable and weak signal change by biomolecules to a measurable level.

Y. Kim et al. established radio frequency biosensing device based on PCB, MEMS equipment and electrical signal change as illustrated in figure (2-10) [81]. Label-free detection is achieved by new label-free immobilisation method on copper layer and PCB surface. Frequency range is above 1 MHz and up to 20 GHz. Their system constructed of a coplanar waveguide transmission line. Applied impedance is 50 Ω. The total length of electrical components equal to 4000 µm only.

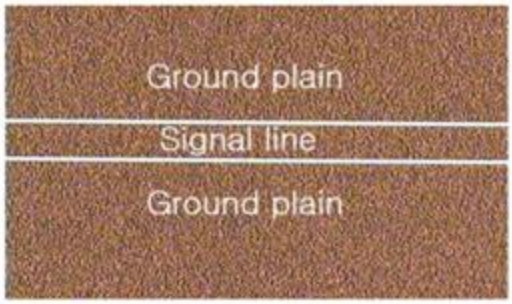

Figure 2-10. Photo of applied coplanar waveguide of Y. Kim et al. [81]

The evaluation method is the scattering matrix, phase shift and resonance frequency recorded. The researchers compared signals before and after loaded samples. Biochemical immobilisation process is applied. Detection surface treated by plasma process to transfer it to hydrophilic and charged with negative charges, to prepare it for the immobilisation process. They concluded that results are the same for Au and Cu. Also, conduction dissipation is the main reason for losses. Biomolecules activity affect power loss due to skin effect.
Moreover, capacitive and inductive parts are best used together in the sensing operation. They referred to control conductive loss of biomolecules as an essential factor. However, they did not show in what way to control molecules layers. The biosensor is disposable, small and straightforward. The final method and devices are useful in biosensing. Although, extra work needed to a functioning surface by the plasma which is a commercial limitation and time consumption procedure.

Proposed study to numerically investigate biosensor based on SRR and high impedance microstrip filter is suggested by J. Zhou [82], research modelled the detection sensitivity difference between asymmetric and symmetric SRR design, configuration of experiment is two ports system constructed by printed board circuit technology, 0.1mm is the width gap between SRR and microstrip, where scattering parameter S_{21} represented response indicator. Experimental results concluded that asymmetric design is highly sensitive in comparison with a symmetric pattern.

F. Deshours et al. introduced biosensor based on two ports microstrip ring resonator (MRR) [83]. Biosensor made on different substrates. Plastic cylindrical opened container incorporated with MRR to hold samples shown in figure (2-11).

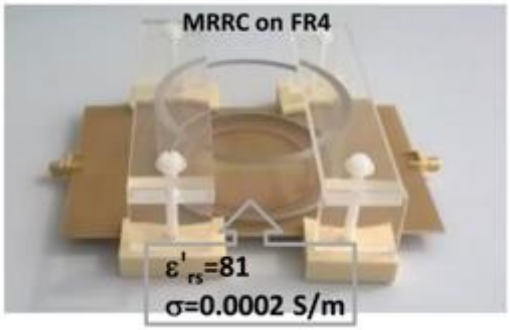

Figure 2-11. MRR with plastic cylinder container by F. Deshours et al. [83]

They have managed to determine the complex permittivity of biological tissue as a function of frequency. Scattering parameter S_{21} is the measurement pointe. High-frequency range applied. A closed-loop transmission line utilised to produce microwave biosensor depending on frequency dependent dielectric parameters of biological tissues. Biosensing device based on split ring resonator deposited on FR4 and RT-Duroid 5880 substrates. Operational frequency of 1 GHz and the frequency band is 1-10GHz. A goal is to improve the determination of complex permittivity of biological tissue by measuring occurred changes in scattering matrix. Geometry modification performed on the two ports resonator. Coupling gap increased and insertion losses decreased. Frequency shift equal to 193 MHz calculated and 3 dB bandwidth multiplied by a factor 7 due to the presence of biological tissues.

M. Zarifi and M. Daneshmand demonstrated a microwave resonator as a fluid sensor based on planar microstrip transmission network [84]. Samples reservoir kept away from microstrip surface. Researchers concluded that remote liquid sensing and sensor response is proportional to the distance between the fluid and resonator surface.

High frequency (microwave) bio-detection method is developed by M. Nikolic-Jaric et al. [85]. The sensing device based on an interferometer incorporated with microwave quarter wavelength resonator. Resonator consists of a coupled transmission line on Rogers Cu-clad 5880 dielectric substrate. Moreover, commercial microfluidic glued and mounted on a Plexiglas. The system includes two main parts, one is a quarter-wavelength sensing resonator of three interdigitated electrodes, and the other is a signal reference. Sensing part supplied with a microfluidic that has an electrode coupled with the resonator. Group is mounted on a Plexiglas block as illustrated in figure (2-12). Detection is achievable at frequency shift equal to 1.5 GHz.

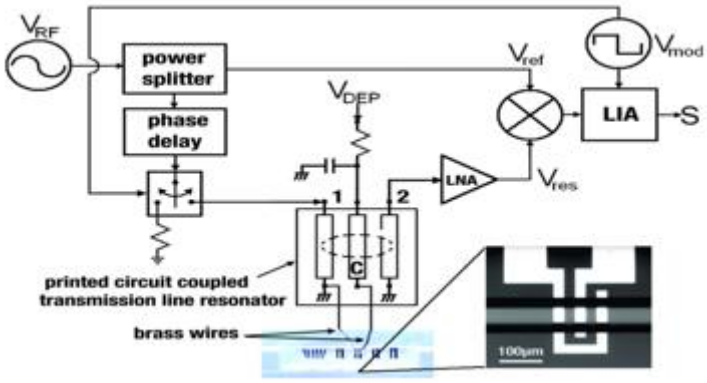

Figure 2-12. Detection apparatus of M. Nikolic-Jaric et al. [85]

Biological samples caused capacitance variation equal to 650 zF over applied bandwidth of 50 Hz. A proposed biosensor can detect biomaterials in low concentrations and identify individual biomolecules. They showed biosensor of zeptofarad sensitivity able to analyse electrical properties of biological samples. Frequency range is gigahertz. The frequency-dependent response showed measurable change related to the material under test.

High radio frequency technology is used by C. Yang et al. to develop multi-layered DNA polymeric label-based biosensor [86]. Two copper coplanar transmission lines deposited on a polymer substrate instead of the traditional one. They are targeting DNA detection, a bio-sensing process enhanced by gold and magnetic nanoparticles. Scattering parameters as a function of frequency represented the indication tool of biosensor responses. Frequency shift indicated the sensing process. The detection limit is 10 pM of DNA concentration. Achieved frequency shifts are 0.7 and 0.9 GHz by triple layers of label particles over a frequency band of 0-8 GHz.

S. Harnsoongnoen et al. proposed a microwave biosensor based on two ports coplanar transmission line in the form of split ring resonator [87]. Organic and inorganic liquids are the targeted samples of detection. Biosensor demonstrated the ability to detect and categorise different chemical solutions depending on sensor responses induced by different concentrations of materials under test.

L. Wang described the use of electronic and microwave biosensor in primary breast cancer diagnosis research [88].

2.4.2. Glucose biosensors

Biosensors based on coplanar transmission line utilised to detect and analyse glucose levels. Recognition is depending on scattering parameters responses. This research field summarised in the next section.

Two ports coplanar transmission line integrated with polydimethylsiloxane (PDMS) microfluidic to produce a glucose level analyser[89]. This research demonstrated by Z. Abedeena and P. Agarwal. 50 Ω coplanar waveguide had a central sensitive region made of an interdigital part and fabricated on FR-4 substrate by PCB technique and experimental configuration shown in figure (2-13). S-parameters are the measurement indicators. Scattering parameters S_{11} and S_{12} showed frequency shift and attenuation variation over different concentrations of glucose.

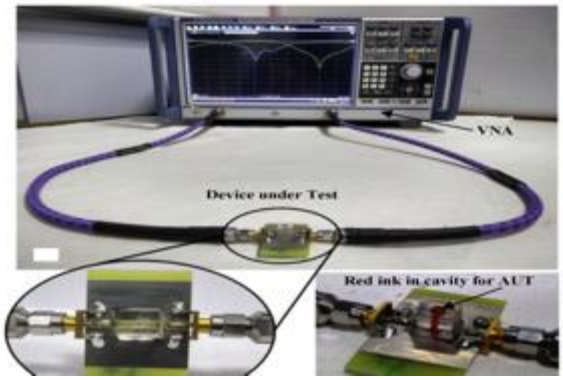

Figure 2-13. Experimental setup of Z. Abedeena and P. Agarwal. [89]

Harsoongnoen [90] introduced a microwave biosensor. Microwave system consists of two ports coplanar transmission line coupled with electric LC resonator examined to detect glucose levels. Scattering coefficient S_{21} implemented as response indicator due to glucose concentration change. Investigated responses are over a frequency band of 2.5-6 GHz. Glucose solutions diluted by deionised water and phosphate buffered saline, a plastic chamber in the form of a cylindrical reservoir connected with electrical parts to fabricate the proposed biosensor. Analysed results of resonance frequency and level of attenuation dip showed linear responsive manner with concentration increment.

B. Camli et al. [91] presented a microwave biosensor for glucose detection. Biosensor constructed from a pair of a microstrip antenna and split ring resonator. The device configured in the form of slit circular conducting copper strip placed on FR-4 dielectric substrate. System cooperated with 2.6 mm thickly stacked sticker reservoir channel. Scattering matrix reflection coefficient S_{21} stands for measurement tool. Response change expressed by frequency shift. Calculated biosensor sensitivity is 0.174 MHz/mgml-1. Over different concentrations of the glucose oxidase enzyme.

New radio frequency biosensor based on microwave resonator proposed by N.Y. Kim et al. [92]. The suggested biosensor can perform label-free identification of glucose concentrations

levels in human serums. Design based on rectangular meandered line resonator. Researchers used passive resonator constructed on a gallium arsenide substrate and consists of a square turned line. Airbridge is added to the resonator to increase detection ability by amplifying of return loss magnitude; experiment arrangement shown in figure (2-14).

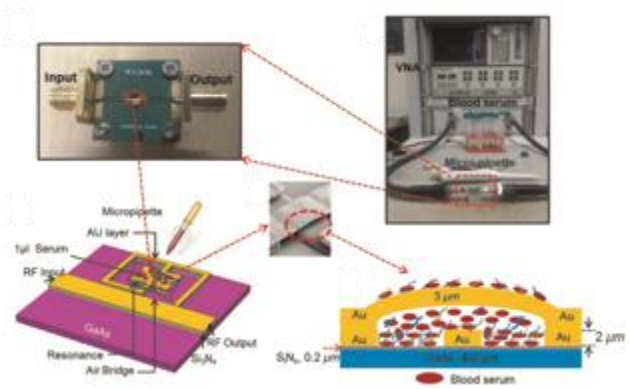

Figure 2-14. Schematic illustration of the biosensing process by N. Y. Kim et al. [92]

Scattering parameters used as detection indicators over a frequency range up to 10 GHz, comparison of characterisation performed to glucose in human serum and deionised water solution. Inductive and capacitive change due to analyte load will induces signal change in the biosensor. Resonance frequency shift and return loss change are the characterisation tools of the biosensor. They found that the electromagnetic interaction between samples and biosensor is responsible for signal change occurrence. Also, they denoted a proportional relationship between exposure time and response quality. Results found a resonance frequency shift equal to 1.08 MHz after using 1 mg/dl of human serum. Although, produced biosensor showed rapid detection level by resonance shifts. Biosensor showed reusability and good sensitivity to extinguish different glucose concentrations.

New radio frequency biosensor for glucose detection is introduced by H. Park et al. [93]. Biosensor constructed of two ports transmission line placed on a silicon oxide substrate. Titanium layer of thickness equal to 10 nm deposited first. After that, 500 nm gold layer deposited on top of the titanium layer. Scattering matrix used to display signals and their change. Operated frequency range is 1-4.5 GHz. The research found that signal proportional with glucose concentrations. They suggested that scattering matrix and derived part of it can be used to describe biosensor behaviour towards glucose detection. Also, they selected the resistance component to represent the best sensitive factor.

An electromagnetic biosensor operates at microwaves range to detects and measures glucose levels introduced by A. Mason et al. [94]. In this research, biosensor consists of two

ports coplanar transmission line supported by adapted tuning system to remove errors. Therefore, the frequency of the resonant peak is adjustable. Thus, the correspondent quality factor is flexible too. Temperature and fluid control systems also included in the design.

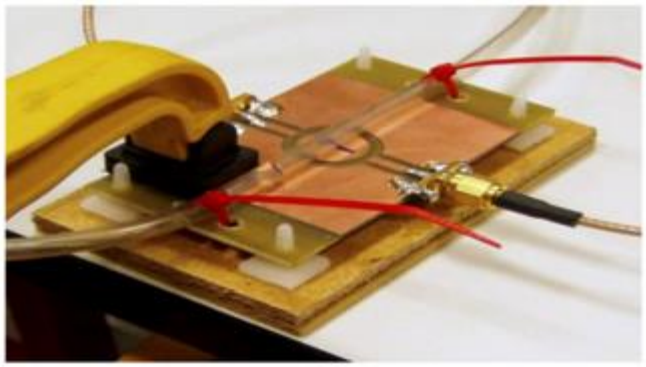

Figure 2-15. Biosensor configuration by A. Mason et al. [94]

The device calibrated at a frequency of 3.64 GHz, supplied power is 0 dBm (1mW). The footprint of a biosensor is 80 mm2. Hence, the device has control function on sensitive and selective responses towards diverse liquid samples. The device configuration is shown in figure (2-15). Scattering parameters represented the measurements indicator because they are changing according to a loaded sample in real-time. Glucose diluted solution is 10-100 mmol to simulate medical standards. Proposed biosensor showed a change in response according to concentration loaded samples. Average of S_{21} amplitude response change is 2 dB. Frequency shift appeared as a result of glucose concentration increment at 3637 MHz of the frequency point.

Biosensor based on a transmission line of a distributed microelectromechanical system reported by L. Li et al. [95], the biosensor consists of a fluidic channel made from acrylic attached to the transmission line network. Transmission line suspended on a resistive silicon substrate. Nickel is waveguide metal. Liquid glucose solution of different concentrations used to test the proposed device via measure resonant frequency shift. Fluidic channel holds a glucose sample during the test to provide interaction of samples with electromagnetic fields. Scattering parameter of reflection S_{11} shifted due to glucose presence. S_{11} response change depends on the loaded concentration of glucose solution. Concentrations of 0-347 mg/ml over frequency range 0-40 GHz exploited. Although, glucose biosensors capable of achieving glucose levels recognition. They might not be able to recognise different loaded material from glucose serums. There is no mechanism to define glucose characteristic to the biosensor such as surface functionalisation and immobilisation.

J. Roelvink et al. presented a microwave sensor based on coplanar transmission network [96]. Measured complex permittivity of fluids and semisolids samples in a wide band of frequencies. Scattering parameters and propagation constant used in permittivity measuring process over the range 1-5 GHz.

In the same context, microwave cavity waveguide tested for biosensing property, a device used as a potential sensor for microfluidic application [97]. H. Hamzah et al. presented split ring resonator with an existing gap equal to 3 mm and operational frequency of 2.5 GHz. Detection device tested over several solvents and chemicals. Sensor responses changed according to pH meter of tested solutions. Therefore, it is an acidity sensor.

2.4.3. Prostate biosensors

Regarding Prostate Specific Antigen (PSA) detection, several procedures and methods are introduced [98-100]. For example, D. Pihikova et al. [42] implemented Electrochemical impedance spectroscopy (EIS) to the purpose of PSA detection. Another study by K. Shin et al. presented biosensor tested by PSA detection [47]. The detection system consists of electrochemical impedance spectroscopy (EIS) supplied with removable magnetic beads. Moreover, the microwell array used to trap magnetic beads. Differently, surface plasmon resonator used to detect PSA biomarkers. PSA prepared on microcontact chip, and this research conducted by G. Erturk et al. [101]. Gold nanoparticles are incorporated with an electrochemical immunosensor to detect PSA biomarkers as showed by L. Suresh et al. [44]. Likewise, PSA sensing by gold nanoparticles used by G. Persunova et al. Gold nano-particles is used to functionalised a silicon nanowire field-effect transistor [102]. L. Su. Et al. introduced PCB piezoelectric biosensor to detect PSA biomarker [103]. Biosensor transducer is a lead titanate zirconate (PZT) ceramic resonator. Two ceramic resonators attached in a parallel manner, one for control and the other one is for sensing process.

2.5. Challenges and problems identification

Reviewed literature exposed several challenges and problems. Challenges to overcome are the integration of electronics with microfluidic, utilisation of assistance circuits and nano-particles, complexity, high-frequency range, slow biochemical experiments. Therefore, problems identified as complex sample and biosensor preparation, high-cost of fabrication, a selectivity of the biosensor and reproducibility, the interaction between biosensor and samples need further studies, commercialisation of radio frequency-based biosensor. Nevertheless, comparison between biosensors against traditional diagnosis tools showing that biosensors should have specific merits, such as rapid diagnosis tool, need small volume of sample in the range of

microliter or less, portable and can be used in different places, disposable for hygiene purpose, simplicity, cost-effective, provides real-time measurement and their sizes are small.

H. Lee and J. Yook introduced a review article about RF biosensors [104]. This review article revised (RF) biosensors and focused on the technology, development and future of biosensing based on radio frequency devices. The study covered passive and active devices. Besides, they classified RF biosensors according to their working principle, operational frequency, and targeted molecules. They showed that two types of RF passive devices of SRR and interdigitated capacitor (IDC) biosensors already employed in previous research. About their work, it is evident that different active mechanisms have also studied. As a result, this and other articles conclude that RF biosensing is a new trend. Besides, the use of active components can enhance passive RF based biosensors. On the other hand, reviewed articles referred to the accompanying problems such as limitations of low sensitivity and expensive tools. However, they suggested future solutions to improve RF biosensors, some of these solutions are; disposable chips, cost-effective and miniaturised biochips, and nano-materials utilisation to improve (RF) biosensors performance.

2.6. Summary of a literature review chapter

Different biosensor researches introduced, and various techniques are involved, but no commercial product realised. However, despite the disadvantages and obstacles, satisfactory progress accomplished alongside with significant development in electronics and fabrication technologies. Furthermore, interest is growing towards the use of microwaves radio frequency (RF) sensors in bio-sensing applications for their valuable properties. They offer non-invasive, rapid and label-free detection. Besides, it observed that biological sensing by microwave means proved to be a readily applicable bio-detection system and can be implemented commercially.

Biosensors technologies including radio frequency-based biosensors are reviewed and expressed according to the material under test and depending on the published research of microwave-based biosensors. There is an excellent focus on coplanar waveguides with operating frequencies up to 45GHz as a biosensor device. Split ring resonator (SRR) is involved too, it consisted of two split parts and used as a radio frequency-based biosensor. Other works used hairpin resonator in the form of stepped impedance resonator-based biosensor.

Some of these devices are supported by electrical circuits and components to enhance the detection process. They are used to detect cancer cells and the dielectric properties of biological molecules. Besides, most of these devices have been used to identify and specify glucose and glucose levels. Nevertheless, there have been few works about PSA sensors; for example, electrochemical impedance spectroscopy applied to investigate PSA recognition. In another

research, PSA biomarkers examined by surface Plasmon resonator technique. Also, Gold nanoparticles employed in an electrochemical immunosensor were also involved in PSA sensing process. Other work indicated the use of a silicon nanowire field-effect transistor to detect PSA biomarkers. In all these works PSA has not been tested by a radio frequency-based biosensor. Nonetheless, microstrip filter based biosensor has not investigated towards PSA analyte detection.

This thesis used microstrip filter-based biosensor to approach possible solutions to previously mentioned problems. Microstrip filters featured simple geometry of transmission line. Furthermore, a low range of operating frequency less than 3 GHz utilised. Fabricated biosensor targeted PSA analyte detection in different concentrations levels.

In the next chapter, a detailed explanation to microstrip filter design process is outlined, passing through numerical analysis and the fabrication of the modelled designs that will eventually lead to the assembly with microfluidic to produce the desired Biosensor.

Chapter 3. Design of microstrip filters

3.1. Introduction

Microwaves are electromagnetic waves of millimetre or micrometre length (micron to meter) and a frequency range from (300 MHz to 300GHz) [105], the shorter wavelength of the micrometre is compatible with biological cells size. Therefore, due to a short wavelength and penetration ability, microwave can be used to detect and penetrate biological tissues within cell level [106]. Employing microwave in biosensing involves the use of transmission line networks [107], transmission lines constructed in different forms, such as microstrip filters which are built by flat metal patches. Radio frequency filter is a device that works within a range of frequencies and has a cut off frequency. Therefore, it is an electric circuit that permits the required signal to pass with lowest power attenuation and highly attenuate unpermitted signals. Microstrip filter has a geometry of precise dimensions in the form of flat and thin metal piece on top of a grounded dielectric substrate [105]. Therefore, the microstrip filter is an ideal system for biosensor and point-of-care applications due to the flat shape and electromagnetic properties. Microstrip filter operates in different frequency ranges suitable for healthcare applications. Regarding a microwave-based biosensor, microstrip filter can be employed because it is compatible with biosensor plane architecture requirements.

This chapter introduces the design of microstrip filters. It started with filter operational requirements and parameters, all through to filter type selection and synthesis. Eventually, physical shape to implement in a final product of microstrip-based biosensor is realised. Design of microstrip filter started by a prototype of a normalised low pass filter, a prototype filter is selected following the operational frequencies of the aimed device [108]. Subsequently, each element of selected normalised filter undergoes a scaling and conversion processes. Scaling processes lead to a realisation of the required practical numerical value of filter's components [109]. After which, all the scaled elements of an efficient filter are transformed into a microstrip filter form by a transformation process. Ultimately, a biosensor is realised by integrating microstrip filters with microfluidic chambers. Microwave filters can be classified into two main categories, active filters, this type requires an external power supply due to the active components. The second type is passive filters, here no active components are included, and no power needed [110]. Both models are applicable in biosensor research.

Microstrip filters utilised in this thesis are passive devices. Next sections introduce filter type selection and microstrip filters design properties in details.

3.2. Transmission line and microstrip filter

The transmission line in the form of a microstrip filter has a unique flat architecture that supports propagation modes of electromagnetic fields. Transmit specific energy from one port to another. Consequently, components of a transmission line are compatible with wavelength itinerant inside it. Lowpass microstrip filter is a series of cascaded metallic patches. Bandpass microstrip filter consists of parallel coupled resonators of separated microstrip patches. Signal transfer by electrical coupling, lowpass and bandpass microstrip filters built on the dielectric substrate connected to the ground conductive layer. Therefore, field lines between a ground plane and microstrip not entirely enclosed in the substrate. They are partially travelling through two different mediums, air and a dielectric substrate. This phenomenon provides surface penetrating fields proper to bio-reaction and sensing processes.

3.2.1. Transmission Line Model

Physical dimensions of electrical circuits at microwave frequency range are comparable with the millimetre wavelength ($1 \leq f \geq 1000$GHz). Moreover, circuit elements defined per unit length and had a small size. Net of connecting wires of circuit elements has impedance rather than resistance due to imperfect conductivity. Although, circuit characteristics of capacitance, inductance and resistance are distributed continuously over the circuit board. Therefore, the name distributed elements model refers to this rule. On the other hand, in the lumped element model, components are combined with perfect wire conductors, consequently, non-uniform voltage and current in each division of the circuit [111].

3.2.2. Lumped and distributed elements filter

The design process of distributed element filter is interested in inductance and capacitance. However, elements are mixed and cannot be treated as a separate "lumped" capacitors and inductors, and they inseparably joined. Lumped elements filter is used to realise microstrip filter. Transform capacitances and inductances of an established lumped elements filter lead to microstrip filter. Transformation produces a corresponding edge coupled or cascaded metal layers of parallel and series linked microstrips. Distributed Element Filter (DEF) can be a microstrip transmission line or coplanar waveguide (CPW) stripline. Therefore, their planar thin shapes could be fabricated by printed circuit board technique (PCB) or other MEMS microfabrication processes [112]. There is no exact frequency beyond which distributed element filters should not be applied. They are mainly associated with high radio frequency microwave group in which wavelengths are less than one metre and in the order of millimetre or micrometre. Besides, LC filters are not able to perform over the range of a hundred megahertz; their low-quality factor leads to poor performance. Lumped model of a filter is not

used in this thesis due to the splitting elements arrangement archetype and confined geometry. Therefore, it will be only used to configure the microstrip filter. Microstrip form provides the advantage to microstrip filter to be an applicable tool in the biosensors research due to flat planar architecture. Microstrip filter made of one or more components of metal patches comprise all components such as capacitors and inductors. These components are cascaded or coupled in a single microstrip filter [106]. Moreover, planar filters used in low power applications such as biosensing because of their low cost, small size and excellent performance. Next sections explain microstrip filters and their design properties.

3.3. Microstrip filter properties

Microstrip concept is related to the integrated microwave circuits (MICs) [113]. General configuration of the microstrip filter is shown in figure (3-1). Metallization suspended on top of the substrate layer that supports the metal strip. Metallic top layer uncovered by any material and it is open to air. Microstrips connected to a dielectric substrate of a certain thickness and grounded. This configuration maintenances improved electromagnetic performance than usual PCB [114].

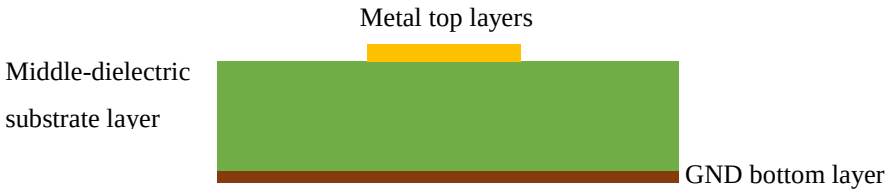

Figure 3-1. Microstrip main components

Microstrip filters are compact, have a small size and short length. Microstrip filters can easily integrate with other components, such as microfluidics. Microstrip filter size decreases as frequency increases. Therefore, microstrip geometry is economically practical as a biosensor at higher frequencies. Several structures of microstrips filters have been made and involved in microwave integrated circuits and biosensing research. Thus, microstrip filters materials are varying depending on the anticipated application [115]. For example, gold and copper for metals. Polymers, glass and even air for a dielectric substrate. Gold and quartz are useful in healthcare applications. Microstrip shape, dimensions and design of a metal layer on the top of a dielectric substrate affect travelling electromagnetic waves. Shape configuration has an impact on the wave propagation and fields through a dielectric substrate to the ground layer. Electromagnetic waves are travelling in different mode [116]. A brief description is given to

propagation mode and microstrip design parameters in the following sections, mode of propagation influences the design of microstrip.

3.3.1. Transverse electromagnetic mode (TEM)

Typically, magnetic and electric fields of travelling waves are perpendicular to each other, and both are transverse to the direction of propagation. Specifically, neither electric field nor magnetic field components are aligning in the path of wave propagation. These travelling waves are transverse electromagnetic waves. They propagate in the transverse electromagnetic mode (TEM) or principle mode [117]. Figure (3-2) showed propagation mode of EM wave. However, this is not the case in microstrip filters.

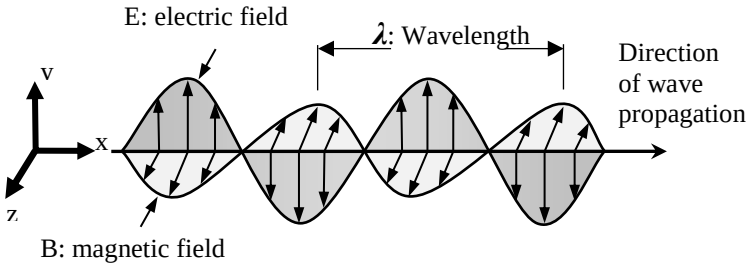

Figure 3-2. TEM normal propagation mode

3.3.2. Quasi-Transverse electromagnetic mode (Quasi-TEM)

Microstrip filter includes different dielectric interfaces alteration. These interfaces are above and below the top layer of microstrips. Specifically, in the region between the air on the top and the dielectric substrate below. Consequently, passing an electric field suffer an immediate change in the interface region. Usually, transmission lines support one mode of propagation over a specific frequency range. TEM, TE or TM due to filling by a uniform dielectric material. Microstrip transmission line does not fill with the same dielectric material. Therefore, it cannot support a single propagation mode. Distribution of fields that generated by transmitted energy through microstrip line is approaching a TEM mode. However, it is not true TEM mode; this approaching mode indicated as a quasi-TEM.

Quasi-mode of propagation describes the complexity of electromagnetic fields in microstrips. In contrast with the simple geometry, electrical fields are transverse and orthogonal to the magnetic fields, and this situation is due to dielectric discontinuity of mixed medium between air and substrate. In other words, the microstrip wave path is a mixture of two different mediums, air and a dielectric substrate. Therefore, a mixed medium does not support TE, TM and TEM mode. Microstrip fields concentrated between the ground layer and metal strip on a substrate. Power fields travel from metal strip towards ground layer. Radiation losses increase

in a high-frequency band over the frequency limit of 60 GHz, losses in microstrip generated from radiation, dielectric and conductor. Hence, changing medium properties stimulate change in fields of travelling wave and microstrip filter response. Approximate representation of magnetic and electric fields showed in figure (3-3-a and 3-3-b). Electrical field lines move from metal microstrip towards ground bottom layer, passing through air and a dielectric substrate. Electric field distribution is shown in figure (3-3-c). Microstrip geometry, the ratio of width to height and substrate material have direct effects on the electrical field distribution over microstrip length [118].

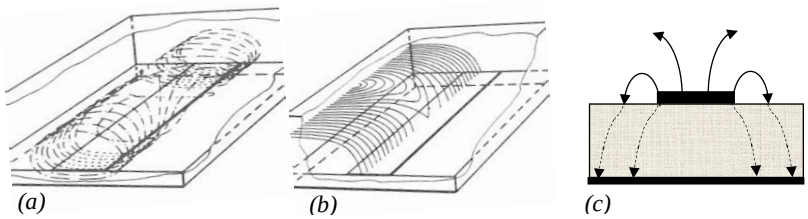

Figure 3-3. a) magnetic field distribution, b) electric field distribution and c) Electrical field of microstrip, cross-section [100]

Propagating velocity of a travelling wave in microstrips depends on physical dimensions of the microstrip and material properties. Moreover, no vanished electrical and magnetic fields longitudinal components. Microstrip discontinuities commonly encountered in the layout of practical filters include steps, open-ends, bends, gaps, and junctions [111]. Quasi-TEM mode of microstrip coupled lines yield velocities of even mode and odd mode, and these modes influenced design equations. Fields relative extents shared between air and dielectric substrate are not equal [119]. In other word, fields are not entirely propagating in the substrate.

3.3.3. Dispersion in microstrip

Microstrip line structure is dispersive and exhibits a nonlinear relationship between frequency and wave number (β) as shown in figure (3-4). The reason behind this condition is the propagation hybrid mode alongside a microstrip transmission line. The hybrid mode occurred as a consequence of the wave travelling between two different mediums [120].

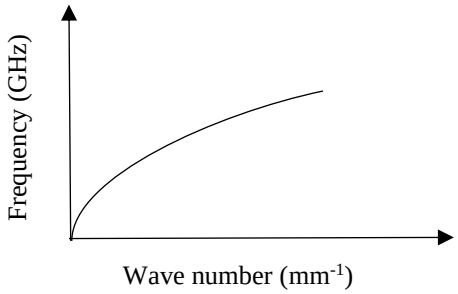

Figure 3-4. Dispersion mode in microstrip transmission line

3.3.4. The impedance of microstrip filters

Regarding a design process, impedance is an essential factor of design criteria. Microstrip impedance is proportional with applied frequency and inversely proportional with microstrip width. Hence, narrow strips impedance is higher than wide strips impedance.

3.3.5. Effective permittivity

Microstrip width depends on two factors, substrate thickness and transmission line characteristic impedance. However, microstrip length depends on wavelength and frequency. Microstrip can be treated as a partial dielectric filling that supports longitudinal section electric (LSE) or longitudinal section magnetic (LSM) modes. Nonetheless, pure TE or TM modes are not possible as mentioned previously. In standard microstrip, currents flow in two directions; transverse and longitudinal on microstrip's skin. LSE and LSM are coupled by flow currents leading to a hybrid mode configuration. Frequency increment increases the efficiency of coupling mode. Consequently, fields concentrate beneath the microstrip region causing relatively large electric displacement in the substrate permittivity. Phenomena of fields concentration towards the substrate with the frequency values raising, producing effective microstrip permittivity as a frequency function ($\varepsilon_{eff}(f)$). Subsequently, it is a frequency dependent, and this point was expressed in equation (3-1). Therefore, slowing down wave propagation through microstrip filter. In general, practical permittivity value reduces to static-TEM at low frequency. Hereafter, at a higher frequency, effective permittivity approaches or become equal to substrate permittivity value as shown in figure (3-5) [118]. Effective permittivity continually increases with frequency. Fields are also partially propagating in the air the substrate surface and the substrate. Subsequently, microstrip is between two mediums, air and a dielectric substrate. The effective permittivity replaces inhomogeneous air-dielectric media [116].

$$\varepsilon_{eff}(f) = \begin{bmatrix} \varepsilon_{eff} & as\ f \to 0 \\ \varepsilon_r & as\ f \to \infty \end{bmatrix} \qquad 3\text{-}1$$

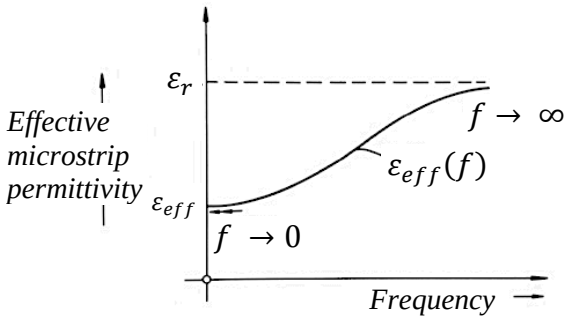

Figure 3-5. Effective permittivity as a function of frequency [108]

One of the equations (3-2) or (3-3) can be used to calculate effective permittivity of microstrip filter depending on the comparison of Z_o with r. Hence, r is an empirical relationship derived experimentally and depends on the electrical permittivity of the dielectric substrate ϵ_r, r = 63-2× ϵ_r. The resultant of the comparison relation identifies the suitable equation, if Z_o > r then equation (3-2) can be applied,

$$\epsilon_{eff} = \frac{\epsilon_r+11}{2}\left\{1 - \frac{1}{2H'}\left(\frac{\epsilon_r-1}{\epsilon_r+1}\right)\left(\ln\frac{\pi}{2} + \frac{1}{\epsilon_r}\ln\frac{4}{\pi}\right)\right\}^{-2} \qquad 3\text{-}2$$

when impedance value is less than r (r=63-2ϵ_r), Z_o < r; equation (3-3) is used

$$\epsilon_{eff} = \frac{\epsilon_r+11}{2}\left\{1 + \frac{29.98}{Z_o}\left(\frac{2}{\epsilon_r+1}\right)^{1/2}\left(\frac{\epsilon_r-1}{\epsilon_r+1}\right)\left(\ln\frac{\pi}{2} + \frac{1}{\epsilon_r}\ln\frac{4}{\pi}\right)\right\}^{-2} \qquad 3\text{-}3$$

Henceforward, effective permittivity is an essential factor in the design process, in addition to height to width ratio and impedance.

3.3.6. Microstrip thickness

Design of an individual microstrip filter, several factors involved, they are microstrip width, length and height. Microstrip height is equal to the dielectric substrate thickness. These factors are essential dimensional criteria. Additionally, the dielectric permittivity of the substrate material as previously stated. The thickness of the metallic top layer of the conducting strip being insignificant to microstrip performance. However, it might be quite often negligible.

Finite strip thickness affects electrical field distribution as shown in figure (3-6). Microstrip has a ratio of $t/h \leq 0.005$, $w/h \geq 0.1$ and electrical permittivity is within 2 to 10.

Thickness effect is insignificant and negligible. Likewise, the substrate height influences the propagation of the surface wave [121]

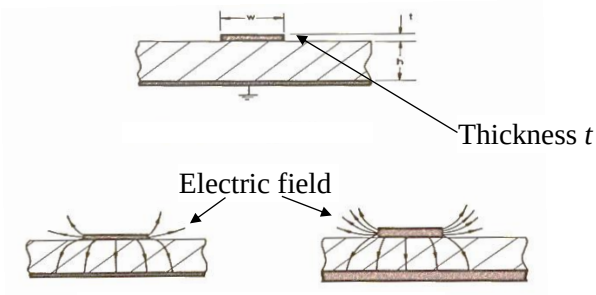

Figure 3-6. Variation of the electric field with microstrip thickness [98]

3.3.7. Even and Odd modes of parallel microstrips

In edge coupled microstrip resonator, travelling voltage wave in one microstrip can be coupled and motivate the second microstrip. Consequently, an opposite polarisation arises from a coupled motivated voltage of accompanied microstrips. Different field configurations occur. Field state of an even mode occurs if voltage polarity is identical on both coupled microstrips. Voltages are negative or positive as shown in figure (3-7-a). On another hand, odd mode of field state will occur if voltage polarity is opposite and not identical on coupled microstrips. Part one is negative, and another part is positive, as shown in figure (3-7-b). Accordingly, in the microstrip design process, calculation of filter parameters considers even and odd mode components and calculate two designation values to every single component. One for even mode and the other one is for an odd mode. Coupling degree influences all design parameters including length, width and separations or spaces between microstrips. Additionally, all parameters are frequency dependent. Equation (3-4) shows the coupling factor as a function of odd and even impedance.

$$C' = 20\log_{10}\left[\frac{Z_{0e}-Z_{0o}}{Z_{0e}+Z_{0o}}\right] \qquad 3\text{-}4$$

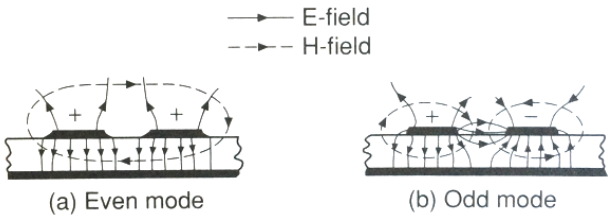

Figure 3-7. Electromagnetic a) even and b) odd modes of parallel coupled microstrip transmission line, only outlines of fields are shown [103].

Coupled microstrips in even mode have similar potential. Nonetheless, the current through parallel conductors' structure is double of a single microstrip. Subsequently, impedance value is equal to a half of even mode impedance (Z_{0e}). Therefore, in an odd mode field situation, potentials of the two microstrips are opposite. A potential difference is double in the value of that for a single microstrip. Though, current is equal to the single microstrip current [122].

3.4. Materials selection

Materials are selected depending on two criteria, microstrip properties and healthcare applications.

3.4.1. Metals

Gold has outstanding electrical properties as well as biocompatibility. A thin layer of gold defines the microstrip thickness over the substrate. Copper is used in the design of other parts of microstrip filters but not the top layer. Although copper is a standard metal in a PCB production, it is chemically unstable in an aqueous test set of biological detection. Consequently, it is a non-biocompatible metal and not applicable to biosensor aqueous nature [123]. Therefore, a combination of copper and nickel with gold to form a microstrip layer of microstrips. Another metal layer consists of gold (Au), and nickel (Ni) applied and attached to copper alloy to surface layer of good biocompatibility. Therefore, gold is insoluble, less reactive and has good resistivity to chemicals. Although gold attachment with quartz is breakable by chemicals, titanium used to secure gold attachment with copper. Therefore, gold has excellent mechanical properties; it has tarnish and corrosion resistance feature. Gold can provide a flat surface to immobilise proteins. Metal smooth surfaces supply a necessary sheet to deposit and attach chemical linkers required to construct the chemical receptors. Configure perpendicular position to increase their capturing functionality. Besides, gold has a good affinity for the immobilisation process of biochemical [102]. Moreover, gold had been used in biomedical applications because of its non-toxic behaviour, stability and innocuous to biological cells.

Gold provides an inert surface to immobilisation protocols in this study. Gold offers strong bond with immobilised biochemical, due to the affinity to immobilisation. Therefore, the ability to biochemical functionalisation. Gold retains its solid state in neutral stable condition over chemical solutions of different pH levels [124]. Surface functionalisation of gold is rapid in comparison to other metals like copper.

3.4.2. Dielectric substrate

In the design, modelling and fabrication processes of proposed microstrip filters; two types of dielectric substrate are used. Correspondingly, a compact and planar architecture of microstrip

filters, as well as condensed electromagnetic fields lines on the surface enabled biosensor design on the flat surface of the microstrip filter supported by a solid dielectric substrate. Moreover, the feasibility of microfluidic integration to a flat and electric dense surface of microstrip filters.

Two types of dielectric substrates used, they are FR-4 for PCB microstrip filters and quartz to evaporated models.

FR-4 substrate

One substrate thickness equal to 1.6 mm applied to all devices. FR-4 is a fire-retardant epoxy resin. Epoxy has excellent heat resistant; its good mechanical properties support suspended microstrip metal layer on it. Moreover, FR-4 and printed circuit board proved to be biocompatible [125]. FR-4 used for PCB microstrip filters of operational frequency within 3GHz. Three designs are submitted on this substrate. Bandpass microstrip filter characterised by Chebyshev response (denoted as 1p). Lowpass microstrip filter characterised by Chebyshev response (indicated as 2p). Lowpass microstrip filter characterised by Butterworth response (denoted as 3p).

Quartz substrate

Quartz's flat surface assists chemical functionalisation and promotes attachment of protein receptors to surface linkers. Besides, quartz is suitable as a substrate for a microstrip filter because metals can be deposit on its surface. Moreover, quartz has high radiation efficiency due its low dielectric losses and permittivity. The orientation of quartz wafer surfaces can be defined in several crystal directions because quartz normally is monocrystalline.

Quartz is used in the design of two more groups of microstrip filters (denoted as 4q and 5q) and reduced size versions of microstrip filters (indicated as 6q and 7q). The first group is working within 3 GHz range and characterised by a Chebyshev response. The second group is the reduced size microstrip filters, an operational frequency of this group is 15-25 GHz. A characteristic response is Chebyshev too. Quartz substrate thickness for the first group is 1 mm. Reduced size devices have substrate thickness equal to 250 μm only.

3.5. Microstrip filter Synthesis

Regarding the microstrip filter design process, essential operational frequencies, attenuations and other design requirements are submitted [126]. Consequently, standard data selected. For example, normalised standard electrical filter satisfied the desired design requirements. A normalised filter used to build the prototype pattern. Prototype filter provides the base for the final filter design. Standardised filters are available in standard tables. Standard table elements represent a general numerical value. They can be selected as capacitive or inductive

components depending on preferred design. Afterwards, scaling equations and formulas used to convert the prototype filter to a practical filter network consists of electrical elements. Subsequently, a transformation synthesis is used to convert electrical elements filter into microstrip filter form. After the synthesis process, electrical components transferred to a single shape geometry.

Components integrated into one thin piece of metal provides different structure geometry and same input and output functionality. Definitively, a realisation of microstrip filters design. Filter properties and functionality conserved. Matlab code is used to compute complex design parameters, synthesis formula. Dimensions of final designs structures calculated by this code. Also, Matlab performed data processing and scattering coefficients plotting. Curve fitting managing and characterisation of microstrip filters and corresponding biosensors. Physical dimensions of the final microstrip filter realised from using prototype numerical values. Design formulas and converting calculations implemented accordingly. An insulator substrate must support microstrips. Manufacturing criteria, a preferred selection substrate of FR-4 dielectric and quartz made.

Matlab program code used to calculate the dimensions and geometry of microstrip filters. Nonetheless, resultant values went through an analysis process to estimate final dimensions that produce desired responses values accomplished with the best useful dimensions. Nevertheless, an approximation is made to modify some microstrip filters dimensions to avoid fabrication problems and offer compatibility with available manufacturing techniques. However, limited design approximation controlled and does not affect microstrip filter design accuracy. Design dimensions requirements are the width (w) of the microstrip, spaces (s) between microstrips for bandpass microstrip filter and lengths (l) of microstrip parts, depending on known height (h) and electrical permittivity of the dielectric substrate [111].

3.5.1. Normalised prototype of standard filter

The design process of microstrip is customizable. Start by selection of a suitable normalised prototype filter. Prototype filter is a low pass filter has cut off frequency equal to 0.150 Hz (Ω_C=1 radian/sec) and a resistance value equal to one ohm for source and load. Figure (3-8) showed a typical response of this filter with ripples in the passband. Low pass prototype filter used as an infrastructure to produce final bandpass and low pass filters in microstrip form [127].

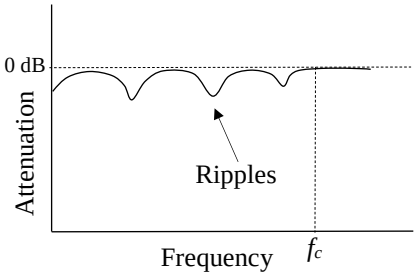

Figure 3-8. Standard low pass filter response

3.5.2. Normalised filter selection process

Different normalised low pass filters consist of several electrical components selected to construct microstrip filters depending on their responses. They are either characterised by Chebyshev response which is not flat passband due to ripples existence or Butterworth which has a maximum flatness of no ripples in the passband. Electrical components of the prototype filters are resistance, capacitors and inductors. Numerical values of these elements shown in tables with each microstrip filter design section. G-values stands for capacitors, inductors and resistors of ladder-type low pass filter. Selection made according to the design requirements. Standard data from tables and charts used to extract the primary prototype filter [128]. Employed filter properties are an analogue, passive, continuous-time signal, and linear. Several parameters should be identified in advance to design a filter. For example, filter type, response form, and application requirements. Lowpass, high pass, bandpass and stop pass filters are the most common filter types. Subsequently, filter response is the next property to be stipulated. Butterworth response, Chebyshev response and Bessel, these are the main filter responses.

Chebyshev ripples enhance the selectivity. Selectivity is a measure of the performance of a radio receiver to respond only to a tuned radio signal. Furthermore, reject other signals nearby in frequency. Ripples of microstrip filter enhance filter response within a narrow bandwidth. This property is beneficial in biosensor application because it enhances signal change and detection process. The filter must be able to permits signals through passband exclusive of distortions. In addition, operational frequencies identified as cut-off frequencies and transmission bandwidth. Other design factors are attenuation level, where the wave power drop significantly, cut-off frequency to the involved frequency ratio. In addition to attenuation characteristic, used to specify the number of electrical elements to construct the prototype filter.

The functionality of the resonant circuits is sensitive to capacitive and inductive elements values. Select proper normalised filter elements regarding the building of the filter according to the attenuation value (dB). A degree of attenuation and the number of elements could be established either by specific calculations or directly from data sheets and graphs [110]. At this work, standard charts and tables are used to figure out normalised lowpass filters. Applying

ratio of the frequency range to central frequency and desired attenuation. The number of filter elements found from standard charts. Figure 3-9 showed a standard chart of attenuation and frequency ratio [128].

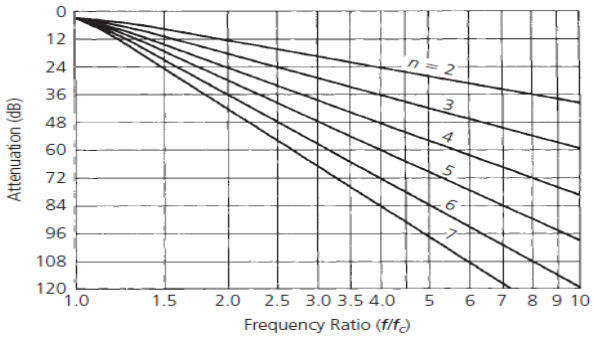

Figure 3-9. Standard attenuation charts for the Chebyshev prototype filter, n is number of electrical components [109]

Approximate attenuation value of Chebyshev response filter predicated by equation (3-5):

$$A_{dB} = 10\log\left[1 + \varepsilon^2 C_n^2\left(\frac{f}{f_c}\right)'\right] \qquad 3\text{-}5$$

where A_{dB} is the attenuation, f is attenuation desired frequency, f_c is the 3dB cut off frequency, n is the order of the filter, $C_n^2\left(\frac{f}{f_c}\right)'$ is the Chebyshev polynomial of order n as shown in table (3-1) and,

$$\varepsilon = \sqrt{10^{R_{dB}/10} - 1} \qquad 3\text{-}6$$

where R_{dB} is passband ripple value. Therefore, for a five-element filter with a ripple of R_{dB}=1, after submitting Chebyshev polynomial for n=5 from the table (3-1), the solution of the attenuation equation (3-5) becomes:

$$\left(\frac{f}{f_c}\right) = \frac{3}{1.5} = 2 \quad \xrightarrow{yields} \quad C_n^2\left(\frac{f}{f_c}\right)' = 16\left(\frac{f}{f_c}\right)^5 - 20\left(\frac{f}{f_c}\right)^3 + 5\left(\frac{f}{f_c}\right)^5$$

$$A_{dB} = 10 \times \log[1 + (10^{0.1} - 1) \times ((16 \times (2^5) - 20 \times (2^3) + 5 \times 2)^2]$$

giving A_{dB}=45.5 dB

Table 3-1. Chebyshev polynomial, up to n=7, n is equal to number of elements

Number of elements	*Chebyshev polynomial*
1	$\left(\frac{f}{f_c}\right)$
2	$\left(\frac{f}{f_c}\right)^2 - 1$
3	$4\left(\frac{f}{f_c}\right)^3 - 3\left(\frac{f}{f_c}\right)$
4	$8\left(\frac{f}{f_c}\right)^4 - 8\left(\frac{f}{f_c}\right)^3 + 1$
5	$16\left(\frac{f}{f_c}\right)^5 - 20\left(\frac{f}{f_c}\right)^3 + 5\left(\frac{f}{f_c}\right)^5$
6	$32\left(\frac{f}{f_c}\right)^6 - 48\left(\frac{f}{f_c}\right)^4 + 18\left(\frac{f}{f_c}\right)^2 - 1$
7	$64\left(\frac{f}{f_c}\right)^7 - 112\left(\frac{f}{f_c}\right)^5 + 58\left(\frac{f}{f_c}\right)^3 - 7\left(\frac{f}{f_c}\right)$

Designated filters are type I Chebyshev filter. Hence, ripples are in the region of passband only. Except on Butterworth lowpass filter, knowing frequency ratio and the desired attenuation enable prototype filter selection [128].

3.5.3. Width to height ratio calculations

In terms of microstrip width, the value of impedance Z_o determines the width equation type depending on relative electrical permittivity ε_r. For narrow strips, if $Z_o > b$, where $(b=44-2\varepsilon_r)$ Ω. Therefore, equation (3-7) compute width to height ratio as a function of relative permittivity ϵ_r and impedance Z_o. Therefore, determine microstrip width because *h* is the dielectric substrate height which is already known [129].

$$\frac{w}{h} = \left(\frac{\exp H'}{8} - \frac{1}{4\exp H'}\right)^{-1} \qquad 3\text{-}7$$

where

$$H' = \frac{Z_o\sqrt{2(\epsilon_r+1)}}{119.9} + \frac{1}{2}\left(\frac{\epsilon_r-1}{\epsilon_r+1}\right)\left(\ln\frac{\pi}{2} + \frac{1}{\epsilon_r}\ln\frac{4}{\pi}\right) \qquad 3\text{-}8$$

H' in equation (3-8) is a part of the equation (3-7), and it is a function of Z_o. Also, it can be a function of *w/h* as shown in equation (3-9).

$$H' = \ln\left\{4\frac{h}{w} + \sqrt{16\left(\frac{h}{w}\right)^2 + 2}\right\} \qquad 3\text{-}9$$

For wide strip formula when $Z_o < b$, $(b=44-2\epsilon_r)$ Ω, equation (3-10) calculate the width to height ratio by using relative permittivity and impedance in order to determine microstrip width.

$$\frac{w}{h} = \frac{2}{\pi}\{(d_\epsilon) - \ln(2d_\epsilon - 1)\} + \frac{\epsilon_r - 1}{\pi\epsilon_r}\left\{\ln(d_\epsilon - 1) + 0.293 - \frac{0.517}{\epsilon_r}\right\} \quad 3\text{-}10$$

$$d_\epsilon = \frac{59.95\pi^2}{Z_o\sqrt{\epsilon_r}} \quad 3\text{-}11$$

where d_ϵ in equation (3-11) is a supplementary part of the equation (3-10)

3.6. Design of Microstrip Filters

Regarding design, two types of microstrip filters characterised by Chebyshev and Butterworth responses. They are two ports bandpass and lowpass filters. Operational frequencies of gigahertz enabled the design of millimetre size of microstrip filters. Therefore, providing small size to biosensor fabrication.

3.6.1. Bandpass microstrip filter (1p)

First proposed transmission line is passive bandpass microstrip filter [114]. It characterised by type-I Chebyshev response. A steep pass/reject band transition with 1 dB ripples in the region of passband [111]. Henceforward, in a bandpass filter, only frequencies within passband are passing from the filter, blocking Frequencies lower than and higher than bandpass frequencies. In other words, Bandpass filter permits certain electromagnetic waves to pass and attenuate other waves above and below the bandpass region [129]. Main design parameters of bandpass filter selected in accordance to four operational frequencies as defined in figure (3-10), specified frequencies at required values of attenuations. Synthesis of coupled resonator circuits will be applied to analyse the bandpass filter.

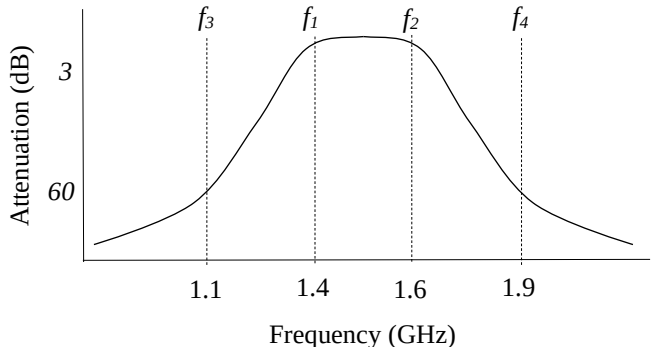

Figure 3-10. Bandpass filter frequencies of a pass and stops bands.
f_1=1.4 GHz, f_2=1.6 GHz, f_3=1.1 GHz and f_4=1.9GHz.

3.7. Design parameters of a bandpass filter

Selected central frequency is 1.5 GHz First cut off frequency is 1.4 GHz at 3dB. Second, cut off frequency is 1.6 GHz at 3dB. First low cut off frequency is 1.1 GHz at 60dB. Second low cut off frequency is 1.9 GHz at 60dB. Response ripple is 1 dB and bandpass is approximately 0.2 GHz. Hence, design parameters selected and computed to suit the proposed biosensor requirements. Involved frequencies are 1.4, 1.5 and 1.6 GHz which represent cut-off frequency, central frequency and stopband frequency, respectively. Standard attenuation curve in figure (3-9) is used to identify the number of elements depending on the attenuation level vs frequency ratio. The number of filter elements represents the order of the filter, and it is five in this case.

BW is the bandwidth at the stopband attenuation. BWc bandwidth of the passband, equation (3-12).

$$\frac{BW}{BW_c} = \frac{f}{f_c} = \frac{f_4 - f_3}{f_2 - f_1} \qquad 3\text{-}12$$

$$\frac{f}{f_c} = \frac{f_4 - f_3}{f_2 - f_1} = \frac{1.9 - 1.1}{1.6 - 1.4} = \frac{0.8}{0.2} = 4$$

Applied in equation (3-12), a ratio of frequencies is equal to 4. Hence, from the chart in figure (3-9), and to obtain a minimum attenuation of 48%. The number of elements should be equal to 5 or more. Selected attenuation value is bigger than the predicted one to overcome potential loss due to fabrication problems. The prototype of a normalised low pass filter consists of five elements.

A normalised filter selected from 1 dB ripples standard Chebyshev chart. Numerical values of elements that construct the normalised prototype low pass filter obtained from standard tables and shown in the table (3-2). Numerical values denoted by g are corresponding to electrical components of inductive and capacitive parts. Source and load resistance are equal to 1 Ω, and filter ripple is 1 dB [128].

Table 3-2. Numerical values of capacitors, inductors and resistors

element	g_o	g_1	g_2	g_3	g_4	g_5	g_6
Value	1	2.207	1.128	3.103	1.128	2.207	1
component	*Rs*	*C/L*	*C/L*	*C/L*	*C/L*	*C/L*	*Rl*

3.7.1. Equivalent circuit of a bandpass filter

Prototype low pass filter undergoes a conversion process to realise the final realistic form of a bandpass filter. Bandpass circuit realised from transform low pass circuit to functional bandpass

circuit requirements. The prototype model is shown in figure (3-11) constructed from elements in the table (3-2). This topology is practical to bandpass configuration. Moreover, facilitates conversion procedure. Equivalent circuit achieved by conversion procedure to a circuit in figure (3-11).

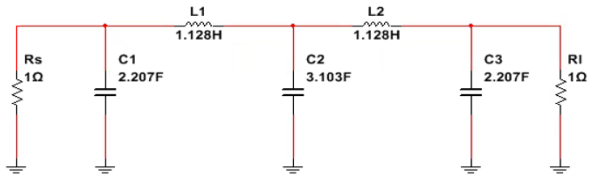

Figure 3-11. Normalised Low pass filter

Normalised low pass prototype circuit transformed to bandpass network by a method explained in figure (3-12). An inductive component will accompany each capacitive component, and a capacitive one will accompany each inductive component in the same connecting manner. [128].

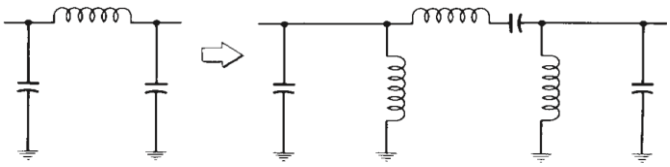

Figure 3-12. Bandpass filter circuit transformation scheme [26]

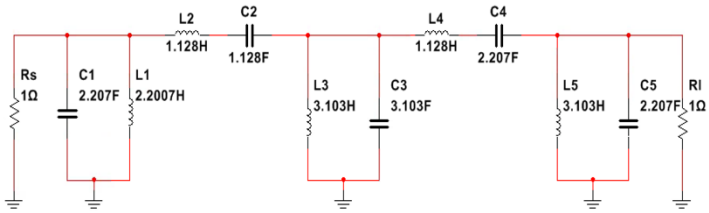

Figure 3-13. Prototype circuit of the bandpass filter

Normalised bandpass network scaled to a final configuration of a bandpass filter. Therefore, implementing scaling equations of frequency and impedance. Bandpass filter circuit consists of series and parallel branches. Each branch has two different components of the same numerical value as shown in figure (3-13). Each parallel and series branch scaled individually by a suitable equation.

Transformation equations (3-13 and 3-14) for branches of parallel resonant are;

$$C = \frac{C_n}{2\pi RB} \quad 3\text{-}13$$

$$L = \frac{RB}{2\pi f_o^2 L_n} \quad 3\text{-}14$$

transformation equations (3-15 and 3-16) for branches of series resonant are;

$$C = \frac{B}{2\pi f_o^2 C_n R} \quad 3\text{-}15$$

$$L = \frac{RL_n}{2\pi B} \quad 3\text{-}16$$

C is the final capacitor. *L* final inductor. *B* final passband width. f_o central frequency. *Cn* normalised capacitor. Ln normalised inductor. *R* impedance of the final load [128].

Design values of scaling are 50 for load impedance *R*, f_o=1.5 GHz which is a bandpass filter central frequency, *B*=0.2 GHz. Calculated components are shown in the table (3-3) and figure (3-14) respectively.

Table 3-3. Scaled data from prototype to final BP filter

Prototype g-value		Series resonators		Parallel resonators	
		Capacitor (F)	Inductor (H)	Capacitor (F)	Inductor (H)
1	2.207			2.341×10^{-11}	4.8076×10^{-10}
2	1.128	3.7625×10^{-13}	2.9921×10^{-8}		
3	3.103			3.2924×10^{-11}	4.194×10^{-10}
4	1.128	3.7625×10^{-13}	2.9921×10^{-8}		
5	2.207			2.341×10^{-11}	4.8076×10^{-10}

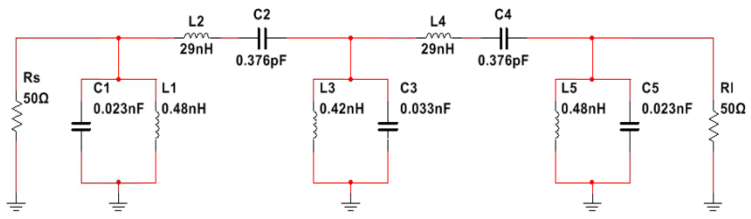

Figure 3-14. Equivalent circuit of Band pass

The designed bandpass filter transformed into a microstrip form depending on g-table. Table (3-2) of the normalised lowpass filter and operational frequencies only. An equivalent circuit is not applicable to the transformation process.

3.8. Microstrip form of bandpass filter

Length of a designed narrowband bandpass filter (BPF) is one-fourth of the wavelength. Proposed microstrip form is parallel edge coupled microstrip filter. Data from the table (3-2) submitted into transformation equations to compute bandpass filter dimensions in the microstrip form.

3.8.1. Bandpass edge coupled microstrip filter (1p)

Electromagnetic waves travel in an adjacent microstrip of an edge coupled microstrip filter will be coupled with locally associated microstrip. Consequently, part of travelling energy will be connected to the adjoining microstrip. Energy coupling will produce two opposite waves oscillating in a contra-directional path to each other. Generated coupled wave propagate in the opposite direction of the incident wave. Design of these edge coupled microstrip filter is flexible. Neither space between microstrips is identical, nor microstrip length and width. Figure (3-15) showed the cross-section of edge coupled microstrip filter.

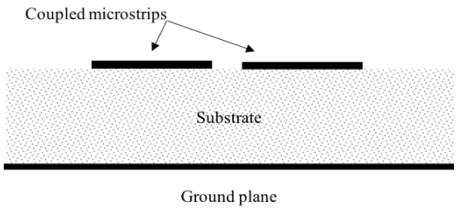

Figure 3-15. Cross section of edge coupled microstrips filter

3.8.2. The admittance inverter parameter (J-inverter)

Admittance (Y) is an expression describing current passing through a conductor. Admittance is a vector function of conductance and susceptance. Thus, admittance is a measure of the charge flow. Susceptance is a measure of material's ability to charge and discharges stored energy throughout current and voltage oscillation. Susceptance is inductive if the energy stored and released in magnetic field form. Susceptance is capacitive if the energy stored and released in electric field form. Symbol *j* used to admittance refers to its complex nature. Admittance equal to reciprocal of impedance. Both admittance and impedance are composed of real and imaginary parts. Equation (3-17) represents the relation between admittance and impedance [6].

$$Y = \frac{1}{Z} \qquad 3\text{-}17$$

3.8.3. Coupling structures

Bandpass microstrip filter is in the form of an edge coupled structures; these structures are microstrip resonators parts. Each part consists of two coupled microstrips separated by a specific space. Equations (3-18 to 3-20) determine these coupling structures. Hence, g_o to g_{n+1} represent numerical values of prototype low pass filter for Chebyshev typical response. Data stated in the table (3-2). Equation (3-18) expressed the first coupling structure.

$$\frac{J_{01}}{Y_o} = \sqrt{\frac{\pi}{2} \frac{FBW}{g_o g_1}} \qquad 3\text{-}18$$

Intermediate coupling structures expressed in equation (3-19).

$$\frac{J_{n,n+1}}{Y_o} = \sqrt{\frac{\pi FBW}{2 g_n g_{n+1}}} \qquad 3\text{-}19$$

Final coupling structure, the opposite end of the coupled microstrip filter, expressed in equation (3-20).

$$\frac{J_{j,j+1}}{Y_o} = \frac{\pi FBW}{2} \frac{1}{\sqrt{g_j g_{j+1}}} \qquad 3\text{-}20$$

where $j=1,2,3,\ldots,n-1$, and $FBW = \frac{w_2 - w_1}{w_o}$ is the fractional bandwidth, w_1 cut off frequency one, w_2 cut off frequency two and wo is the central frequency of bandpass filter, J_j, $_{j+1}$ is representative of the characteristic electrical admittances of J-inverters. Y_o represents the characteristic admittance of the terminating lines. j is the sequence of the element in the normalised filter table [116].

Feeding line and characteristic impedances of the system are 50 Ω. Designed coupled microstrip geometry computations included the following calculations. Shape ratios calculations started by admittance determination.

$$FBW = \frac{w_2 - w_1}{w_o} = 0.133$$

$$\frac{J_{0,1}}{Y_o} = \sqrt{\frac{\pi}{2} \frac{FBW}{g_o g_1}} = 0.3$$

$$\frac{J_{j,j+1}}{Y_o} = \frac{\pi FBW}{2} \frac{1}{\sqrt{g_j g_{j+1}}}$$

$$\frac{J_{1,2}}{Y_o} = \frac{\pi FBW}{2} \frac{1}{\sqrt{g_1 g_2}} = 0.1324$$

$$\frac{J_{2,3}}{Y_o} = \frac{\pi FBW}{2} \frac{1}{\sqrt{g_2 g_3}} = 0.3$$

$$\frac{J_{3,4}}{Y_o} = 0.1324$$

$$\frac{J_{4,5}}{Y_o} = 0.1324$$

$$\frac{J_{5,6}}{Y_o} = \sqrt{\frac{\pi}{2}\ \frac{FBW}{g_5 g_6}} = 0.3$$

3.8.4. Even and odd impedances

Characteristic odd and even impedances Z_{0e} and Z_{0o} for coupled microstrips are functions of coupling degree C. Additionally, they are depending on terminating characteristic impedance of the single line. They will be used to calculate equivalent single shape ratios. Equations (3-21) and (3-22) used to compute impedances as a function of admittance [121].

$$(Z_{0e})_{0,1} = \frac{1}{Y_o}\left(1 + \frac{J_{0,1}}{Y_o} + \left(\frac{J_{0,1}}{Y_o}\right)^2\right) \qquad 3\text{-}21$$

$$(Z_{0o})_{0,1} = \frac{1}{Y_o}\left(1 - \frac{J_{0,1}}{Y_o} + \left(\frac{J_{0,1}}{Y_o}\right)^2\right) \qquad 3\text{-}22$$

for *j=0*

$$(Z_{0e})_{0,1} = 69.5\ \Omega$$

$$(Z_{0o})_{0,1} = 39.5\ \Omega$$

for *j=1*

$$(Z_{0e})_{1,2} = 57.5\ \Omega$$

$$(Z_{0o})_{1,2} = 42.5\ \Omega$$

for *j=2*

$$(Z_{0e})_{2,3} = 56.2\ \Omega$$

$$(Z_{0o})_{2,3} = 45.0\ \Omega$$

Final values of admittances and impedances shown in the table (3-4).

Table 3-4. Final calculated admittances and impedances of bandpass microstrip filter

j	$J_{j,j+1}$	$Z_{0e})_{j,j+n}$	$Z_{0e})_{j,j+n}/2$	$Z_{0o})_{j,j+n}$	$Z_{0o})_{j,j+n}/2$
0	0.30	69.50	34.75	39.50	19.80
1	0.13	57.50	28.75	42.50	21.20
2	0.11	56.20	28.10	45.00	22.50

3.8.5. Determination of shape ratio w/h

For calculated odd and even impedances, related and required width to height ratios given by equation (3-23) [104]. Equation (3-29) apply odd and even impedances to calculate odd and even width to height ratios [121]. The dielectric substrate is FR-4 of height equal to 1.6 mm.

$$\frac{w}{h} = \frac{8e^{A}}{e^{2A}-2} \qquad 3\text{-}23$$

$$A = \frac{Z_o}{60}\left[\frac{\varepsilon_r + 1}{2}\right]^{0.5} + \frac{\varepsilon_r - 1}{\varepsilon_r + 1}\left\{0.23 + \frac{0.11}{\varepsilon_r}\right\}$$

where FR-4 height (h) is *1.6 mm*, ε_r*=4.4.* For feed lines, Z_o=50 Ω giving *A=1.521 and* $\left(\frac{w}{h}\right)_o = 1.932 < 2$, whilst for values of *j=0*, 1 and *2*. Calculated ratios are shown in the table (3-5).

Table 3-5. Even and odd width to height ratios of bandpass microstrip filter

j	$Z_{0e})_{j,j+n}/2$	$(w/h)_{0e}$	$Z_{0o})_{j,j+n}/2$	$(w/h)_{0o}$
0	34.75	3.36	19.75	7.84
1	28.75	4.44	21.25	6.97
2	28.10	4.58	22.52	6.38

Space to height ratios (*s/h*) and shape ratios for single microstrip equations (3-24 to 3-38) are to determine space to height ratio. Depending on even and odd width to height ratios calculated in the previous section, table (3-5).

$$\left(\frac{w}{h}\right)_{se} = \frac{2}{\pi}\cosh^{-1}\left(\frac{2d-g+1}{g+1}\right) \qquad 3\text{-}24$$

$$d = \cosh\left(\pi\frac{w}{h} + \frac{\pi s}{2h}\right) \qquad 3\text{-}25$$

$$g = \cosh\left(\frac{\pi s}{2h}\right) \qquad 3\text{-}26$$

for $\varepsilon_r \leq 6$

$$\left(\frac{w}{h}\right)_{so} = \frac{2}{\pi}\cosh^{-1}\left(\frac{2d-g-1}{g-1}\right) + \frac{4}{\pi\left(1+\frac{\varepsilon_r}{2}\right)}\cosh^{-1}\left(1 + 2\frac{w/h}{s/h}\right) \qquad 3\text{-}27$$

for $\varepsilon_r \geq 6$

$$\left(\frac{w}{h}\right)_{so} = \frac{2}{\pi}\cosh^{-1}\left(\frac{2d-g-1}{g-1}\right) + \frac{1}{\pi}\cosh^{-1}\left(1 + 2\frac{w/h}{s/h}\right) \qquad 3\text{-}28$$

The second part of equations (3-27) and (3-28) can be ignored because in close-fitting coupling *s/h* ratio will be less than *w/h*. Subsequently, a right formula to calculate *s/h* ratio can be made under this condition [129]. Equation (3-29) define space to height ratio as a function of odd and even ratios.

$$\frac{s}{h} = \frac{2}{\pi}\cosh^{-1}\left[\frac{\cosh\left(\left(\frac{\pi}{2}\right)\left(\frac{w}{h}\right)_{se}\right)+\cosh\left(\left(\frac{\pi}{2}\right)\left(\frac{w}{h}\right)_{so}\right)-2}{\cosh\left(\left(\frac{\pi}{2}\right)\left(\frac{w}{h}\right)_{so}\right)-\cosh\left(\left(\frac{\pi}{2}\right)\left(\frac{w}{h}\right)_{se}\right)}\right] \qquad 3\text{-}29$$

3.8.6. Space between each two microstrips calculation

Space gap and related width for each resonator find by equations (3-29) and (3-30) respectively. Results are in the table (3-6). Cross section of edge coupled microstrip filter showing calculated dimensions illustrated in figure (3-16).

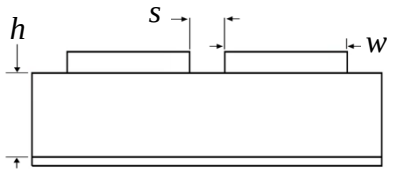

Figure 3-16. Cross-section illustrated dimensions of an edge coupled microstrip filter

For *J=0,* submitting previous results of odd and even ratios in equation (3-29) to obtain

$$\frac{s}{h} = 0.038$$

equation (3-30) is to find final width to height ratio of microstrip design [129] .

$$\frac{w}{h} = \frac{1}{\pi}\left[\cosh^{-1}\left(\frac{1}{2}\left[\left(\cosh\left(\frac{\pi s}{2h}\right)-1\right)+\left(\cosh\left(\frac{\pi s}{2h}\right)+1\right)\cosh\left(\frac{\pi}{2}\left(\frac{w}{h}\right)_{se}\right)\right]\right)-\frac{\pi}{2}\frac{s}{h}\right] \qquad 3\text{-}30$$

$$\frac{w}{h} = 1.661166$$

similarly,

j=1 $\quad \frac{s}{h} = 0.18 \Longrightarrow \frac{w}{h} = 2.135$

j=2 $\quad \frac{s}{h} = 0.32 \Longrightarrow \frac{w}{h} = 2.15$

Table 3-6. Space to height ratios and width to height ratios of bandpass microstrip filter

j	*s/h*	*w/h*
0	0.038	1.66
1	0.18	2.14
2	0.32	2.15

microstrip widths and spaces width calculated for edge coupled microstrip filter. Configure complete final shape by determining the length of each resonator.

3.8.7. Wavelength and microstrip length

Wavelength is the distance between two points of similar electrical phase. The relative dielectric constant of the wave propagation medium and frequency are the factors that affect the wavelength. Wave velocity reduced by a factor as a function of relative permittivity, equation 3-31.

$$\lambda = \frac{1}{\sqrt{\epsilon_r}} \qquad 3\text{-}31$$

microstrip length *l* calculated by equation 3-32,

$$l = \frac{\lambda_g}{4} \qquad 3\text{-}32$$

$$\lambda_g = \frac{300}{F\sqrt{\epsilon_{eff}}} \ \ (mm) \qquad 3\text{-}33$$

3.8.8. Microstrips lengths

Wavelength determination is related to relative permittivity and width to height ratio, equations (3-34 and 3-35)

$$\varepsilon_{re} = \frac{\varepsilon_r+1}{2} + \frac{\varepsilon_r-1}{2}\frac{1}{\sqrt{1+\frac{12h}{w}}} \qquad 3\text{-}34$$

$$\lambda_g = \frac{\lambda_o}{\sqrt{\varepsilon_{re}}} \qquad 3\text{-}35$$

In order to reach maximum coupling. Length of a coupled region must be equal to a complete numeral of a quarter wavelength. This case expressed by equation (3-36).

$$\frac{(n-1)\lambda_g}{4} \qquad 3\text{-}36$$

At higher frequencies, the quarter wavelength condition may lead to a repeated response phenomenon of harmonic effects. The solution is to make coupled region length equal to a quarter wavelength, as expressed by equation (3-37).

$$l = \frac{\lambda_g}{4} \ \ (mm) \qquad 3\text{-}37$$

Even and odd modes have different phase velocities and wavelengths. Thus, an expression to weighted mean phase velocity described by equation (3-38). Involving characteristic impedances of each mode. Thenceforward, an appropriate wavelength of microstrip given by equation (3-39)

$$\lambda_{gn} = \frac{v_n}{f_o} \qquad 3\text{-}38$$

where

$$v_n = \frac{Z_{0e}+Z_{oo}}{(Z_{0r}/v_e)+(Z_{oo}/v_o)}$$

Due to manufacturing criteria and design requirements, equation (3-37) only will be used to find the length of microstrips in the bandpass filter.

j=0 $\quad \frac{w}{h} = 1.661166,\ \varepsilon_{re} = 3.3, \quad \lambda_g = 109.1 \Longrightarrow l = 27.27\ mm$

j=1 $\quad \frac{w}{h} = 2.135,\ \varepsilon_{re} = 3.36, \quad \lambda_g = 109.1 \Longrightarrow l = 27.27\ mm$

j=2 $\quad \frac{w}{h} = 2.15,\ \varepsilon_{re} = 3.36, \quad \lambda_g = 109.1 \Longrightarrow l = 27.27\ mm$

Calculated dimensions are shown in the table (3-7). Some of these dimensions modified slightly to fit the manufacturer's tolerance.

Table 3-7. Physical dimensions of each microstrip resonator and corresponding spaces.

j	w_j/h	w_j *(mm)*	s_j/h	s_j *(mm)*	l (mm)	ε_r
0	1.66	2.65	0.04	0.06	27.50	3.30
1	2.13	3.41	0.18	0.29	27.27	3.36
2	2.15	3.44	0.32	0.51	27.27	3.36

w: width of microstrip, h: substrate height, s: space between microstrips, length of microstrip, ε_r: relative permittivity

3.8.9. Final geometry of bandpass microstrip filter

Computer code is made by Matlab software to perform the calculation and solutions of design formula. The final configuration is shown in figure (3-17), structure is symmetric about the centre. Bandwidth is sensitive to the separations of the terminal coupled sections. Correspondingly, they might be reform by increasing them to modify the bandwidth and response of the filter. Microstrip spaces increased slightly and appropriately to improve transmission passband and mixed coupling [116]. Modified dimensions showed in the table (3-8).

Table 3-8. Final physical dimensions of each microstrip resonator and corresponding modified spaces

j	w_j/h	w_j (mm)	s_j/h	s_j (mm)	l (mm)	ε_r
0	1.66	2.65	0.04	0.3	27.50	3.30
1	2.13	3.41	0.18	0.3	27.27	3.36
2	2.15	3.44	0.32	0.5	27.27	3.36

w: width of microstrip, h: substrate height, s: space between microstrips, l: length of microstrip, ε_r: relative permittivity

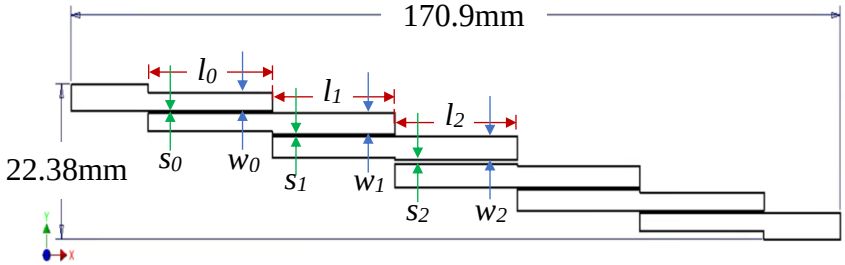

Figure 3-17. Final geometry of bandpass microstrip filter. Dimensions are in millimetres; total length is 170.9 mm, and total width is 22.38mm.

3.9. Low pass microstrip filters

Low pass filter is a circuit that consists of an inductor, capacitors and resistors (RLC). Filter out or passes frequencies lower than or equal to cut off frequency and attenuates all frequencies above cut off frequency, operation due to the low capacitor reactance equal to resistance at cut-off. Works as a short circuit, terminate all signals and yielding zero outputs in the terminal of the circuit. A bandwidth of a lowpass filter is passband zone includes frequencies within the region from 0 frequency to cut off frequency fc of the filter. Wherever attenuated frequencies are in the stop band zone. Low pass filter components cascaded together. The filter is two poles transmission network consists of some repeated passive first order circuits, connected to form the final filter. Filter order expressed by a number of cascaded stages of an RC circuit. Therefore, filter order is equal to the number of connected RC circuits. A design process is similar to the previous one described in the design of the bandpass filter. Prototype selection, scaling process and equivalent circuit. Microstrip made by transformation formulas from equivalent circuit form to a metallic microstrip form of low pass filter.

3.9.1. Chebyshev low pass filter

Designated lowpass filter characterised by Chebyshev response. Chebyshev response is shown in figure (3-1). The passband is not flat, therefore, improve the initial slope of the stop band and produce semi-rectangular attenuation curve shape [113].

3.9.2. Design parameters of Chebyshev low pass filter (2p)

Cut off frequency at 3 dB is 1.3 GHz. Attenuation value > -50 dB. Insertion loss is -50 dB at 1.95 GHz. Ripple value is 1 dB. Source and load impedance are equal to 50Ω. Recall the selection process used previously in bandpass filter design to accomplish normalised low pass filter prototype. Determined frequency ratio calculated to the value 1.5. This value projected over the attenuation curve in figure (3-9) to find the number of elements that give the required attenuation value of the filter.

$$\frac{f}{f_c} = \frac{1.95}{1.3} = 1.5$$

3.9.3. Prototype of low pass filter

The obtained frequency ratio projected on the figure (3-9). Extracted number of elements to realise configured attenuation is seven elements. The number of elements (n) is 7. Thus, filter order is 7. Standard tables of Chebyshev response of 1 dB ripple are used to determine elements values of a low pass prototype filter [119] . These values are shown in the table (3-9).

Table 3-9. Numerical values of capacitors, inductors and resistors for normalised low pass filter for 1dB ripple

element	g_0	g_1	g_2	g_3	g_4	g_5	g_6	g_7	g_8
Value	1	2.204	1.131	3.147	1.194	3.147	1.131	2.204	1
Filter components	*Rs*	*C*	*I*	*C*	*I*	*C*	*I*	*C*	*Rl*

These elements from the table (3-9) can be arranged in two possible topologies, figures 3-18.

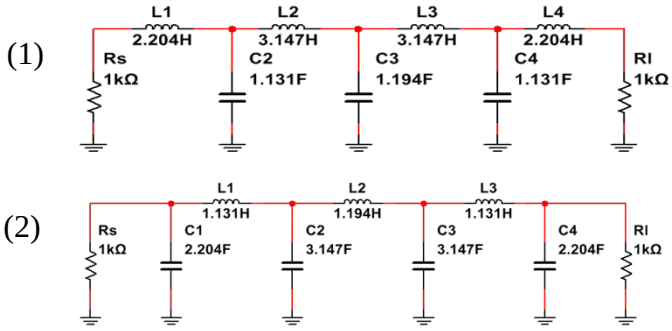

Figure 3-18. Two possible topologies of a lowpass filter

First topology (1) in figure (3-18) is not selected to configure lowpass filter. Avoiding using circuit started by an inductive element to prevent the effect of impedance and increase the loss. As well as, increase capacitive parts will enhance bio-detection act; therefore, topology start by capacitor selected.

3.9.4. Chebyshev low pass filter realisation

The circuit of low pass normalised filter is transformed to a Chebyshev low pass filter by application of appropriate scaling process. The second configuration in figure (3-18) selected to build the final filter circuit.

Scaling prototype lowpass filter to a functional lowpass filter completed;

for capacitive parts, equation (3-39) refers to capacitance scaling.

$$C = \frac{C_n}{2\pi f_c R} \qquad 3\text{-}39$$

$$C_{1=}C_4 = \frac{2.204}{2\pi \times 1.3 \times 10^9 \times 50} = 5.4 \times 10^{-12}\ F$$

$$C_{2=}C_3 = \frac{3.147}{2\pi \times 1.3 \times 10^9 \times 50} = 7.7 \times 10^{-12}\ F$$

for inductive parts, using equation (3-40) of inductive scaling.

$$L = \frac{RL_n}{2\pi f_c} \qquad 3\text{-}40$$

$$L_1 = L_3 = \frac{50 \times 1.131}{2\pi \times 1.3 \times 10^9} = 6.9 \times 10^{-9}\ H$$

$$L_2 = \frac{50 \times 1.194}{2\pi \times 1.3 \times 10^9} = 7.4 \times 10^{-9}\ H$$

Table 3-10. Parameters of lowpass network of Chebyshev filter circuit

element	g_0	g_1	g_2	g_3	g_4	g_5	g_6	g_7	g_8
Value	1	2.204	1.131	3.147	1.194	3.147	1.131	2.204	1
Scaled	50Ω	5.4 pF	6.9 nH	7.7 pF	7.4 nH	7.7 pF	6.7 nH	5.4 pF	50Ω
component	*Rs*	*C*	*L*	*C*	*L*	*C*	*L*	*C*	*Rl*

Numerical values of resultants seven components and 50 Ω resistance of source and load in the table (3-10). Submitted into the distributed element circuit to construct equivalent filter circuit in figure (3-19)[128].

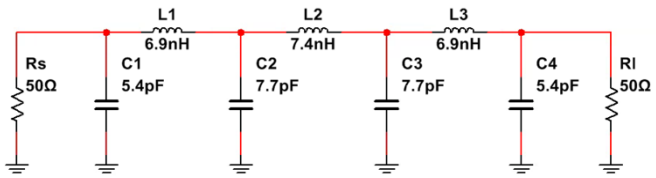

Figure 3-19. Chebyshev low pass filter equivalent circuit of lumped elements

3.9.5. Microstrip form of low pass Chebyshev filter

Convert the lumped elements network into a microstrip form is made by using transformation formula and equations for inductive and capacitive parts. The impedance of the inductive parts is not substantial. Therefore, narrow line inductors become hard to manufacture and restricted ability to carry current through narrow inductive elements [114].

Dispersion effect might be neglected in this transmission line due to the moderately low cut-off frequency of 1.3 GHz in order to realise the microstrip form. Appropriate cascaded microstrip parts will replace electrical circuit; these parts have a definite length, width and height. Parts calculation worked out one by one through the transformation process. Matlab code used to determine dimensions. Some factors need to define in advance because they included in capacitive and inductive expressions. They are the length and a characteristic impedance of each element. The occurrence of transverse resonance must be restricted at higher frequencies, restriction achieved by control width of each part. Seven sections configuration containing low-high-low impedance cascade lines will shape the microstrip form [114]. Figure (3-20) showed the transformation process.

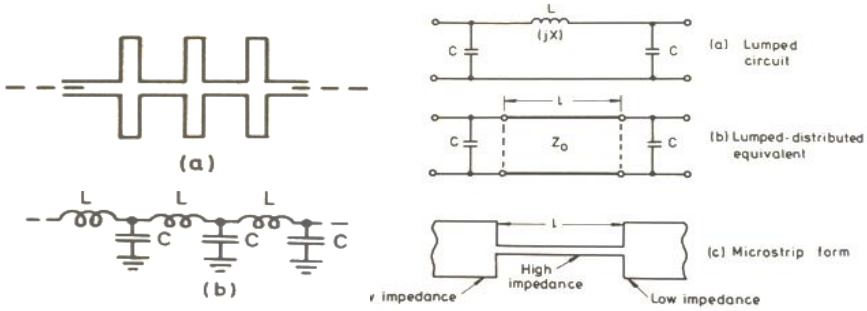

Figure 3-20. Circuit parts transformation [94]

3.9.6. Transformation of low pass filter to a microstrip low pass filter

Regarding microstrip filter realisation, width and length are required to be determined by an adequate formula. Required dimensions showed in figure 3-21.

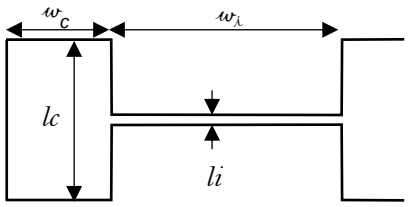

Figure 3-21. Length and width of inductive and capacitive parts

Width of microstrips

Transformations equations of inductive or narrow strip parts [116]. Type of applied equation to define microstrip width is depending on the value of Z_o, if Z_o > b, where (b=44-2ε_r) Ω, and $\frac{w}{h} < 1.3$, equation (3-41) can be used.

$$\frac{w}{h} = \left(\frac{\exp H'}{8} - \frac{1}{4\exp H'}\right)^{-1} \qquad 3\text{-}41$$

$$H' = \frac{Z_o\sqrt{2(\epsilon_r+1)}}{119.9} + \frac{1}{2}\left(\frac{\epsilon_r-1}{\epsilon_r+1}\right)\left(\ln\frac{\pi}{2} + \frac{1}{\epsilon_r}\ln\frac{4}{\pi}\right)$$

$$\varepsilon_{eff} = \frac{\epsilon_r+1}{2}\left\{1 - \frac{1}{2H'}\left(\frac{\epsilon_r-1}{\epsilon_r+1}\right)\left(\ln\frac{\pi}{2} + \frac{1}{\epsilon_r}\ln\frac{4}{\pi}\right)\right\}^{-2} \qquad 3\text{-}42$$

For Capacitive or wide strip parts, equation (3-35) can be used.

$$\frac{w}{h} = \frac{2}{\pi}\{(d_\epsilon - 1) - \ln(2d_\epsilon - 1)\} + \frac{\epsilon_r-1}{\pi\epsilon_r}\left\{\ln(d_\epsilon - 1) + 0.293 - \frac{0.517}{\epsilon_r}\right\} \qquad 3\text{-}43$$

$d = \frac{59.95\pi^2}{Z_o\sqrt{\epsilon_r}}$ is part of equation (3-43),

and $\varepsilon_{eff} = \frac{\epsilon_r+1}{2} + \frac{\epsilon_r-1}{2}\left(1 + 10\frac{h}{w}\right)^{-0.55}$

widths of each part have been determined by using dielectric substrate height (*h*) equal to 1.6 mm for microstrip on FR-4. Calculated widths are shown in the table (3-11).

Table 3-11. Calculated widths of microstrips parts

Parts	C_1	C_3	C_5	C_7	L_2	L_4	L_6
Width (mm)	8.1	12.05	12.05	8.1	6.08	7.15	6.08

3.9.7. Microstrips Lengths

The previous formula of effective permittivity and wavelength of equations (3-32 and 3-33) are applicable to this filter. Determine the length of each part;

Inductive elements length

$$X_L = Z_{0L}\sin\left(\frac{2\pi l_L}{\lambda_{gL}}\right) \qquad 3\text{-}44$$

$$C_L = \frac{l_L}{2fZ_{0L}\lambda_{gL}} \qquad 3\text{-}45$$

$$l_L = \frac{\lambda_{gL}}{2\pi}\sin^{-1}\left(\frac{\omega L}{Z_{oL}}\right) \qquad 3\text{-}46$$

for short length, the equation can be reduced to the form of equation (3-47)

$$l_L = \frac{f\lambda_{gL}L}{Z_{oL}} \qquad 3\text{-}47$$

where f is a cut-off frequency of the filter, λ_{gL} is wavelength at inductor, L inductive electrical value, Z_{oL} is impedance at inductor and l_L is an inductive part length.

Capacitive elements length

$$B_c = \frac{1}{Z_{0c}} \sin\left(\frac{2\pi l_c}{\lambda_{gc}}\right) \qquad 3\text{-}48$$

$$L_C = \frac{l_c Z_{0c}}{2f\lambda_{gc}} \qquad 3\text{-}49$$

$$l_C = \frac{\lambda_{gc}}{2\pi} 2\pi \sin^{-1}(\omega C Z_{0c}) \qquad 3\text{-}50$$

Approximation of length expression can be applied, thus, for short length equation (3-50) can be reduced to the form in equation (3-51).

$$l_C \cong f\lambda_{gc} Z_{0cC} \qquad 3\text{-}51$$

$$\lambda_g = \frac{300}{F\sqrt{\varepsilon_{eff}(f)}}$$

lengths of inductive and capacitive parts calculated to the effective electrical permittivity of ($\varepsilon_{eff} \approx 3.14$); results are shown in the table (3-12).

Table 3-12. Calculated lengths of microstrip parts, effective permittivity= 3.14

Length of inductive parts	30.76 mm	Impedance ≅ 75Ω
Length of capacitive parts	1.43 mm	Impedance ≅ 40Ω

Microstrip filter dimensions realised. Filter's electrical values transformed to one part cascaded physical geometry by using the previous synthesis formulas for length and width.

3.9.8. Final dimensions and microstrip Thickness of lowpass filter

Thickness can be neglected as mentioned previously. Although, the thickness should provide adequate skin depth to the current passing through it. Final dimensions of the microstrip shown in figure (3-22).

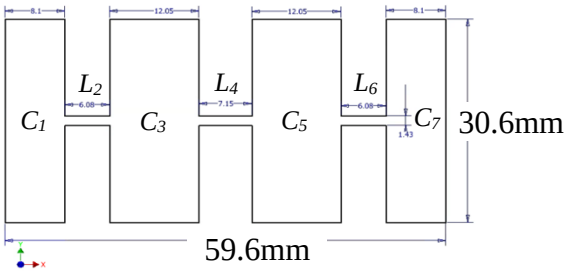

Figure 3-22. Calculated microstrip dimensions of Chebyshev lowpass filter, total width is 30.6 mm, and total length is 59.6 mm

3.10. Butterworth low pass filter (3p)

Butterworth filter passband described by an extremely flat response in the output signal with no ripples in the passband and satisfactory roll off. In contrary to Chebyshev filter. Frequency response is ideally flat in passband region of -3 dB. Flatter response is not realisable in practice. Although with increased cascade number of resonators. However, ripple might be generated. Parameters of the design process are edges of stop and passband, passband attenuation and stopband attenuation. The number of elements in the filter specifies the poles of a filter, therefore, a falloff response rate [130].

3.10.1. Butterworth Filter in Low Pass configuration

The parameters of Butterworth filter are selected to be as following, cut off frequency at 3 dB is equal to 0.8706 GHz, attenuation value > -30 dB, insertion loss =-30 dB at 2 GHz, ripple = 0 dB. Source and load impedances are equal to 50Ω.

$$\frac{f}{f_c} = \frac{3}{0.8706} = 3.4459 \approx 3.5$$

The selection process of prototype normalised filter applied as described previously. A prototype of normalised Butterworth low pass filter nominated in agreement with design criteria and frequency ratio. Determined frequency ratio is 3.5. From attenuation curve in figure (3-23) of Butterworth standard table [128], number of elements that gives the required attenuation value of designed filter specified to be four.

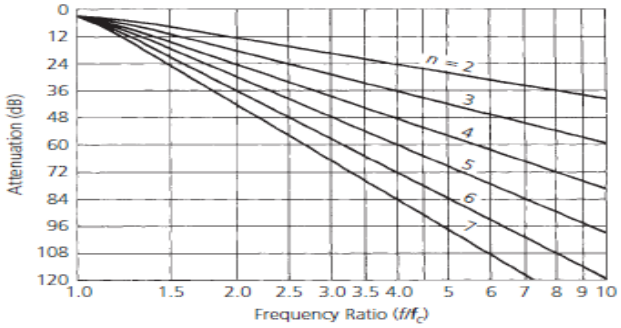

Figure 3-23. Standard attenuation curves of Butterworth filters [109]

3.10.2. Prototype of Butterworth low pass filter

From curves and data sheets. Four elements circuit selected that give the targeted attenuation. Filter order is 4. Standard tables of Butterworth response are used to determine elements values of normalised low pass prototype filter [111]. Load and source resistances are equal to 1 Ω. Numerical values shown in the table (3-13). Prototype filter is shown in figure (3-24).

Table 3-13. Numerical values of capacitors, inductors and resistors for the normalised low pass filter for 1dB ripple

Element	g_o	g_1	g_2	g_3	g_4	g_5
Value	1	0.765	1.848	1.848	0.765	1

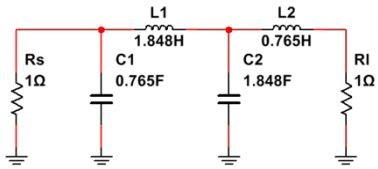

Figure 3-24. Normalised Butterworth filter circuit

Equivalent circuits of the final filter can be constructed in two possible topologies. Either start by a capacitor or inductor, as shown in figure (3-25). Prototype filter circuit consists of four elements, two inductances and two capacitances in addition to resistors.

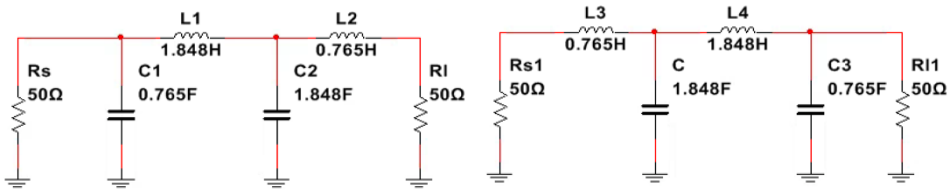

Figure 3-25. Two possible topologies of normalised Butterworth low

3.10.3. Scaling of Frequency and Impedance

The low pass prototype circuit scaled to a practical filter. Transformation achieved by applying scaling formulas (3-52) for capacitive components and (3-53) for inductive components of normalised low pass filter.

$$C = \frac{C_n}{2\pi f_c R} \qquad 3\text{-}52$$

$$L = \frac{RL_n}{2\pi f_c} \qquad 3\text{-}53$$

where C and L are the final capacitance and inductance respectively, R is the load resistance, f_c is cut off frequency and C_n, L_n are prototype values [128].

Butterworth low pass filter is realised by the calculations below.

$$C1 = \frac{C_n}{2\pi f_c R} = 0.003 \times 10^{-9}$$

$$C2 = \frac{C_n}{2\pi f_c R} = 0.007 \times 10^{-9}$$

$$L1 = \frac{RL_n}{2\pi f_c} = 18.4 \times 10^{-9}$$

$$L2 = \frac{RL_n}{2\pi f_c} = 7.6 \times 10^{-9}$$

3.10.4. Equivalent circuit

Topology started with a capacitive part is selected to represent the equivalent circuit of the Butterworth filter. Table (3-14) and figure (3-26) are showing elements and circuit topology, respectively.

Table 3-14. Parameters of the lumped low pass network of Butterworth filter circuit

Element	g_o	g_1	g_2	g_3	g_4	g_8
Value	1	0.765	1.848	1.848	0.765	1
Scaled	50Ω	3 pF	18.4 nH	7 pF	7.6 nH	50Ω
component	*Rs*	*C*	*L*	*C*	*L*	*Rl*

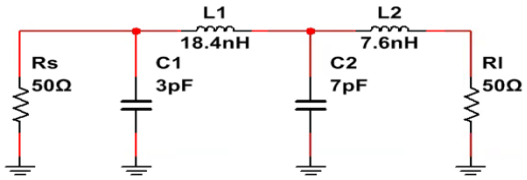

Figure 3-26. Butterworth low pass filter equivalent circuit

3.10.5. Microstrip filter realisation

Apply the same technique used before to transform lumped elements form of Chebyshev filter to a metallic microstrip form, on this filter to produce microstrip form of it.

3.10.6. Synthesis of microstrip filter

Synthesis of microstrip design requires values of length and width to be identified. Length l and width w values conformed to characteristic impedance Z_o. Relative electrical permittivity ε_r and

height *h* of the substrate. Additionally, frequency have a governor rule in determines these dimensions, table (3-15). Same mathematical operations of previous Chebyshev microstrip filter used to determine the width and length of Butterworth low pass microstrip filter.

Table 3-15. Physical dimensions of Butterworth microstrip filter

Microstrip part	*Length (mm)*	*Width (mm)*
Capacitive (C_1)	20.4	8.8
Inductive (L_2)	0.6	13.5
Capacitive (C_3)	20.3	14.8
Inductive (L_4)	0.6	12.5

Final Butterworth microstrip filter geometry realised. Started by a capacitive element, thus, a configuration of microstrip filter shown in figure (3-27).

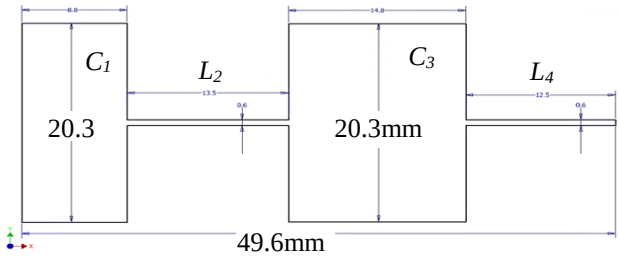

Figure 3-27. Microstrip geometry of Butterworth low pass filter, total length is 49.6 mm, and total width is 20.3 mm.

3.11. Microstrips on a quartz substrate

Preceding design method of microstrip filters used to design new group of microstrip filters, quartz used as dielectric substrate material. Quartz provides maximum surface flatness which provides good infrastructure to metal microstrip. Therefore, flat surface to biochemical functionalisation of bio-sensing operation.

3.11.1. Low pass Chebyshev microstrip filter (4q)

This filter configuration is identical with the previous Chebyshev lowpass microstrip filter except the dielectric substrate is quartz. Therefore, different dielectric permittivity. Cut-off frequency f_c=1.45 GHz, microstrip height=1 mm, numerical values of prototype and scaled elements of the final filter shown in the table (3-16). The geometry of the microstrip filter showed in figure (3-28). Total width and length dimensions are 75×19.6 mm.

Table 3-16. Parameters of the lumped low pass network of Chebyshev filter circuit

element	g_0	g_1	g_2	g_3	g_4	g_5	g_8
Value	1	2.204	1.131	3.147	1.194	3.147	1
Scaled	50Ω	5.4 pF	6.9 nH	7.7 pF	7.4 nH	7.7 pF	50Ω
component	*Rs*	C_1	L_2	C_3	L_4	C_5	*Rl*

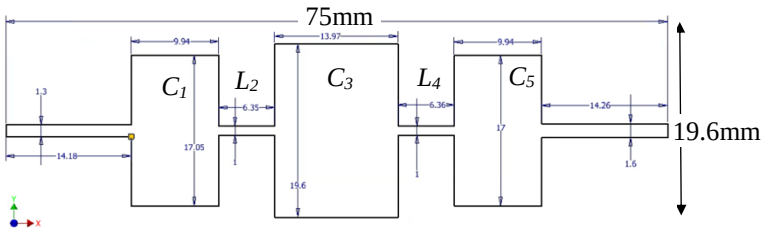

Figure 3-28. The geometry of microstrip Chebyshev low pass filter on quartz, dimensions are in millimetre, 75×19.6mm

3.11.2. V-shaped Bandpass microstrip filter (5q)

Bandpass microstrip filter designed in V-shaped geometry targeting compact device, standard edge coupled microstrip filter separated from the middle, and one half is rotated 180o, and then the two parts joined together as shown in figure (3-29). They have built on quartz dielectric substrate of 1 mm thick. V-shaped geometry is untraditional and aims to reduce the length and size of the microstrip filter. They are replacing the longitudinal configuration with asymmetry reflected format of similar sides. All design criteria are the same except microstrips distribution over a dielectric substrate. Dimensions of microstrip form shown in the table (3-17). Figure (3-29) showed microstrip form of the filter, 25×64.8 mm. Therefore, same procedures of selection, scaling and transformation of previously designed bandpass microstrip filter applied to produce V-shaped bandpass microstrip filter. The design parameters are 1.55 GHz of central frequency. First cut off frequency is 1.45GHz. Second, cut off frequency is 1.8 GHz.

Table 3-17. Physical dimensions of V-shaped microstrip filter

j	$w_{j\,(}mm)$	$s_{j\,(}mm)$	*l* (mm)	ε_r
0	2.65	0.3	27.55	3.30
1	3.04	0.3	27.25	3.36
3	3.45	0.2	27.25	3.36

w: width of microstrip, h: height of substrate, s: space between microstrips, l: length of microstrip, ε_r: relative permittivity

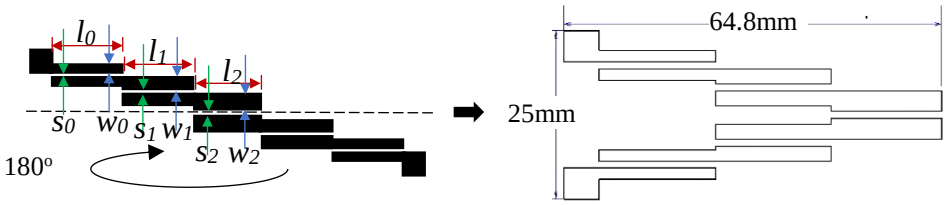

Figure 3-29. V-shaped microstrip bandpass filter, total length is 64.8mm, and total width is 25mm

3.12. Reduced size models

In order to compare the functionality of proposed biosensors with smaller versions of them, a reduced size microstrip filters of higher operational frequency and micro size is designed [131, 132]. New two ultra-compact and reduced size microstrip filters designed. Therefore, small size is beneficial in bio-sensing application due to biological sample size reduction, integration, cost-effectiveness and mass production. Dimensions parameters of these microstrips filter are in mm and μm while their thickness is 350 nm only. Additionally, they designed on a dielectric substrate of quartz has a thickness equal to 250 μm. These dimensions with further electromagnetic and materials properties represent good base to bio-sensing performance. Simplicity is an essential factor of the designed microstrip filters. Previously described design steps applied to design the new microstrip filters, considering the small size and accompanied higher frequency.

Miniaturized and lightweight is the desired trend in electronic biosensors [57, 133]. Higher frequencies and miniaturised devices aimed to boost productivity, applications of microstrips and their biosensor. Length and size of microwave microstrip filter are reversely proportional with the operating frequency and wavelength. Therefore, an increase in operating frequency will reduce the size and length of the microstrip filter. Hence, dimensions of the miniaturised microstrip filters providing a compromise between targeted biomolecules and electromagnetic waves propagate through them. Size reduction aid cost of manufacturing and application as well as handling. Higher frequencies (f >10GHz) enhance the sensitivity of the biosensor. Reduce sample size to less than one microliter or few nanoliters of liquid. Increases the ability to detect low concentrations less than one nano per ml or one cell only. The similar design procedure of miniaturised microstrips filter in the form of edge coupled and cascade-connected microstrip filter. It is same as the previously practised procedure of designed microstrip filters except for operating frequencies and thickness of a dielectric substrate. Two types of microstrip filters designed with Chebyshev characteristic response; bandpass in the form of edge coupled microstrip filter, and lowpass cascaded microstrip filters [134].

3.12.1. Chebyshev bandpass microstrip filter (6q)

Selected central frequency is 15 GHz. First cut off frequency is 14 GHz at 3dB. Second, cut off frequency is 18 GHz at 3dB. First low cut off frequency is 10 GHz at 50dB. Second low cut off frequency is 22 GHz at 50dB. Response ripple is 1 dB and bandpass is approximately 4 GHz. Design carried out by the same previously used technique in the section of bandpass microstrip filters in this chapter. Calculated and potential dimensions are driven from the same prototype shown table (3-2). Parameters of reduced size bandpass microstrip filter shown in the table (3-18). The proposed design is shown in figure (3-30), structure is symmetric about centre. Dimensions are 11×4.66 mm.

Table 3-18. Dimensions of the first half of edge coupled filter (mm)

j	*W (mm)*	*S (mm)*	*L (mm)*
0	*0.349*	*0.0023140*	*2.73*
1	*0.462*	*0.0113550*	*2.70*
2	*0.490*	*0.0181240*	*2.70*

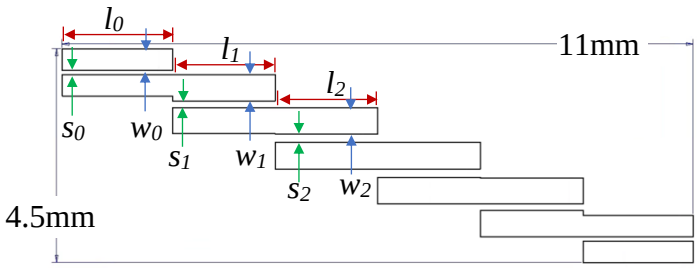

Figure 3-30. The proposed design of the reduced size bandpass microstrip filter, total length is11mm and total width is 4.5mm

3.12.2. Chebyshev low pass microstrip filter (7q)

Design procedures for this filter are similar to the previous low pass filter of Chebyshev response except frequency are higher. The cutoff frequency is equal to 20 GHz. The thickness of the substrate dielectric layer is 250 µm. Normalized low pass filter is the same one used previously to design low pass Chebyshev filter in the table (3-9). Therefore, identical equivalent circuit showed in figure (3-20). Calculated geometry and possible physical dimensions of width and length are shown in the table (3-19). Figure (3-31) showed a device's configuration, and total dimensions are 7.3×1.6mm ×350nm.

Table 3-19. Physical dimensions of reduced size lowpass Chebyshev filter

Inductive			Capacitive		
	Length (mm)	Width (mm)		Length (mm)	Width (mm)
L_1	1.2408	0.2051	C_2	0.510	0.83
L_3	1.7717	0.2051	C_4	0.538	0.83
L_5	1.7717	0.2051	C_6	0.510	0.83
L_7	1.2408	0.2051			

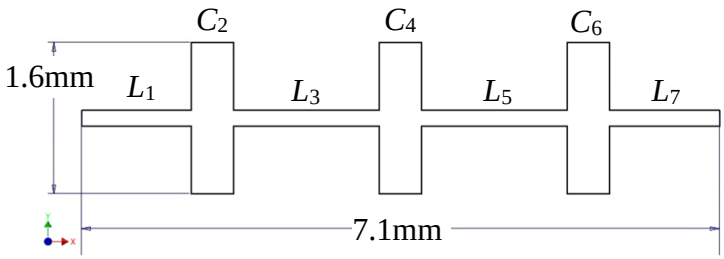

Figure 3-31. Design of reduced size microstrip of lowpass Chebyshev filter, dimensions are 7.1mm×1.6mm×350nm.

3.13. Summary of microstrip filters design chapter

This chapter yielded the design of seven microstrip filters, three of them were fabricated by PCB technique on FR-4 dielectric substrate. Two microstrip filters were designed and fabricated by evaporation technique on a quartz substrate, one of them is V-shaped microstrip filter. Two more reduced sizes of microstrip filters were designed targeting miniaturised version of the sensor; they fabricated by evaporating on quartz. Regarding the microstrip filter design process, several parameters and their values are considered. These parameters are, operating frequencies, the number of elements, response type, cut off frequency points, centre frequency, attenuation, materials of microstrip and dielectric substrate, ripples number which is determined by appropriate filter response. These parameters and factors are used to select and build the normalised lowpass filter or the prototype. Prototype filters selected from standard data books and standard tables. The calculated ratio between the cutoff frequency and appropriate frequency range used to determine the order of the prototype filter depending on the required attenuation. Attenuation curve, or standard forms, identify the number of elements depending on frequency ratio. Produced prototype filter have the same number of elements and order with the final one. The prototype filter had a circuit of normalised values, and elements then scaled to operational and practical filter values. Afterwards, a practical filter was converted to a

microstrip form by specific transformations. Five microstrip filters were then designed, in addition to these, two reduced size microstrip filters designed by the same methods of the previous microstrip filters, all design parameters are the same except higher frequency applied and different dielectric substrate thickness and permittivity. Electrical filters transformed to microstrip filters in order to be used in biosensor assembly, this is because microstrips provide a flat surface to construct microfluidic on it. It allows travelling electrical field lines that travel from microstrip through microfluidic and materials inside it, regarding biosensor fabrication, designed. Microstrip filters will be modelled, fabricated and integrated with microfluidic to realise the targeted biosensor.

Chapter 4. Modelling of microstrip filters

4.1. Introduction

Designed microstrip filters characteristic responses are modelled and analysed in this chapter. Regarding simulations, two 3D full electromagnetic wave simulators used, Sonnet Lite and Ansys electromagnetic Suite. Sonnet Lite used to analyse microstrip filters that have an operational frequency less than 3GHz; they are 1p, 2p,3p and 4q. Ansys electromagnetic simulator was used to analyse reduced size versions 6q and 7q, in addition to V-shaped microstrip filter 5q. Ansys has more flexibility in comparison with the light version of Sonnet Lite. Ansys produced more consistency results at high frequency. Scattering parameters of an incident, transmitted and reflected waves used in the modelling and evaluation processes. Scattering matrix represents an adequate characterisation tool for transmission lines and microstrip filters. It is based on the three dimensions modelling based on Maxwell's equations. These equations comprise all parasitic, cross-coupling, enclosure and bundle resonance possessions. Modelling parameters of interest are model dimensions, dielectric substrate type, metal type and frequency band [135].

4.1.1. Electromagnetic waves in transmission lines

An electromagnetic wave travels along the skin of the transmission line. Travelling wave propagate over transmission line as a function of a position over time. Electromagnetic coupling between microstrips allow waves travel over discontinuities and spaces [118], this merit is useful in biosensing applications.

4.1.2. Power flow

Current and voltage of waves are propagating with constant shape and magnitude. Power is restrained and flows with speed similar to the speed of an electromagnetic wave propagating in-between two conductors. Also, some power will escape as losses in the form of radiation or heat. Additionally, power can be absorbed by the materials close to microstrip patches, such as material under test in a biosensor.

4.1.3. Transmission lines geometry

Wavelength is comparable to transmission line dimensions. Therefore, transmission line theory analysis of the travelling wave is convenient to verify and analyse transmission lines with parameters other than voltage. The transmission line might be expressed as a continuous path between two ports to guide and transmit electromagnetic power, path geometry made of conducting and insulating materials that have definite borders and properties. The geometry of cross-section is constant, and a transmission line of constant geometry is uniform. Henceforth,

geometry discontinuities change the consistency of the transmission line [114]. According to this concept, the addition of biological materials will affect travelling waves.

4.1.4. Travelling wave in a transmission line

Electromagnetic waves in transmission networks are sinusoidal and analysed as an oscillating wave. Voltage and resultant current in a transmission line can be expressed in the form of exponential equations of a periodical wave. Equations (4-1) and (4-2) describe travelling wave as a function of displacement (x) [136].

$$V(x) = V_o^+ e^{-\gamma x} + V_o^- e^{\gamma x} \qquad 4\text{-}1$$

$$I(x) = I_o^+ e^{-\gamma x} + I_o^- e^{\gamma x} \qquad 4\text{-}2$$

γ is wave complex propagation constant.

4.1.5. Attenuation

Voltage attenuates exponentially as a wave travelling along a transmission line. Attenuation indicated in equation (4-3).

$$V_1 = V_{1p} e^{(\alpha + j\beta)l} \qquad 4\text{-}3$$

Component α is the attenuation constant using units of (Np/length unit) Np or Neper. Np is a logarithmic ratios measurements unit for quantities like loss and gain in electronic systems ($1Np=20\log_{10}e=8.6858896$ dB). Component β is the phase constant (radians, or degrees/length unit).

4.1.6. Relation of Incident and reflected waves with impedance

Transmission line had an incident, reflected and transmitted waves due to load and mismatched impedance. Part of travelling energy will be transmitted, and another part will be reflected. Reflected wave will travel in the opposite direction to the incident wave direction. Both waves will have an incident and reflected components.

Relative phases and amplitudes of the two opposite waves are dependent on the characteristic impedance of the transmission line (Z_o). Controversy, waves magnitudes are determined by source impedance. Impedance can be affected by the materials under test in the biosensor.

4.1.7. Reflection coefficient

A forward and backward travelling wave of voltage can define the transmission line. The reflection coefficient is a position dependent function. It can be expressed as a function of impedances. Therefore, the relation between the reflection coefficient and impedance of a

transmission line is linked. In terms of response analysis, modification of geometry and impedance will affect reflection coefficient and device characteristic response [106]. Therefore, biosensor's response.

4.2. Transmission line circuit analysis

Short and open circuit method is appropriate to low-frequency circuits only. However, it is not efficient to analyse circuits that operate at microwave frequency. Therefore, termination by open-short circuit method might cause two ports microwave network to oscillate, and stability problem arises [137].

4.2.1. Scattering parameters and microstrip filters modelling

In terms of network analysis, scattering parameters are a handy tool. The circuit can be analysed without the need to identify its internal components. Thus, when microwave enters and travels through a transmission line, it will partially reflect, and the rest of the wave will transmit with a ratio of attenuation to the opposite port of the transmission line. Analysis of two ports transmission line network considers a superposition of two identical waves oscillating in opposite directions to each other. Regarding microstrip filters analysis. Two ports transmission network representation will be used to characterise filters functionality.

An electromagnetic analysis might be described in high-frequency parameters set, and the scattering matrix well interprets it. Scattering matrix described the electrical behaviour of the microstrip filter and produced a biosensor. Scattering parameters refer to the incident, transmitted and reflected electromagnetic waves. Linear two ports transmission network can be characterised by scattering matrix consists of four elements. Scattering and reflection coefficients define incident and transmitted waves at each port, this situation illustrated in figure (4-1). A notation refers to incident wave on each port, b refers to the reflected wave from each port. They are dependent on position. Variables a_1 and a_2 are the incoming incident waves from each port, b_1 and b_2 are the outgoing waves at each port.

Scattering parameters denoted as S_{11}, S_{12}, S_{21} and S_{22} and they compose scattering matrix. S_{11} and S_{22} are the reflection coefficients. S_{12} and S_{21} are the transmission coefficients

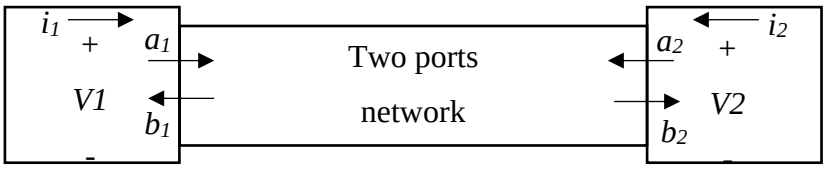

Figure 4-1. Two ports network, conventionally, each port contains two nodes referring to the two waves in it.

Accordingly, powers of forward and reverse travelling waves are equal to $|a|^2\ and\ |b|^2$. Travelled power affected by attenuation and geometry changes due to external materials [106]. Net power at one port is equal to ($|a|^2 - |b|^2$).

4.2.2. Scattering matrix

S-parameters can be measured from the matched network. That, characterised impedance is equal to a load impedance, Z_o=Z_L. Consequently, in the matched case, reflected wave from load would be zero, a_2=0. Scattering matrix is expressed in the form of equation (4-4), and for two ports network, it will 2×2 matrix.

$$b = Sa \Rightarrow \begin{bmatrix} b_1 \\ b_2 \end{bmatrix} = \begin{bmatrix} S_{11} & S_{12} \\ S_{21} & S_{22} \end{bmatrix} \begin{bmatrix} a_1 \\ a_2 \end{bmatrix} \quad 4\text{-}4$$

Scattering parameter in any port might be defined as the ratio between b(x) and an (x) which is equal to the reflection coefficient value. Reflection scattering parameter equation describes the quantity of reflected power from network port, equation (4-5).

$$S(x) = \frac{b(x)}{a(x)} = \Gamma(x) \quad 4\text{-}5$$

Scattering matrix general formula can be decomposed. Equations (4-8) and (4-9) give the reflection coefficient S_{11} and transmission coefficient S_{21} respectively. Similarly, S_{12} and S_{22} can be extracted.

$$P_L = P_{S,max} - P_{refl} = |a_1|^2(1 - \Gamma^2) \quad 4\text{-}6$$

$$S_{ij} = \left.\frac{b_i}{a_j}\right|_{Z_o=Z_L} \quad 4\text{-}7$$

Reflection coefficients are S_{11} and S_{22}, and transmission coefficients are S_{21} and S_{12},

$for\ a_2 = 0$

$$S_{11} = \left.\frac{b_1}{a_1}\right|_{Z_o=Z_L} \quad 4\text{-}8$$

$$S_{21} = \left.\frac{b_2}{a_1}\right|_{Z_o=Z_L} \quad 4\text{-}9$$

$for\ a_1 = 0$

$$S_{12} = \left.\frac{b_1}{a_2}\right|_{Z_o=Z_L} \quad 4\text{-}10$$

$$S_{22} = \left.\frac{b_2}{a_2}\right|_{Z_o=Z_L} \quad 4\text{-}11$$

$$[S] = \begin{bmatrix} [S_{11}] & [S_{12}] \\ [S_{21}] & [S_{22}] \end{bmatrix} \quad 4\text{-}12$$

Scattering coefficients expressed by equations (4-8) to (4-11) describe the scattering matrix, equation (4-12). Asymmetry of two ports network leads to equal scattering parameters and reflected parameters. After that, symmetrical networks have $S_{11}=S_{22}$ and $S_{12}=S_{21}$.

For specific frequency, two ports network might be expressed by various parameters. Therefore, they are connected, and they can be converted from one form of a matrix to another. S matrix might be described by different matrix form through standard conversions to an incident and reflected amplitudes of voltage waves from ports. Standard tables of matrix conversions are available in many references [117].

4.2.3. Scattering and reflection coefficients of a microstrip filter

Scattering parameters are a useful technique for high-frequency filters characterisation. Travelling waves have been used to define high-frequency networks instead of electrical components of current and voltage. Through the measurement of the scattering degree which represents the amount of amplification or attenuation as a function of electrical power square root.

Scattering term refers to resultant reflection and transmission waves of an incident electromagnetic wave on a surface between two different mediums. Reflection produces from the surface towards the source, opposites the propagation of the source wave in the reverse direction. While transmission occurs through the material in the same direction of the source propagating wave direction beyond the surface. Figure (4-2) showed S_{11} and S_{22}. They represent reflection coefficients. Transmitted parameters defined by S_{12} and S_{21}.

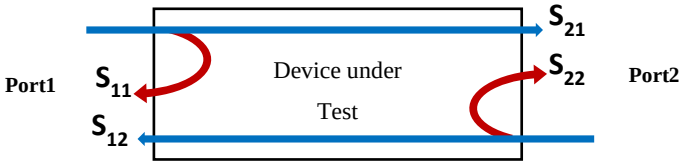

Figure 4-2, Scattering parameters sketch for two ports device

Scattering parameters are non-dimensional variables. They are ratios only. However, a decibel (dB) unit is used to label the magnitude of the S-parameter.

Scattering parameters for a passive two-port device are defined by the equation of power scattering ratio below:

$$|S_{11}|^2 + |S_{21}|^2 \leq 1$$

Equal sign indicates that scattering parameters are unitary for a lossless device. At the same time, scattering parameters are not exceeding the value of one which is equal to 0 dB value. An equation of power scattering ratio is a measurement function for power consumption by the

device. The loss is proportional to the power consumption. Minimum result refers to a more extensive loss.

$$|S_{11}|^2 + |S_{21}|^2 = PS \qquad (0 \leq PS \leq 1)$$

Defining scattering coefficients as a ratio of reflected to incident power at each port, equations (4-13 to 4-16)

$$|S_{11}|^2 = \frac{power\ reflected\ from\ \ input}{power\ incident\ on\ input} = \frac{|b_1|^2}{|a_1|^2} \qquad 4\text{-}13$$

$$|S_{22}|^2 = \frac{power\ reflected\ from\ \ network\ output\ port}{power\ incident\ on\ output} = \frac{|b_2|^2}{|a_2|^2} \qquad 4\text{-}14$$

$$|S_{12}|^2 = \frac{power\ reflected\ from\ \ network\ input\ port}{power\ incident\ on\ output} = \frac{|b_1|^2}{|a_2|^2} \qquad 4\text{-}15$$

$$|S_{21}|^2 = \frac{power\ reflected\ from\ \ network\ output\ port}{power\ incident\ on\ input} = \frac{|b_2|^2}{|a_1|^2} \qquad 4\text{-}16$$

Scattering parameters are very useful tools to analyse passive networks such as microstrip filter circuits [117]. Scattering matrix used to analyse designed microstrip filters of this research.

4.3. Electromagnetic modelling

Scattering parameters or S-matrix define electromagnetic characteristics of transmission lines. Responses of microstrip filter affected by design and dimensions change. Network parameters and their phases measured as a function of applied frequency.

Simulators performed de-embedded computations; microstrip filters analysed as a lossless conductor. Computer software used to synthesis, construct, analyse and evaluate the microstrip filters. Equivalent circuits of filters analysed by NI Multisim program. Next sections present an overview of designed microstrip filters simulation and modelling.

4.4. Patches dimensions and feed lines

Microstrip divided into several metallic strips called patches. In the modelling process, microstrip filters constructed from patches of rectangular shapes. They connected directly to form microstrip filter's body. A thickness of patches is selected depending on targeted application and manufacturing processes criteria. The characteristic impedance of feeding lines is selected to be 50 Ω, in order to make it compatible with cables and connectors. The width of the feed line calculated as a function of impedance, thickness and electrical permittivity of the dielectric substrate. Length of feeding line is defined to match SMA connectors' purpose. Feed lines added to the calculated dimensions of microstrips in the modelling process.

4.5. Sonnet Lite electromagnetic simulator

Regarding modelling, final geometry of microstrip filters except for reduced size versions and V-shaped microstrip filter is modelled by Sonnet Lite electromagnetic simulator. This programme is using the scattering matrix to characterise microstrip networks. Three dimensions geometry is submitted first. Consequently, the dielectric layer is specified as FR-4 dielectric material, which is a laminated pane of strengthened epoxy. Dielectric thickness is equal to the one used in the design calculations; it is equal to 1.6 mm. Thickness selected to meet requirements of printed circuit board (PCB) fabrication criteria. The dimensions of the SMA connectors (SubMiniature version A). Scanning frequencies are within the range from 0.1 GHz to 3 GHz, and attenuation range is up to -100 dB. Finite elements method adopted by the simulator to analyse microstrip transmission lines, mesh subsections are 1200. Gold conductivity is 4.09×10^7 S/m and is considered lossless, the thickness is 10 µm, FR-4 dielectric permittivity is 4.4, and dielectric loss tangent is 0.02, microstrip height is 1.6 mm. An applied frequency band is 0.01-3 GHz. Ports impedance is 50 Ω. Analysis results will be discussed in the next sections.

4.6. Modelling of microstrip filters on FR-4

Microstrip filters modelled in order to examine the design and its operational features. Also, modify some dimensions. Microstrip filter dimensions are selected and modelled following the preferred frequency. Electromagnetic modelling and simulation of the filters are realised by Sonnet Lite which it is a full wave electromagnetic simulator [138, 139].

Preliminary, proposed microstrip filter is accomplished from prototype filter, transformed to a microstrip filter by transformation process from electrical components form to physical metal form. A substrate made of FR-4 dielectric material has a dielectric constant equal to 4.4. The thickness of the substrate is 1.6 mm. Microstrips surface metal is gold. Applied thickness is 10 µm. Input and output feed lines of 50 Ω impedance are connected to the two terminal ports located in the right and left ends of each filter. Modelled results of scattering parameters as a function of frequency showed that designs are correct and have a standard bandpass and bandstop responses within the selected band and frequencies. Some dimensions are modified to suit the fabrication process without affecting filters responses. Current density patterns are identified as a sensitive surface region to bio-sensing process.

4.6.1. Bandpass microstrip Chebyshev filter (1p)

Bandpass microstrip filter layout consists of six edge-coupled microstrip resonators separated by spaces of micro gaps, figure 8. Overall dimensions of the filter are 170.9 mm length and

21.98 mm width. Gaps between strips are 100 microns and 350 microns respectively. Feed lines length is 17mm. The design showed in figure (3-17). Edge coupled microstrip filter consists of 14 gold patches, attached to the top of FR-4 dielectric substrate. Twelve patches represent resonators with a gap between them. Mesh pattern model of the microstrip filter is shown in figure (4-3).

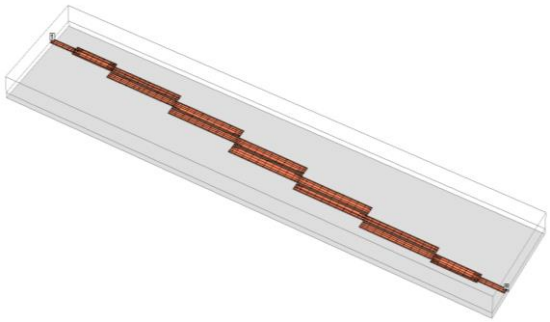

Figure 4-3. 3D representation of bandpass microstrip filter geometry and 1785 mesh subsections in Sonnet Lite

Scattering parameters in figure (4-4) showing that S_{12} and S_{21} are mostly identical due to shape symmetry. Slight differences might be due to connection port to a power source which determines the length of a wave path, micro differences in spaces of resonators. Results confirmed design functionality. Phases are shown in figure (4-5), typical responses of microstrip filter. Current density pattern showed in figure (4-6). Passband has a high current density on microstrips edges.

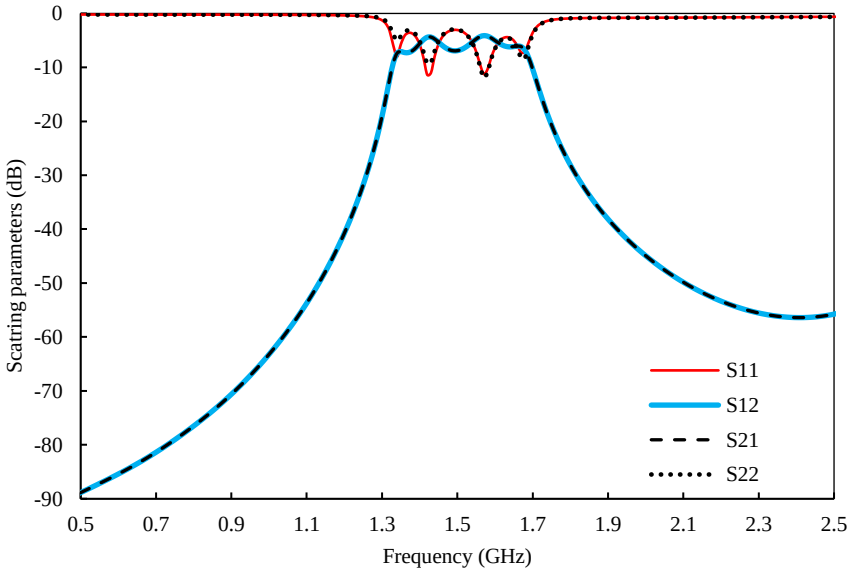

Figure 4-4. Scattering parameter S_{11}, S_{12}, S_{21} and S_{22} of bandpass Chebyshev microstrip filter on FR-4 substrate

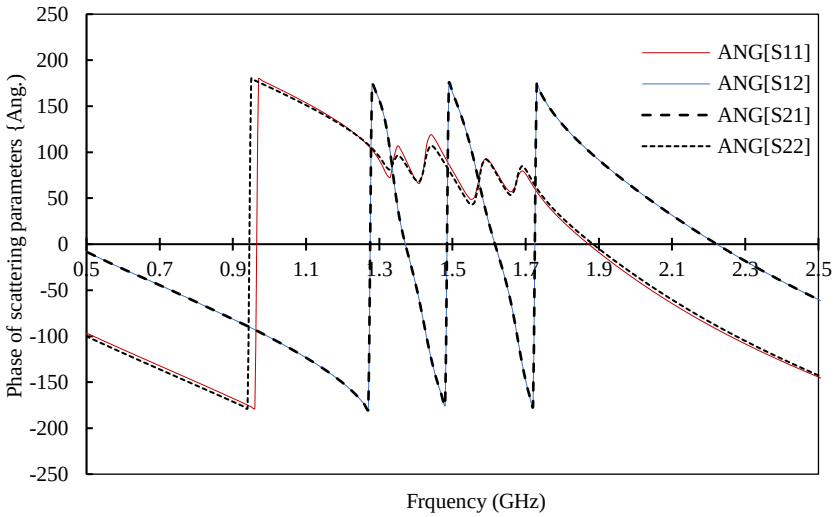

Figure 4-5. Phase of scattering parameter S_{11}, S_{12}, S_{21} and S_{22} of bandpass Chebyshev microstrip filter on FR-4 substrate

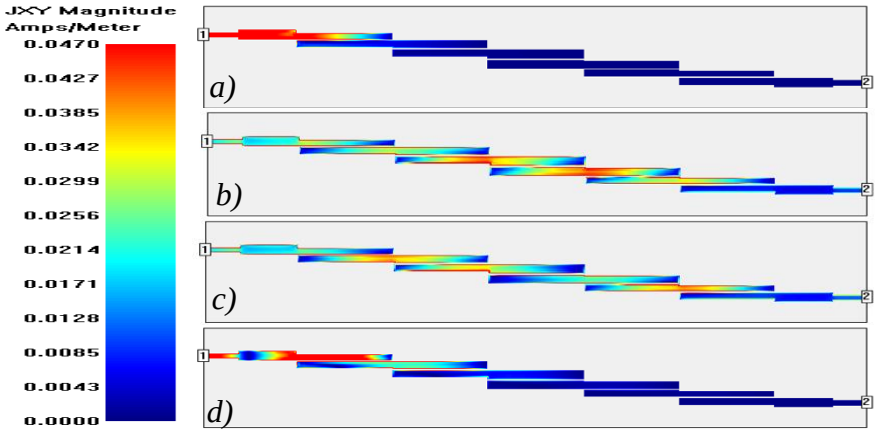

Figure 4-6. Surface current density distribution pattern over a frequency band, a) 0.01GHz, b) 1.35GHz, c) 1.44GHz and d) 1.98GH GHz. Current density shows the connectivity of a transmission line is restricted within passband only

Modelling data and results of bandpass microstrip filter by scattering matrix simulation approved the initial design. Parameters and dimensions updated as necessary. After that, the device can go through the manufacturing process.

4.6.2. Lowpass microstrip Chebyshev filter (2p)

Lowpass microstrip filter layout consists of seven cascaded microstrips golden patches connected directly: four capacitive and three inductive. Shown in figure (3-22). Overall dimensions of the filter are 89 mm length and 31 mm width. Feed lines length is 13.23mm.

Microstrips are placed on top of the FR-4 dielectric substrate. This microstrip of seven sections represents seven electrical components of the lowpass filter. Figure (4-7) showed a mesh pattern of a microstrip model.

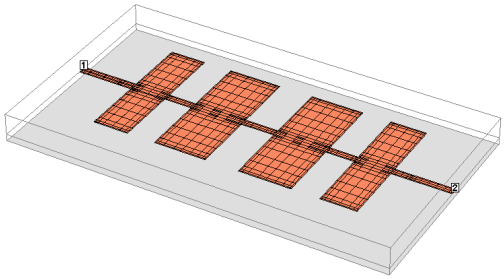

Figure 4-7. 3D mesh subsections of lowpass Chebyshev microstrip filter

Graphs of scattering parameters S_{12}, S_{21} are identical and reflection coefficients S_{11}, S_{22} are identical too due to shape symmetry, figure (4-8). Phases are shown in figure (4-9), typical responses of microstrip filter. Current density pattern showed in figure (4-10). Connection band has a high current density on a connection path between capacitive and inductive parts.

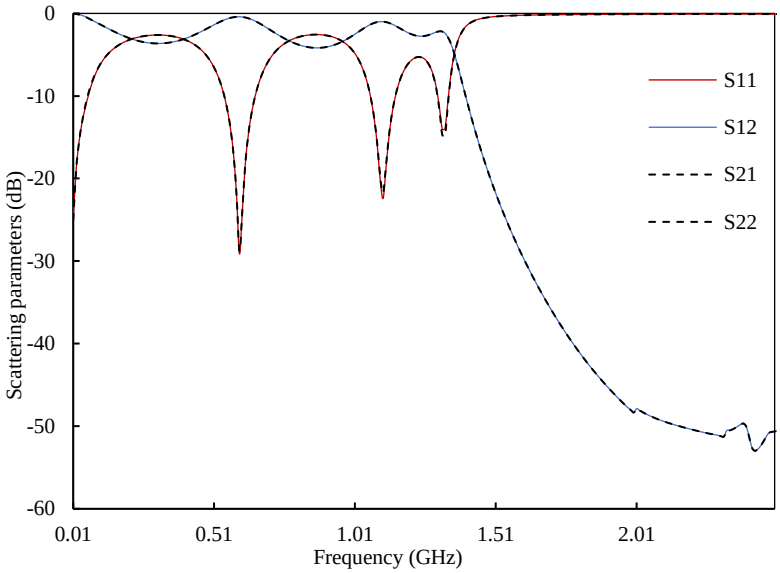

Figure 4-8. Scattering parameter S_{11}, S_{12}, S_{21} and S_{22} of lowpass Chebyshev microstrip filter on FR-4 substrate

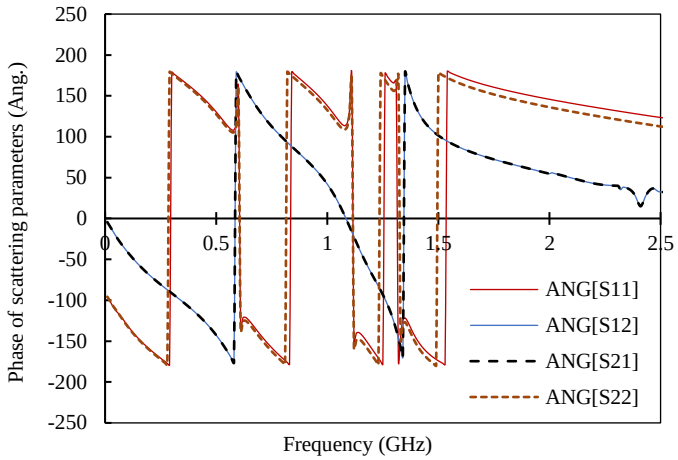

Figure 4-9. Phase of scattering parameter S_{11}, S_{12}, S_{21} and S_{22} of lowpass Chebyshev microstrip filter on FR-4 substrate

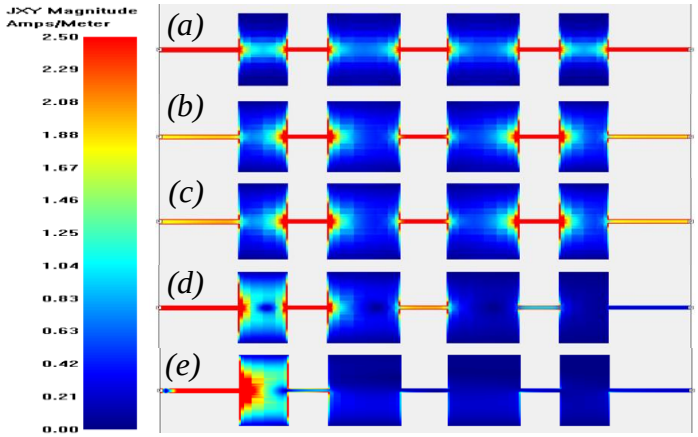

Figure 4-10. Surface current density distribution pattern over frequency passband and stopband, a) 0.051GHz, b) 1.1GHz, c) 1.38GHz, d) 1.55GH GHz and e)3GHz. Current density shows the regions that rich with fields.

Modelling performed over passband and stopband of lowpass microstrip Chebyshev filter. Scattering matrix simulation showed filter's responses are in a good agreement with initial design factors.

4.6.3. Lowpass microstrip Butterworth filter (3p)

Butterworth lowpass microstrip filter involves four components microstrip elements cascaded together. Overall dimensions of the filter are 81 mm length with feed lines and 20 mm width. Feed lines length is 5.8mm and 5.5mm respectively shown in figure (3-27). Microstrip filter consists of four components, two capacitive and two inductive. Besides, feed lines connected to the input port and output port. The modelled design is shown in figure (4-11).

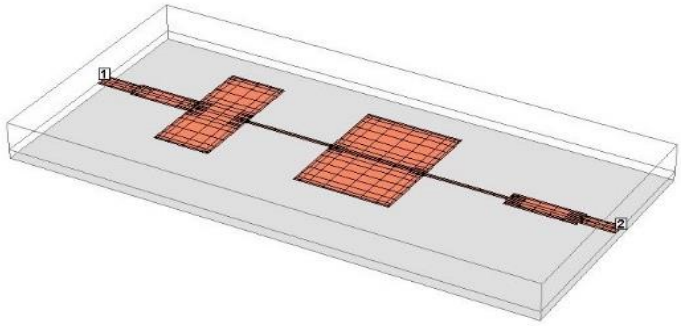

Figure 4-11. 3D mesh of lowpass Butterworth microstrip filter modelling

Scattering parameters S_{12}, S_{21}, S_{11} and S_{22} shown in figure (4-12). They represent designated response of the filter. Phases are shown in figure (4-13). Scattering parameters are according to design criteria. Current density pattern showed in figure (4-14). Passband had a high current density on capacitive part close to port one.

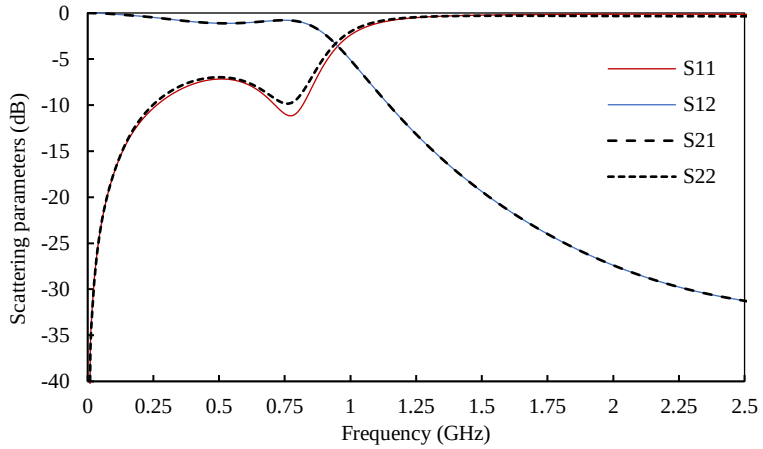

Figure 4-12. Scattering parameter S_{11}, S_{12}, S_{21} and S_{22} of lowpass Butterworth microstrip filter on FR-4 substrate

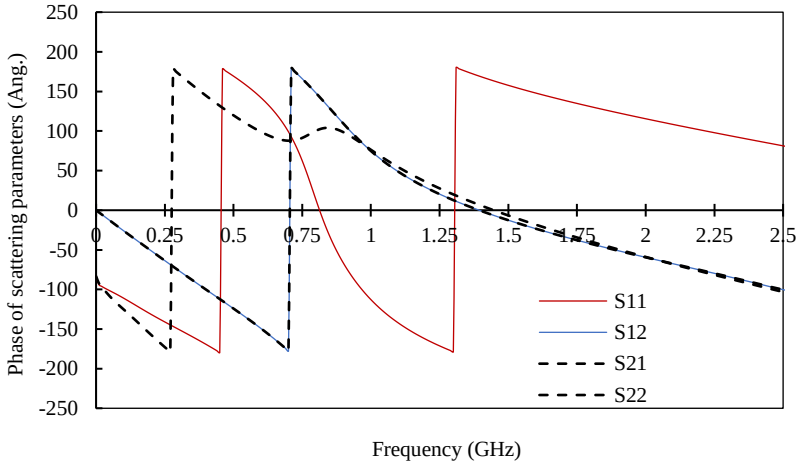

Figure 4-13. Phase of scattering parameter S_{11}, S_{12}, S_{21} and S_{22} of lowpass Butterworth microstrip filter on FR-4 substrate

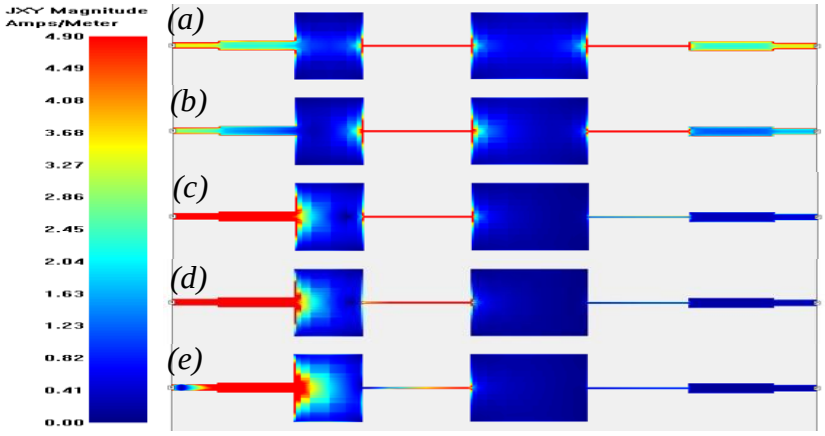

Figure 4-14. Surface current density distribution pattern over frequency passband and stopband, a) 0.01GHz, b) 0.55GHz, c) 1.55GHz, d) 1.88GH GHz and e) 3GHz. Current density shows the regions that rich with fields. These regions are more sensitive to surface changes.

Modelling performed over passband and stopband of lowpass microstrip Butterworth filter. Scattering matrix simulation confirmed filter's functionality under operational frequency. Results are according to design factors and dimensions. Subsequently, the device is prepared to manufacture.

4.7. Modelling of microstrip filter on quartz

Two microstrip filters on quartz dielectric substrate modelled by Sonnet Lite. Lowpass and V-shaped bandpass microstrip filter that has Chebyshev characteristic response. Modelling of microstrip Chebyshev filters on quartz completed. Resultants scattering matrix data showed filter functionality over operational frequencies. Results are in a good agreement with design criteria. Subsequently, it is possible to manufacture these microstrip filter.

4.7.1. Lowpass microstrip Chebyshev filter (4q)

Lowpass microstrip filter layout consists of five microstrips parts cascaded directly: three capacitive and two inductive. Feed lines added. Overall dimensions of the filter are 46.5 mm length and 19.6 mm width. Excluding Feed lines length of 13.23 mm. Figure (3-28). The modelled design is shown in figure (4-15).

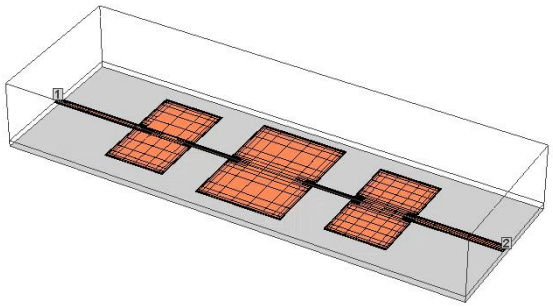

Figure 4-15. 3D geometry of Chebyshev lowpass microstrip filter

Analysis showed that scattering parameters S_{12} and S_{21} are identical and reflection coefficients S_{11} are S_{22} are not. These responses are shown in figure (4-16). This can explain by unequal length of feed lines from each port. Similar behaviour of phases shown in figure (4-17). Current density pattern showed in figure (4-18), current density pattern showed over a passband.

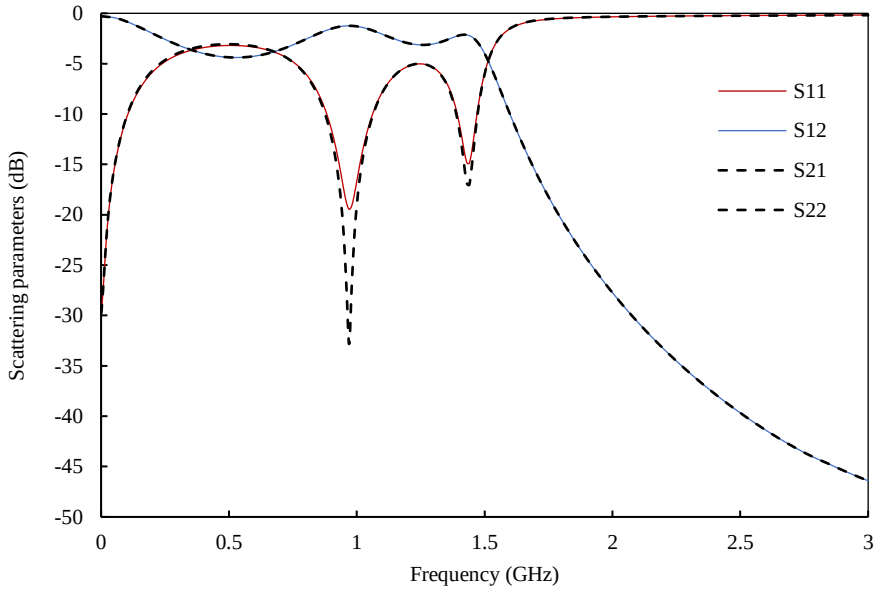

Figure 4-16. Scattering parameter S_{11}, S_{12}, S_{21} and S_{22} of lowpass Chebyshev microstrip filter on a quartz substrate

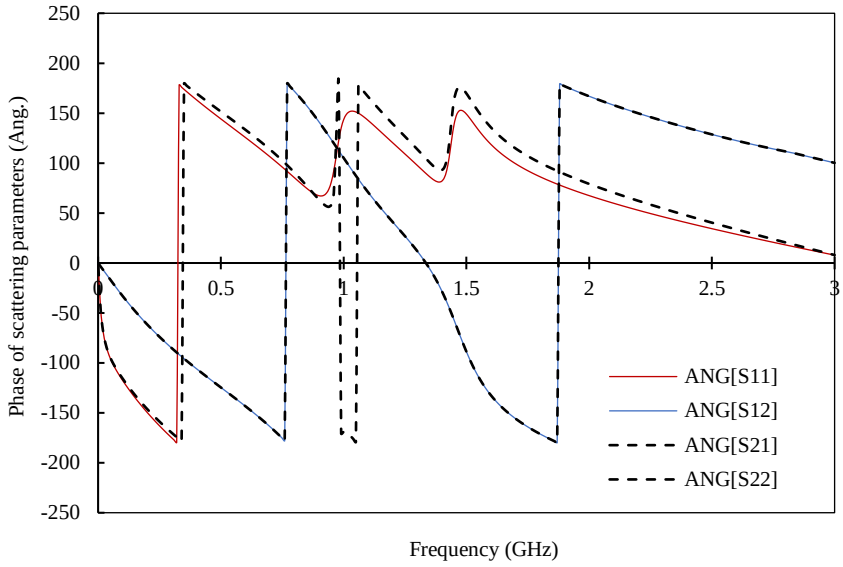

Figure 4-17. The phase of scattering parameter S_{11}, S_{12}, S_{21} and S_{22} of lowpass Chebyshev microstrip filter on a quartz substrate

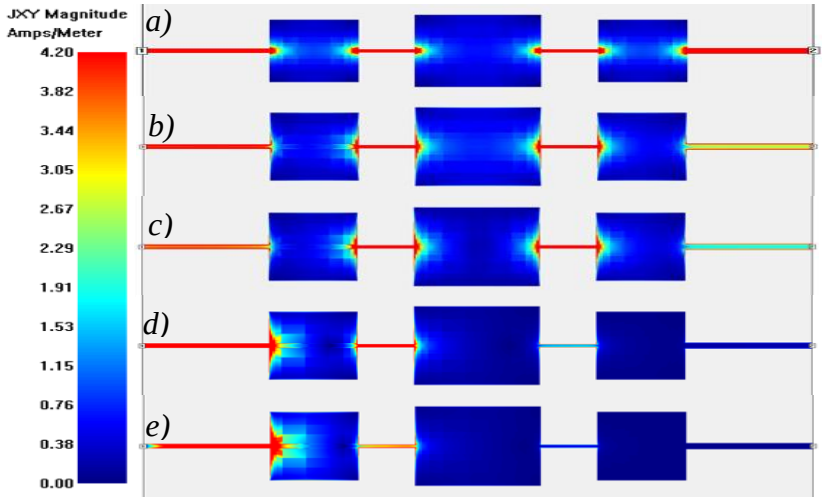

Figure 4-18. Surface current density distribution pattern over frequency passband and stopband, a) 0.001GHz, b) 0.97GHz, c) 1.43GHz, d) 2.1GH GHz and e) 3GHz. Current density shows the connectivity of a transmission line is restricted within passband only. Besides, it shows the regions that rich with fields. These regions are more sensitive to surface changes

4.7.2. V-shaped Bandpass microstrip Chebyshev filter (5q)

An attempt made to design a V-shaped bandpass microstrip filter by vertical rotation around the central line of coupled microstrip filter. Benefited from two symmetrical sides of microstrip, as shown in figure (3-35). This design reduces microstrip length by half and size will be compacted. The feature of compactness is advantageous in different applications.

V-shaped bandpass microstrip filter layout consists of six edge-coupled microstrip resonators separated by constant spaces of micro gaps. Overall dimensions of the filter are 59.6

mm length and 18.9 mm width. Gaps between microstrips are made to be 1 mm to the adequate mask fabrication process. Feed lines dimensions are 4.5×5mm, figure (3-29).

A model showed in figure (4-19). Metallic microstrip thickness is 350 nm. Substrate dielectric is flat quartz of 1mm height. A frequency band is 3 GHz, the filter centre frequency is 2 GHz. Gold is used to form both top microstrip layer and ground bottom layer with the same thickness of 350 nm. Spaces width among microstrips are increased to 1 mm to compile with laser machining of the mask due to manufacturing limits.

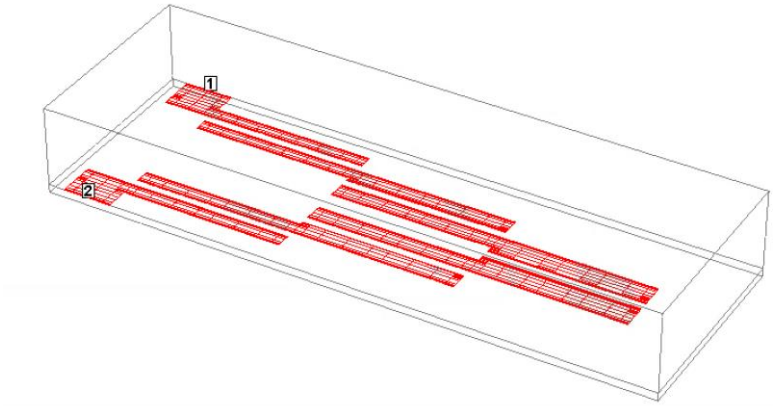

Figure 4-19. 3D modelling configuration of V-shaped bandpass microstrip filter

Responses of V-shaped microstrip filter are in good operational shape except passband attenuation is around -10 dB, figure (4-20). Therefore, it is possible to use it as a reduced size biosensor. Phases are shown in figure (4-21). Current density distribution at passband shown in figure (4-22). Give the possibility to use any part of the rich fields' surface.

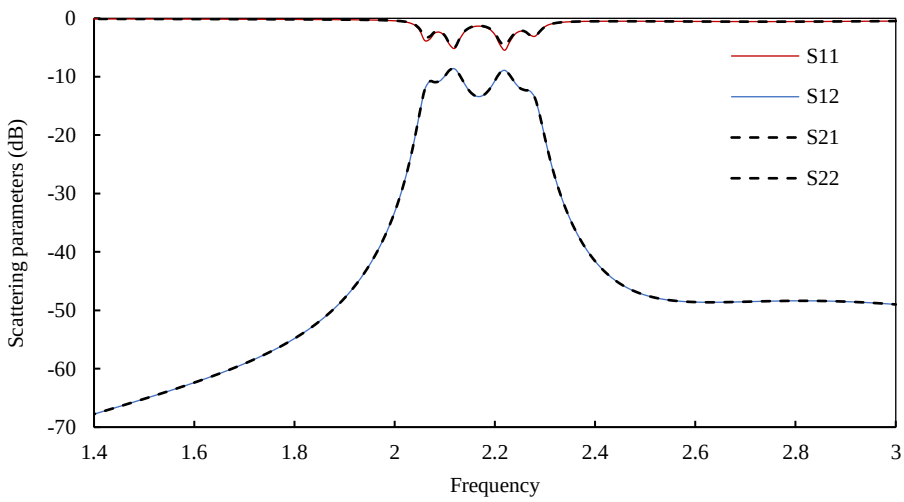

Figure 4-20. Scattering parameter S_{11}, S_{12}, S_{21} and S_{22} of V-shaped bandpass Chebyshev microstrip filter on the quartz substrate

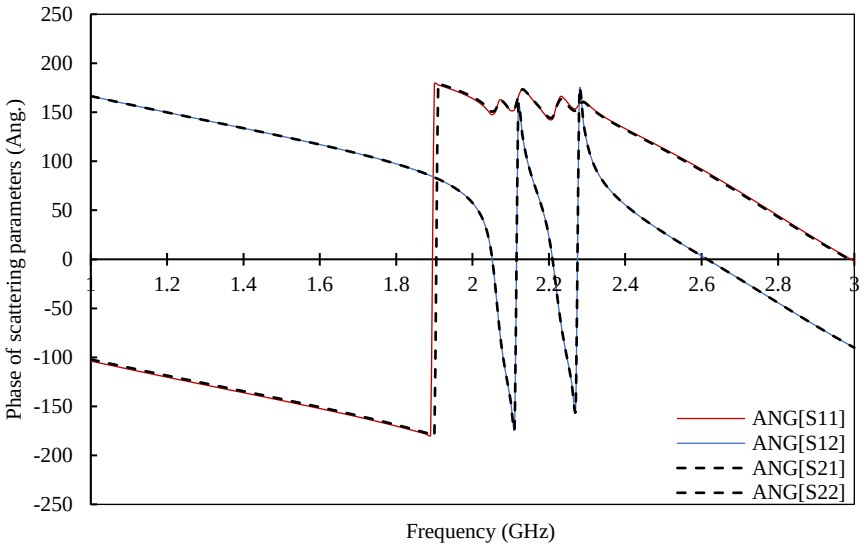

Figure 4-21. The phase of scattering parameter S_{11}, S_{12}, S_{21} and S_{22} of bandpass Chebyshev V-shaped microstrip filter on quartz substrate

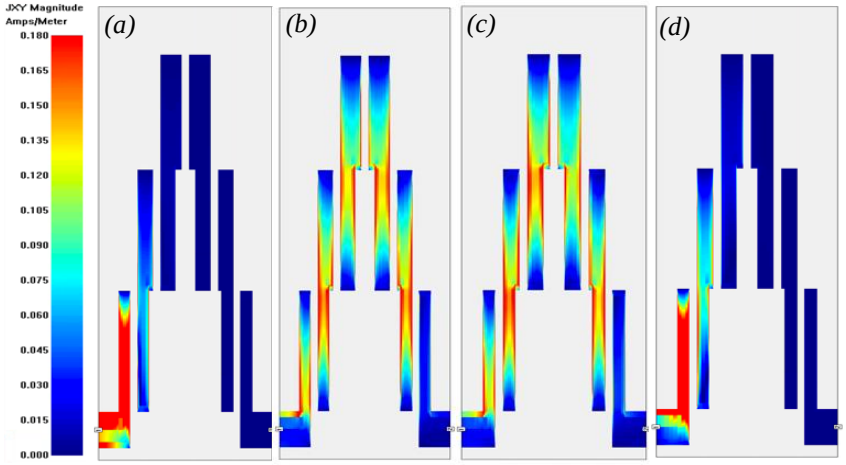

Figure 4-22. Surface current density distribution over frequency passband and stopband, a) 1.6 GHz, b) 2.01 GHz, c) GHz, and d) 2.6GH GHz. Current density shows the regions that rich with field. These regions are more sensitive to surface changes.

Increased spaces of V-shaped microstrip filter influenced performance over an operational frequency band. However, the modelled filter showed good functionality and responses to a potential microstrip filter.

4.8. Modelling of reduced size microstrip filters

Reduced size microstrip filters modelled by Ansys HFSS package software. Ansys provides more flexibility and consistency over higher frequencies and complex geometry. ANSYS HFSS simulation suite has mesh automation property yielding precise accuracy towards high-frequency simulations. Modelling parameters setting is 350 nm for metal thickness. This

thickness is practised to the top and bottom ground layers. Proposed metal is gold. The dielectric substrate is flat quartz of 250 μm thickness. An applied frequency band is 1-30 GHz because of designed frequencies of submitted microstrip filters are over 15 GHz. Additionally, submitted geometry of microstrip filters.

4.8.1. Bandpass microstrip Chebyshev filter (6q)

Previously designed geometry shown in figure (3-30), submitted to Ansys software simulator. Dimensions of reduced size bandpass microstrip filter are 4.66 ×11.08mm×350nm. Height is equal to a quartz substrate thickness of 250 μm. Modelling results are in good agreement with design criteria, central frequency is 16GHz, the passband is 8GHz, and passband attenuation is 4dB. Scattering parameters and phases are shown in figures 24 and 25 respectively.

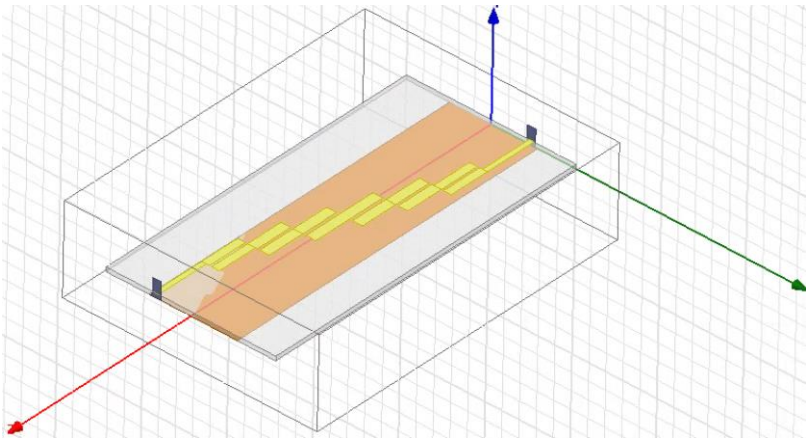

Figure 4-23. General modelling configuration of reduced size bandpass microstrip on quartz

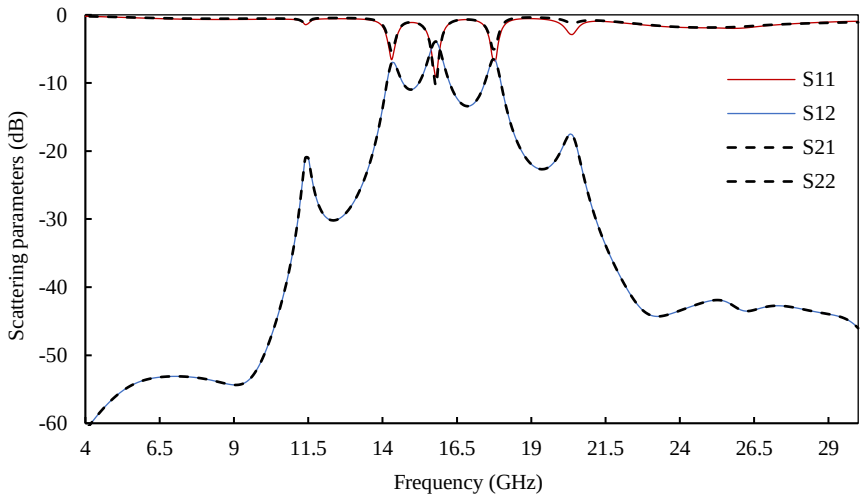

Figure 4-24. Scattering parameter S_{11}, S_{12}, S_{21} and S_{22} of reduced size bandpass Chebyshev microstrip filter on quartz substrate

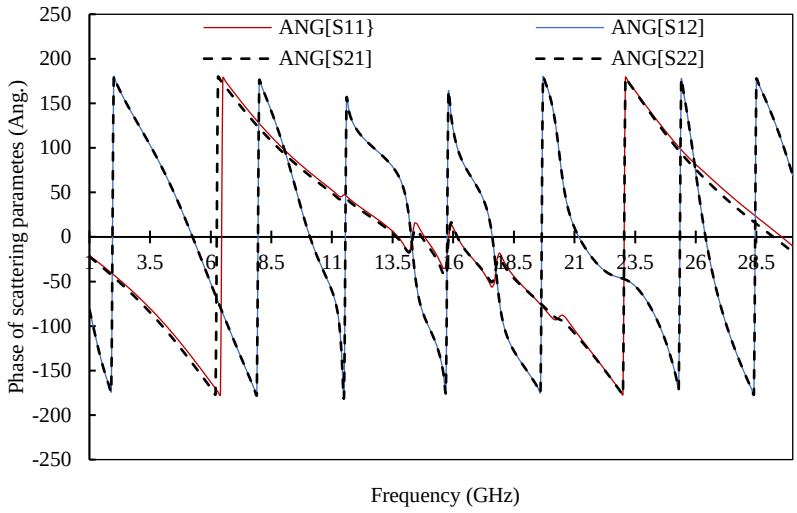

Figure 4-25. Phase of scattering parameter S_{11}, S_{12}, S_{21} and S_{22} of reduced size bandpass Chebyshev microstrip filter

4.8.2. Reduced size lowpass microstrip Chebyshev filter on quartz (7q)

Two models of reduced size lowpass microstrip filter are designed depending on ground layer architecture. Ground layers designs are a wide and narrow plate under microstrip of feed lines; the purpose is to investigate appropriate size reduction.

4.8.3. Lowpass microstrip Chebyshev filter on 2 mm width ground layer

Reduced size lowpass microstrip filter is designed previously, figure (3-31), the dielectric substrate is quartz and microstrips is covered by gold. Dimensions are 7x1.68mm, and thickness is equal to 350nm, height is 250 µm.

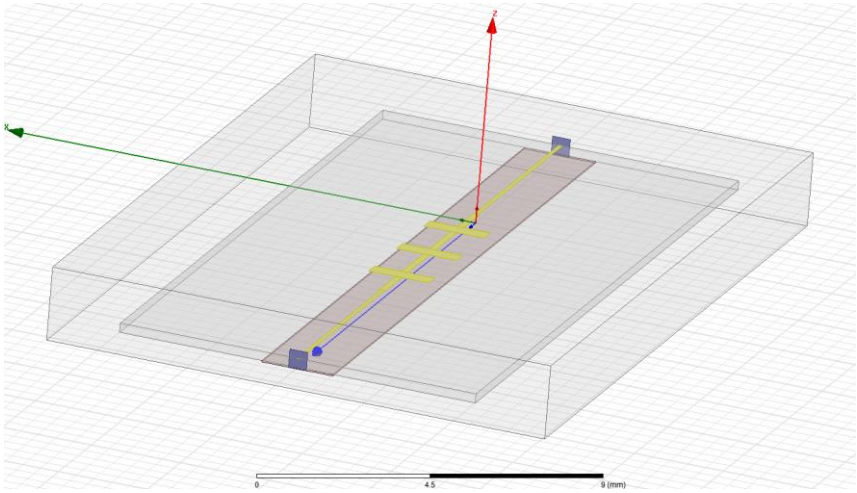

Figure 4-26. Reduced size lowpass microstrip Chebyshev filter on 2 mm width ground layer

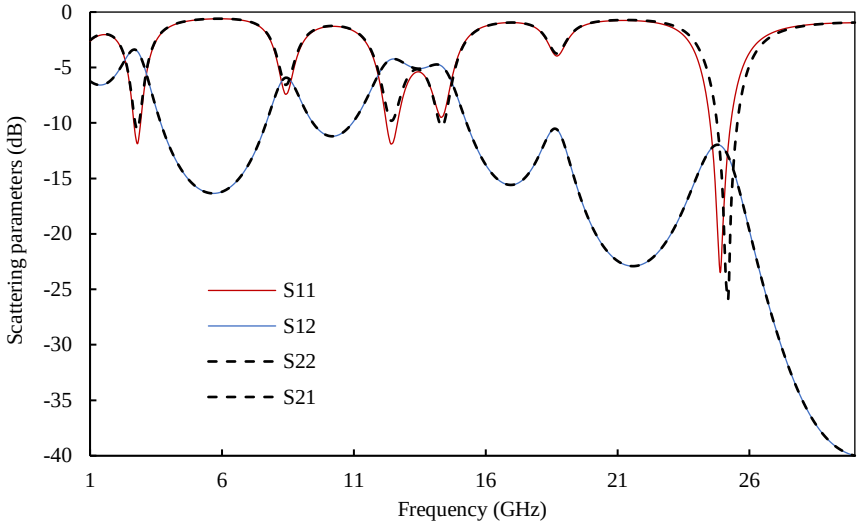

Figure 4-27. Scattering parameter S_{11}, S_{12}, S_{21} and S_{22} of reduced size lowpass Chebyshev microstrip filter

Collected data of modelling, figure (4-27) of scattering parameters and figure (2-28) of phases responses. Results showed good responses of this device over the selected operational frequency band. No modification made to microstrips dimensions.

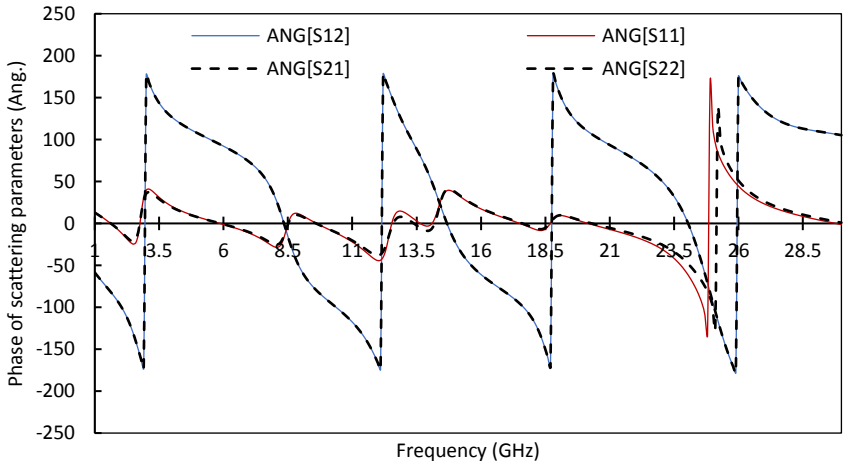

Figure 4-28. Phase of scattering parameter S_{11}, S_{12}, S_{21} and S_{22} of reduced size lowpass Chebyshev microstrip filter

4.8.4. Lowpass microstrip Chebyshev filter with narrow ground layer feed lines

The second version of reduced size lowpass microstrip filter, a ground layer below feed lines narrowed to be identical in width with microstrip feed lines, while original dimensions of

microstrip filter ground layer preserved as shown in figure (4-29). The purpose of this design is to reduce fabrication cost and signal disturbance. Results from the modelled device are approximately identical with the first design.

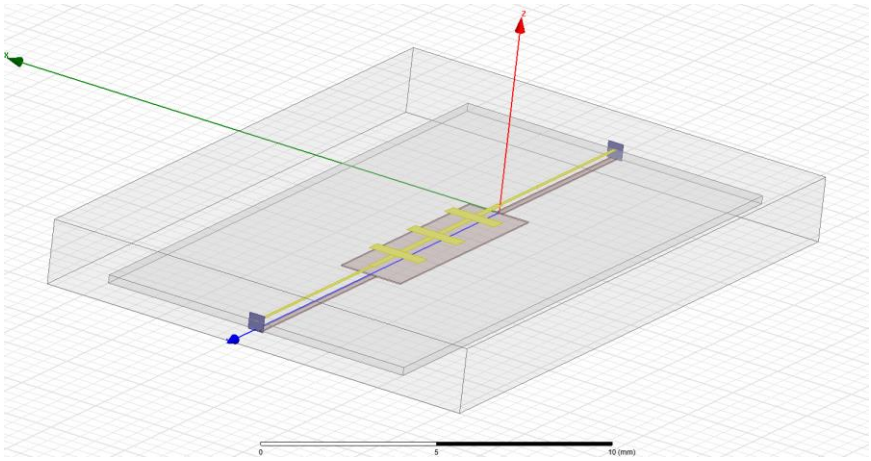

Figure 4-29. Architecture of reduced size lowpass microstrip filter
of narrow ground under feedlines

Reduced size versions of microstrip filters showed good responsive results over operational frequencies. Despite reduced size, microstrip filters showed good functionality according to design criteria. Results corresponding to cut-off frequency are within expected values. Modelling is indicating they will be correct functioning when fabricated.

4.9. Summary of microstrip filters modelling chapter

In this chapter, microstrip filters modelling is achieved, and their characteristic responses were found to be as projected in the design chapter. Before the fabrication step, the designed microstrip filters that have presented in chapter 3 were modelled and analysed in this chapter by finite elements electromagnetic method. The modelling programmes are Sonnet Lite electromagnetic simulator and Ansys HFSS package. Ansys was used to analyse the V-shaped and reduced size microstrip filters only. Scattering matrix is used to characterise microstrip filters in the modelling process. Also, current patterns extracted in order to recognise regions of rich current density, and they represent high sensitivity regions for the biosensing process.

The modelling results and responses all agreed with the design criteria of microstrip filters. However, appropriate adjustment to some dimensions made, modelled and analysed. Modelling results were within the selected design parameters and specifications. Therefore, the

microstrip filters preserved their original responses over the desired frequency band as such; the designed devices were approved to meet design requirements.

Depending on the obtained results from electromagnetic simulators, all microstrip filters designs can be used in later stages of the research. At this level, microstrip filters were modelled and proved; they will be fabricated before integrating them with microfluidic to build a microstrip-based biosensor. The fabricated microstrip filter based biosensor will be tested in a biomedical experiment to detect PSA analyte.

Chapter 5 Microstrip filters fabrication, verification and biosensor assembly

5.1 Introduction

Design and modelling processes of microstrip filters explained in chapters three and four respectively. This chapter is committed for fabrication processes of previously designed and modelled microstrip filters. In addition to fabrication and verification of microstrip filters, fabrication of microchambers and biosensors assembly described in this chapter. Utilised fabrication techniques introduced and explained.

The designed models were appropriately prepared to meet manufacturer's requirements and tolerance. The employed manufacturing techniques can be classified into two categories, printed circuit board and clean room evaporation process. Fabrication method selection depends on the dimensions and size of each device. Regarding the materials of microstrip filters and microfluidic, the selection process of materials depends on their electrical properties and their suitability for healthcare application. More importantly, they are biocompatible and convenient to biochemical functionalisation protocols.

Afterwards, fabricated microstrip filters undergo a verification process by vector network analysers. Obtained results of microstrip filters' responses showed a good match with modelled designs. Besides, the microfluidic and microchambers designed, fabricated and integrated with microstrip filters. Finally, biosensors constructed and ready to examine experimentally.

5.2 Materials of microstrip filters and biosensors

5.2.1 Metals

Gold is an ideal metal for microstrip filter based biosensors due to its outstanding biocompatibility. Gold is suitable to perform chemical and biological functions with biological cells and tissues without affecting them or provokes changes, as previously mentioned in the design chapter. Although gold is an inert element, it might affect by buffers and de-attached from the dielectric substrate surface. Therefore, in addition to pure gold (Au), metals like nickel (Ni), titanium (Ti) and copper (Cu) used with gold to form the top and ground bottom layers to prevent gold removal. A very thin layer of titanium is used to conserve gold persistence on quartz and avoid gold breakdown due to biochemical solutions in functionalising and testing biosensor procedures. Cracking of gold layer over quartz surface cause failure of bio-detecting setup and devices. However, gold is suitable for immobilisation of proposed biochemical protocols in this proposed research. Additionally, gold has excellent chemical resistance, and it is a non-reactive element with applied biochemical.

5.2.2 Polymethyl methacrylate (PMMA)

Polymethyl methacrylate (PMMA), trade names of it are Plexiglas. Perspex or acrylic used to fabricate microchannel and microfluidic of the biosensor, it is also used to fabricate microstrip jigs. PMMA is selected because it is thermoplastic, robust and transparent. It has suitable mechanical properties and machinability, and it is accessible by laser machining. PMMA is integrated with microstrip filters utilising adhesive tape. PMMA machining and application can be completed with ease; it is presenting no fabrication difficulties or complicated tools.

5.2.3 Dielectric substrate

Dielectric substrate materials selected depending on their relative properties. Electric and thermal stability in addition to the economic factor. Two types used, quartz and FR-4.

Quartz (SiO_2) substrate

Quartz is an excellent insulator, and it selected as a dielectric substrate due to it is low permittivity, low thermal expansion, and stability of frequency over temperature, inert to chemicals and has flat well-polished surfaces. Quartz tiles used in this study supplied by PI-KEM Co. and their properties are shown in the table (5-1). Quartz illustrated in section 3.2.2.

Table 5-1, Properties of quartz thin tiles employed in this research

Dimensions	20 mm×10 mm×250 µm
Orientation	random
Polished	2 sides
Colour	clear

FR-4 dielectric

FR-4 is a fire-retardant epoxy resin; it has excellent heat resistant; its good mechanical properties support suspended microstrip metal layer and microfluidic on it. FR-4 is supplied directly by the manufacturer. FR-4 explained in chapter three, section 3.2.2.

5.2.4 Adhesive and tapes

Epoxy liquid glue is first applied. Therefore, double-sided adhesive tape consists of thin film foam of approximate thickness equal to 100 µm and 25.4 mm width used to attach microchannel and microfluidic with microstrip filter. Cold bonding provided by tape prevent the use of mixed epoxy glue and maintained microchannel from being blocked by spread liquid glue Hence, epoxy glue slides to channel before it solidifies due to the pressure of channel weight and aqueous state of glue. Adhesive tape paste state preserved microchannel boundaries in high precision. Double-sided tapes products made in several thicknesses and adhesives types, both

sides of the tape are well protected by special paper. Moreover, double-sided tapes can cut by laser, and they have excellent thermal and chemical resistance.

5.3 Manufacturing of microstrip filters by PCB method

Designs of three microstrip filters are sent to Faraday Printed Circuits Co. for fabrication. They are two lowpass and one bandpass microstrip filters. A 10 μm nickel/gold metal layer is patterned on the front surface to construct the filter geometry with a continuous metal backplane on the rear of the 1.6 mm FR-4 dielectric substrate. A solder resists layer placed on the backside ground plane. However, gold on the front surface is left exposed to allow for microfluidic and biochemical functionalization, footprints of designs drawings made by Autodesk invertor. 3D footprints of build-up layers are shown in figure (5-1). Files transferred to a (dxf) file format.

Converted and edited by layout editor which is a design software. Transferred to a Gerber file format and viewed and checked by GC-prevue programme before sending them to the manufacturer.

Figure 5-1. Schematic illustration of build-up PCB layers to construct microstrip filter

Three microstrip filters made by PCB standard technology, filters are Chebyshev bandpass microstrip filter (denoted by 1p), Chebyshev lowpass microstrip filter (denoted by 2p) and Butterworth lowpass microstrip filter (denoted by 3p). Fabricated devices and their rectangular architecture shown in figure (5-2), the top golden layer is left free.

Once fabricated, SMA connectors soldered to the PCB microstrips filters terminal ports in order to connect to VNA.

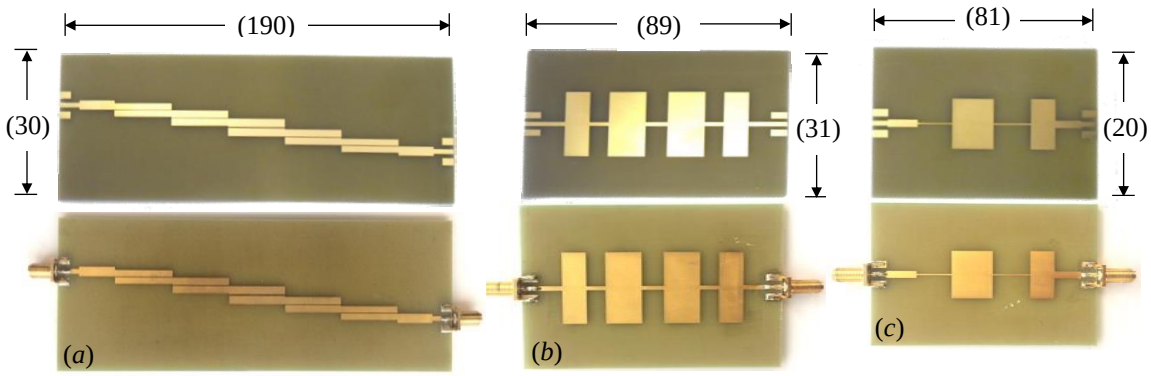

Figure 5-2. Fabricated microstrip filters, *a)* 1p, *b)* 2p and *c)* 3p without and with SMA connectors attached, dimensions are in millimeter.

5.4 Shadow mask

5.4.1 Shadow masks ofminiaturisd microstrip filters

Shadow masks designs sent to Fotofab Co. This company supplies photochemically machined metal sheet components and masks. Mask made by a photolithographic process of chemical etching. This method provides quick production of the required parts, ease of repeatability of the fabrication process, inexpensive prices in comparison to other mask production methods and a high number of patterns per sheet. Regarding shadow mask design, a soft copy of mask drew by Autodesk inventor and transferred to a Gerber file format. Final copy sent to the company; more than one design distributed in one sheet area as shown in figure (5-3). Shadow mask thickness is 100 µm, two shadow masks designed and fabricated to cover top and bottom sides of quartz sheet in order to produce complete microstrip filter. Steel shadow masks made for reduced size bandpass microstrip filter (5q) and lowpass microstrip filter (6q).

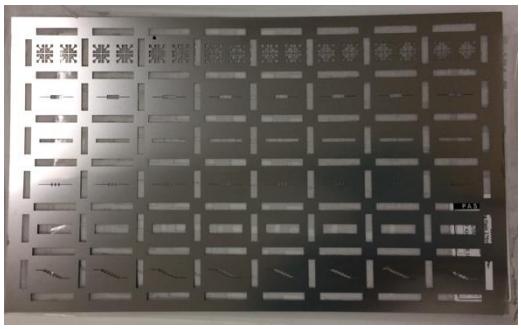

Figure 5-3. Steel sheet of shadow masks.

5.4.2 Preparation of reduced size microstrip filters

Regarding reduced size microstrip filters evaporation, quartz tiles of 250 µm thick and 10×20 mm sandwiched between two shadow masks of microstrip mould and ground layer. The top mask represents microstrip patterns, and the bottom layer represents the ground layer. A

sandwiched group mounted on an acrylic rectangular frame holder of 5mm height, and 2.5 mm thick, holders attached to open windows on a circular jig, a jig made of transparent PMMA disk of 150 mm diameter, disk supplied with rectangular windows to allow evaporation over quartz surface from both sides. Disk carries eleven holders of microstrip filters. The double-sided tape used to put all parts together started with a shadow mask to frame and ended by attaching frames to disk. A rectangular frame, shadow mask on quartz, jig disk and samples attached to it shown in figure (5-4).

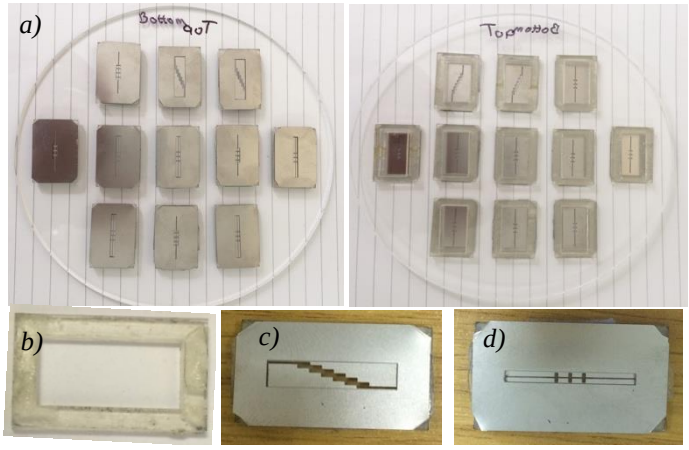

Figure 5-4. Prepared patterns and Jig of the reduced size microstrip filters, a) top and bottom layers of the disk, disk diameter is 150 mm, b) holders and c) bandpass filter masks, d) lowpass filter mask. Holder and masks dimensions are 20 × 10 mm.

5.4.3 Shadow mask of V-shaped bandpass and cascaded lowpass microstrip filters

PMMA Disk of diameter is designed to embody the shadow mask of V-shaped bandpass and lowpass Chebyshev microstrip filters. Moreover, Disk has another function; it services as a jig to hold samples during the evaporation process. A disk made by laser machining. PMMA disk embraces two designs, and they are V-shaped bandpass and lowpass Chebyshev microstrip filters (4q and 5q). Disk diameter is 150mm and its height equal to 3mm. Dielectric substrates of these microstrip filters are a 100 µm thick quartz tiles, dimensions of quartz tile are 20×75×1 mm. Laser machining used to cut mask patterns on the disk. Jig disk can carry five patterns only of microstrip filters as shown in figure (5-5). Small pieces of double-sided tape used to mount quartz piles on disks directly.

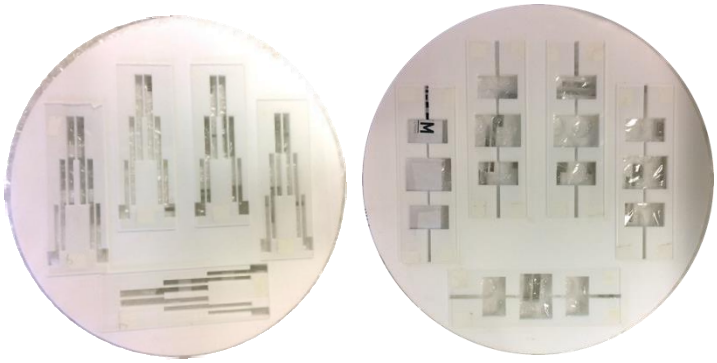

Figure 5-5. Disk jig of V-shaped and lowpass 3GHz microstrip filters with quartz tiles attached, disk diameter is equal to 150 mm and thickness is 5mm.

A slight increment made in spaces between microstrip resonators of V-shaped microstrip filters pattern. Mask adjusted because of machining tolerance. Laser machine had one beam radius. For original spaces, they either be bend or melted by laser beam because the laser beam is wider than the spaces. Therefore, spaces distance increased to avoid this problem. Dimension change modelled, and approximate original responses maintained. Increased dimension has an insignificant influence on the filter's performance and characteristic response.

5.4.4 Evaporation mechanism

The evaporation process made by INEX MICRO Co., metals deposited on a quartz substrate through a shadow mask in a controlled clean room. Deposition made by an evaporated metal beam from a pure metallic chip. Evaporated metals coated entire jigs surface area. Top and bottom layers of the microstrip patterns first coated by 50 nm titanium layer. Afterwards, gold deposited on titanium and created a layer of 300 nm thickness. The final thickness of microstrips is 350 nm, same thickness for the ground layer. These two layers of metals formed microstrip filters shapes. Therefore, three dimensions physical shapes of microstrip filters accomplished. In order to realise microstrip filters, shadow masks are lift-off from evaporated samples. Microstrip filters prepared for a verification process. Figure (5-6) showed fabrication steps of reduced size microstrip filters (6q and 7q). Sample preparation started by fastening masks on quartz, attached to jigs, evaporated and released to obtain the final product.

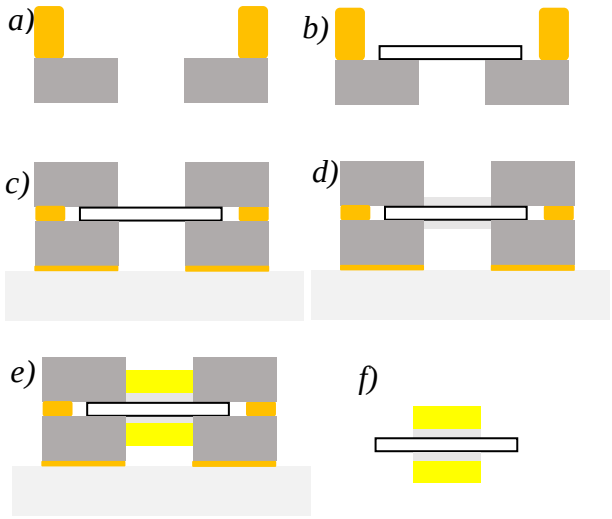

Figure 5-6. Illustration of preparing steps of the masks on the quartz and evaporation process stages for the reduced size microstrip filters, first a) adhesive type applied on bottom mask, then b) quartz aligned, c) top mask added, d) masked e) quartz attached to square frame and jig, *f*) evaporated and microstrip filter realised.

In terms of V-shaped bandpass and lowpass microstrip filters on a quartz substrate (4q and 5q), quartz tiles of 1mm thickness and area of 20×75 mm mounted directly on the 5 mm thick disk jig by double-sided tape from corners of quartz pieces. The top layer of microstrip filters is shaped on the plastic jig. Simultaneously, the jig is working as a holder and shadow mask. Therefore, the ground bottom layer is left uncovered to keep it in total exposure to evaporated atoms. Preparation configuration illustrated in sketches of the figure (5-7). First, quartz tiles attached to jig disk, exposure to gold and de-attached from jig to realise microstrip filters.

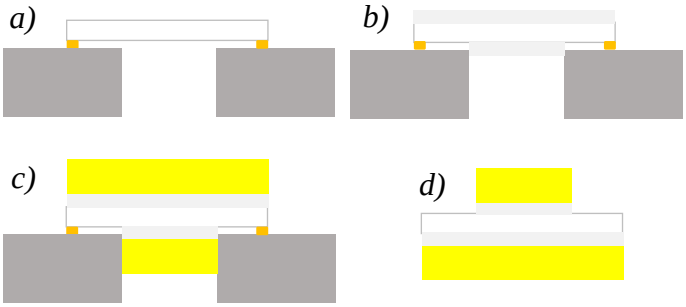

Figure 5-7. Preparing steps of the masks and evaporation process stages for V-shaped and lowpass 3GHz microstrip filters, a) quartz aligned to adhesive tape on a bottom mask, b) first metal layer deposited, c) second metal layer deposited and d) final device layers.

Evaporated jigs surface covered by deposited gold as shown in figure (5-8). A careful handle is made to de-attached samples from disks and preparing them due to the fragile nature of thin quartz tiles.

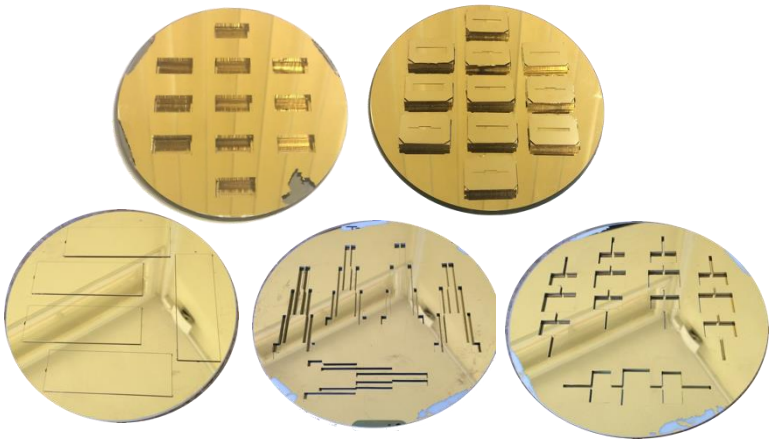

Figure 5-8. Evaporated disk jigs covered with gold, disks diameter is 150 mm, and disks thickness is 5 mm.

Fabricated reduced size edge coupled bandpass (6q), lowpass (5q), lowpass and V-shaped bandpass microstrip filters shown in figure (5-9). Grey colour belongs to titanium layer on the ground of microstrip filters.

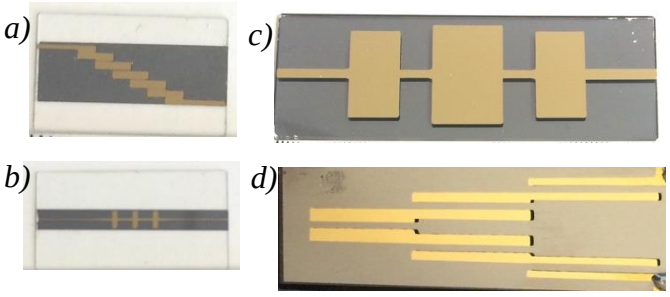

Figure 5-9. Fabricated microstrip filters by an evaporation process. *a)* Reduced size bandpass microstrip filter 11×4.66 mm, *b)* Reduced size lowpass microstrip filter 7.3×1.6mm, *c)* Lowpass microstrip filter 75×19.6 mm, *d)* V-shaped bandpass microstrip filter 25×64.8 mm.

5.5 Measurement jigs

Microstrip filters made on a quartz substrate are very thin, 250 µm and 1mm of thickness. They breakable due to mechanical stress by manual handling, preparing, VNA cables connection and movements during testing. In addition, soldering might fracture and de-attached because of

mechanical forces. Therefore, a plastic jig designed and constructed from 5mm thick Plexiglas to hold microstrip filters in a constant fixture. Jig prevents crack and fracture problem. Jig dimensions are compatible with microstrip filters. Also, the jig has rigid holders for SMA connectors against connecting and disconnect of cables. Reduced size microstrip filters have an adjustable jig due to their reduced size: soldering configuration and SMA connector's lengths. The jig can be adjusted according to these factors to realise the best fitting of the device. Jigs have windows in their base layer to facilitate the grounding soldering work. Jig also provides physical protection for the microstrip filters inside it before and during measurements.

Assembling practice involves microstrip, SMA connectors and jigs. There are no other complex components. SMA connectors are soldered manually to the feed lines and dedicated pads by solder joints over feed lines to supply power to the transmission line. They are keeping exposed microstrip surface unaffected. Jigs provided necessary protection while soldering SMA connectors to microstrip filters as shown in figure (5-10) showed fabricated jigs, one of them are holding microstrip filters.

Figure 5-10. Jigs of fabricated microstrip filters.

5.6 VNA measurements

In terms of transmission network analysis and verification, a vector network analyser (VNA) used. A network analyser is an instrument produces radio frequency sinusoidal signals that propagate into the network under test, it measures input and output signals. Amplitude and phase of a backward signal from the network to the analyser are dissimilar to forward signal from analyser to network. A network analyser measures response of the network to these applied signals. Signals differences used to characterise and analyse microstrip filter. Hence, phase and amplitude of both incident and reflected waves can be measured. VNA performs two ports or one port analysis. Resultant data from VNA is frequency domain, and it is transformable to a time domain data. VNA uses the scattering matrix to define microstrips electromagnetic characteristics. Two ports configuration identical to modelling configuration imposed in the experiment. Two types of two ports VNA models are used individually in the

characterisation process of scattering parameters. They are Rohde & Schwarz ZVL and Agilent PNR analysers.

5.6.1 Rohde & Schwarz analyser

Rohde & Schwarz analyser shown in figure (5-11). This machine has an operational frequency band from 9 KHz to 3GHz, dynamic range up to 140dB, extreme measurement speed, temperature stability and high precision. Also, speed synthesisers for measurement of high speed. This model is used to characterise S-matrix of microstrip filters on FR-4 (denoted by 1p, 2p, 3p) and on a quartz substrate (denoted by 4q and 5) respectively and operate within the range of the 3GHz band. Calibration set a number of points depending on measurement type.

Figure 5-11. Rohde & Schwarz network analyser,
frequency range from 9 kHz to 3GHz.

5.6.2 Agilent E8363b PNR analyser

Agilent E8363b PNR analyser showed in figure (5-12), is a general use instrument and has a programmability property to be customised for the applications. Operational frequency is 10 MHz to 40 GHz, 110 dB of dynamic range. This machine is used to characterise S-matrix of reduced size microstrip filters on a quartz substrate (denoted by 6q and 7q). They are Chebyshev bandpass, and lowpass microstrip filters and their operating frequencies are over 16 GHz and up to 26 GHz.

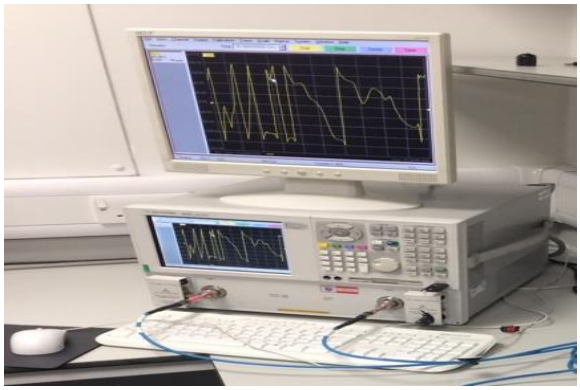

Figure 5-12. Agilent PNR analyser, frequency range is up to 40GHz.

Moreover, trace data of scattering parameters produced by VNA can be saved and exported in the form of plain text format of an ASCII file and PNR format. Thus, further post-processing calculations and analysis by external application. Such as MATLAB analysis and plotting, an external USB memory drive is used to data transfer purpose.

5.6.3 VNA Calibration

Regarding de-embedding measurements, and prior to using VNA instruments for microstrip filters characterisation, VNAs are calibrated to manufacturer's specifications. Calibration can mathematically eliminate and correct potential measurements errors during the test, removing unnecessary signals, especially from the connecting cables between instrument ports and microstrip filters ports. Therefore, enhance measurement accuracy of scattering parameters, calibration completed in room temperature. VNAs calibrated by the method of Through, Open, Short, and Match standards (TOSM).

In addition, measurement inaccuracies due to hardware imperfections, setup problems, cables errors and measurement uncertainty. These errors might not be possible to remove.

5.6.3.1 Calibration setup of Rohde & Schwarz ZVL analyser

Two ports manual calibrating method is applied by using mechanical calibration kit shown in figure (5-13), in addition to calibration software wizard. Before the calibration process, many parameters need to be set. They are the number of scanned points, required power, type of measurement, start, stop and central frequencies. First, select cables type from the calibration wizard. Then, each port is directly connected and calibrated with "single-Through" kit consists of open, short, match and then across (thru) common case, are the two ports connected to calibration kit at the same time. The selected power level is -10 dBm (0.1 mW) to avoid thermal stress of samples. Standard impedance is 50 Ω for ports. Cables and calibration kit.

Figure 5-13. Standard mechanical calibration kit of R&S VNA.

5.6.3.2 Calibration setup of Agilent PNA

PNA calibrated by two methods, electronic and manual (mechanical). Electronic and mechanical calibration kits shown in figure (5-14). A calibration method is similar to previously mentioned one; open, short, load and a direct connection or thru between two ports. Calibration frequency is from 1 to 26 GHz, power is equal to -17 dBm, and impedance is 50 Ω.

Figure 5-14. Standard mechanical and electronic calibration kits for Agilent PNA.

VNA is efficiently calibrated to measure S-matrix. Although, there is a calibration problem with the analyser. In order to connect cables to devices and calibration kit, an adaptor needed as shown in figure (5-15). After calibration and adaptor kept connected to the cable of port one. Deformed dip signal occurs in the reflected wave at frequency 21 GHz, removing the adaptor cause dip disappearing. Figure (5-15) showing a cable with and without the adaptor. This problem might be due to that a connector's length is compatible with wavelength at this frequency and cause response change. More than one connector is tested, and all of them showed the same problem. Signal dip due to connector appeared at frequency 21 GHz is showed in figure (5-16).

Figure 5-15. VNA Cable with and without a connector.

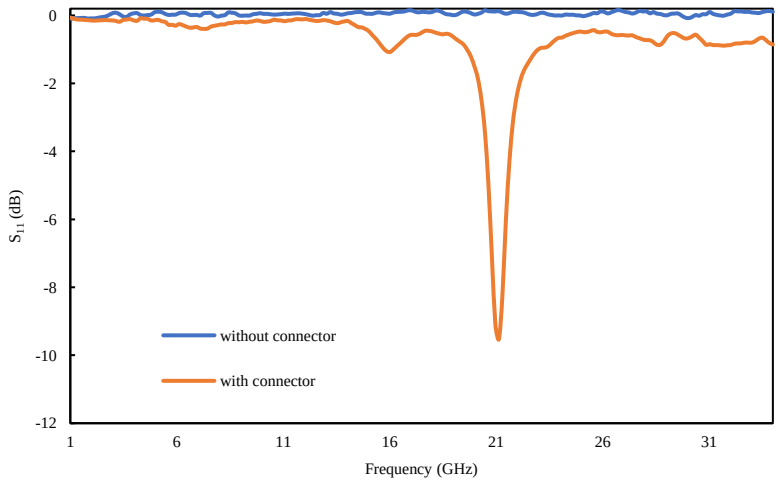

Figure 5-16. Defected S_{11} signal at 21GHz after adaptor connected to the cable.

However, connect microstrip filters reduces the deformation to its minimum value. Also, below 21 GHz deformation in transmitted signals can be neglected. Subsequently, signals beyond 21 GHz frequency showed the noised response.

5.7 Experimental setup

5.7.1 Rohde and Schwartz VNA measurements

Rohde and Schwartz VNA used to characterise five microstrip filters with an operational frequency less than 3GHz. Three of them made on FR-4 dielectric substrate, denoted as 1p, 2p and 3p. Moreover, two made on a quartz substrate, and they are 4q and 5q. All included microstrip filters supplied with 50 Ω SMA female connectors suitable to the VNA frequency range and male cables. They are soldered manually. SMA connectors are attached firmly alongside board edges, and the centre contact pin positioned parallel. Flat and centred against a signal trace of microstrip board. SMA legs and pins bonded to the board ports from each side.

Although no fixture included in the soldering process, except microstrips on quartz, jigs are used.

5.7.2 Agilent PNA

Reduced size microstrip filters (6q and 7q) characterised by Agilent PNA because of their higher operational frequency which is up to 26 GHz. They are provided with a high frequency of 3.5 mm SMA connectors in a match with VNA cables male connectors. A special jig is made to hold them during measurements in order to protect them from being broken while handling due to their fragility and miniature size. Calibration is made before each device measurement to prevent errors and ensure best results. Therefore, microstrip filters connected directly to the analyser ports by approved standard cables to ensure maximum connectivity and minimise attenuation lose.

Modelling results showed the behaviour of microstrip filters regarding design criteria. Hence, fabricated devices carried out regarding modelled designs. A standard measurement of scattering parameters is implemented to characterise physical models' responses and verify their functionality.

5.7.3 Measured S-parameters

Fabrication conditions might impact evaluation of S-parameters and their accuracy of fabricated models. Consequently, modified responses occurred to some of the microstrip filters. Four S-parameters of reflection and scattering and their phases are investigated to each microstrip filter according to design requirements. Moreover, a comparison is made between modelled and measured S-parameters to determine the precision of the fabricated design.

Microstrip filters evaluation includes frequency characteristics, electrical and thermal stability, systematic characterisation to investigate the match between computed models of microstrip filters and the fabricated patterns. Characterisation performed by analysing collected data from VNAs. S-parameters and accompanied phases plotted against frequency. S_{11}, S_{12}, S_{21} and S_{22} are measured and shown in supplemented figures to each device. S_{11} and S_{12} plots are included only due to the symmetrical similarity of S_{21} with S_{21} and S_{22} with S_{11}, S_{22} and S_{21} have similar responses to S_{11} and S_{12} respectively. Since the shape of microstrip filters are symmetrical from both sides, same power and waves applied to both ports, therefore, same results.

5.8 VNAs Characterization results

5.8.1 Chebyshev bandpass microstrip filter (1p)

The Rohde & Schwarz ZVL analyser characterised bandpass microstrip filter. Measurement setting is configured according to device properties, and central frequency is 1.5 GHz, power is -1dBm and spontaneous dB dynamic range. Impedance is 50 Ω for ports and cables.

Measurements results of reflected and transmitted waves in comparison to the modelled data are shown in figures (5-17) and (5-18). Phases are shown in figures (5-19) and (5-20) respectively.

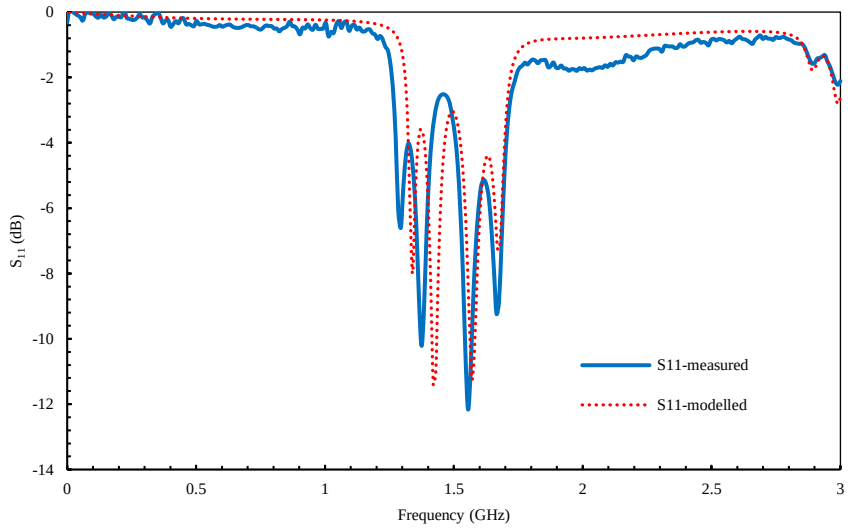

Figure 5-17. Reflection coefficient S_{11} of bandpass microstrip filter (1p)

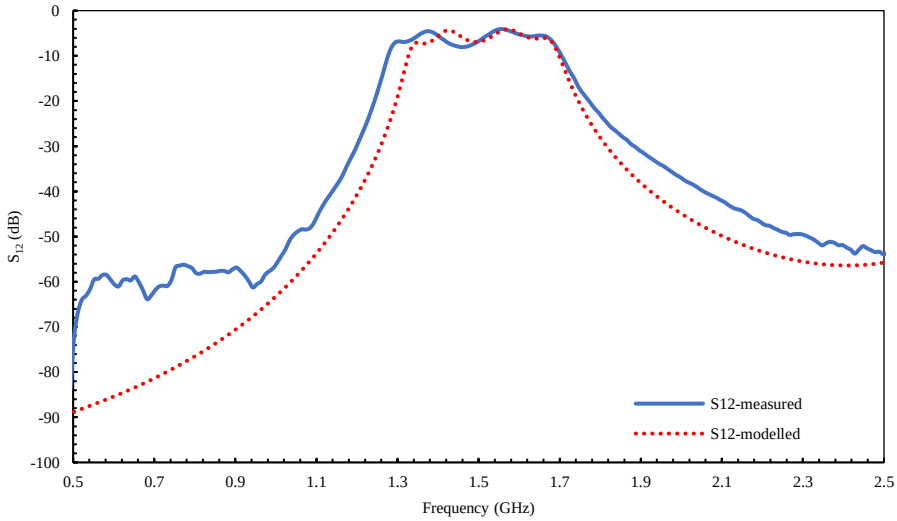

Figure 5-18. Scattering parameter S_{12} of bandpass microstrip filter (1p)

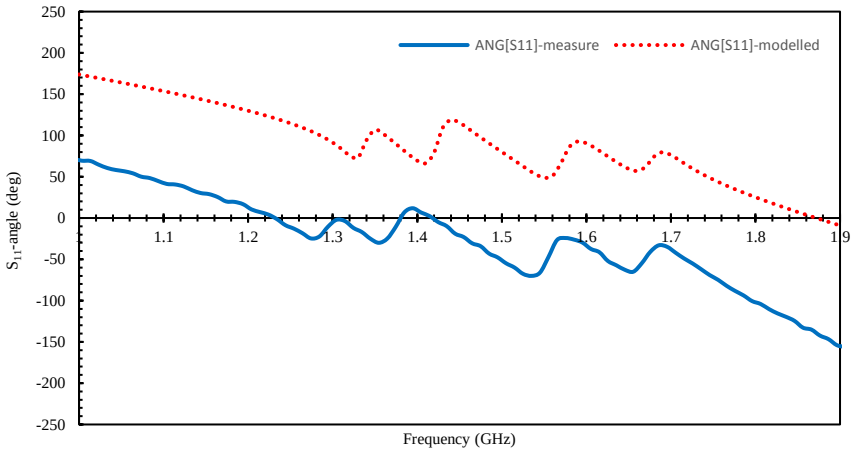

Figure 5-19. S_{11} phase diagram of bandpass microstrip filter (1p)

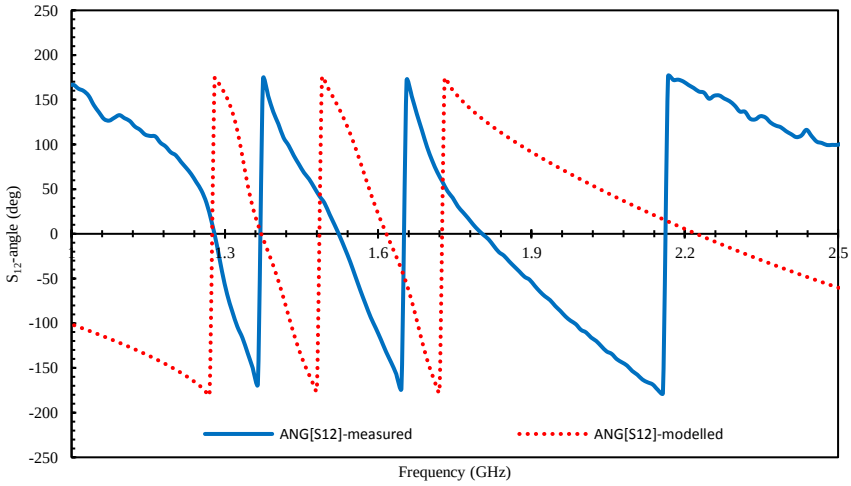

Figure 5-20. S_{12} phase diagram of bandpass microstrip filter (1p)

5.8.2 Chebyshev lowpass microstrip filter (2p)

Rohde & Schwarz ZVL analyser used to verify this lowpass microstrip filter. Measurements parameters are; cut off frequency 1.35 GHz, ripple 1-1dB, applied power is equal to -1dBm and spontaneous dB dynamic range is 80 dB, impedance is 50 Ω for ports and cables. Figures (5-21) to (5-24) are showing modelled and measured data of the resultants scattering parameters and their phases respectively.

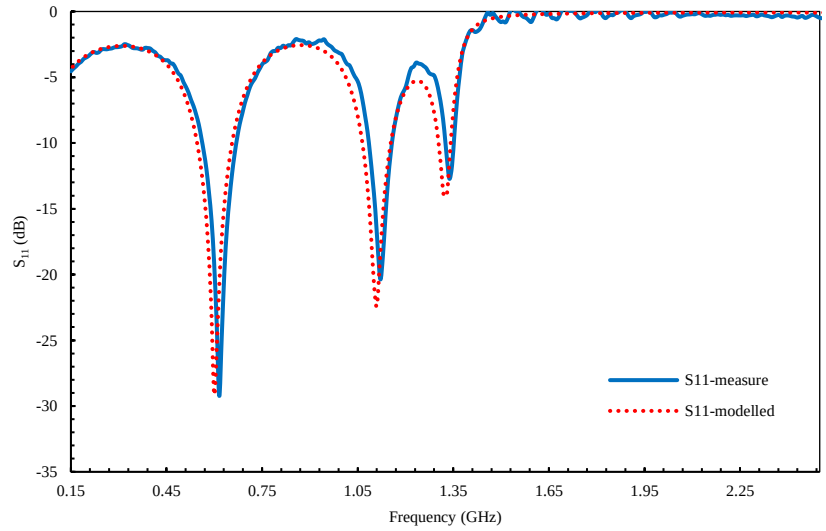

Figure 5-21. Measured and modelled S_{11} responses of Chebyshev lowpass microstrip filter (2p)

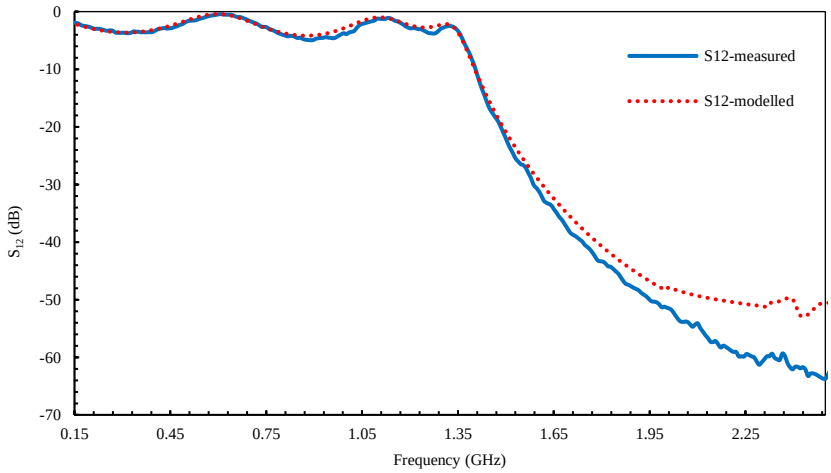

Figure 5-22. Measured and modelled S_{12} responses of Chebyshev lowpass microstrip filter (2p)

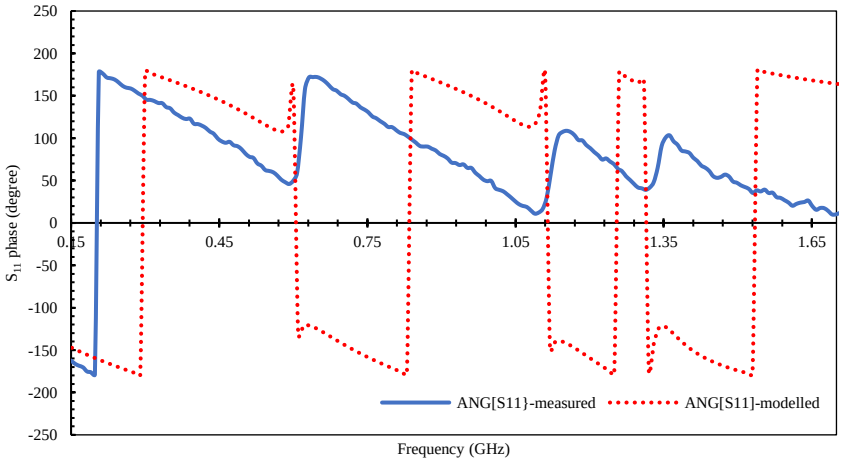

Figure 5-23, S_{11} phase diagram of Chebyshev lowpass microstrip filter (2p)

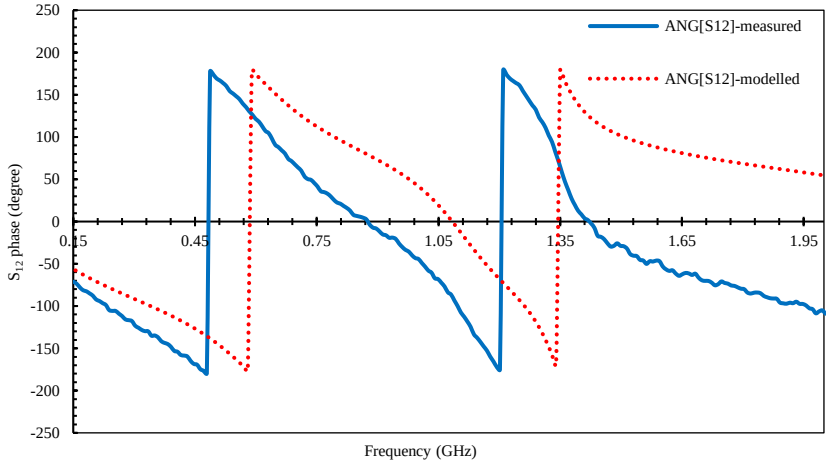

Figure 5-24. S_{12} phase diagram of Chebyshev lowpass microstrip filter (2p)

5.8.3 Butterworth lowpass microstrip filter (3p)

This device is analysed by Rohde & Schwarz ZVL analyser, and factors are; cut off frequency of lowpass microstrip filter is 0.9 GHz, applied power is equal to -1dBm, and spontaneous dB dynamic range is 80dB, impedance is 50 Ω for ports and cables. Comparisons between modelled and measured data are shown in figures (5-25) to (5-28).

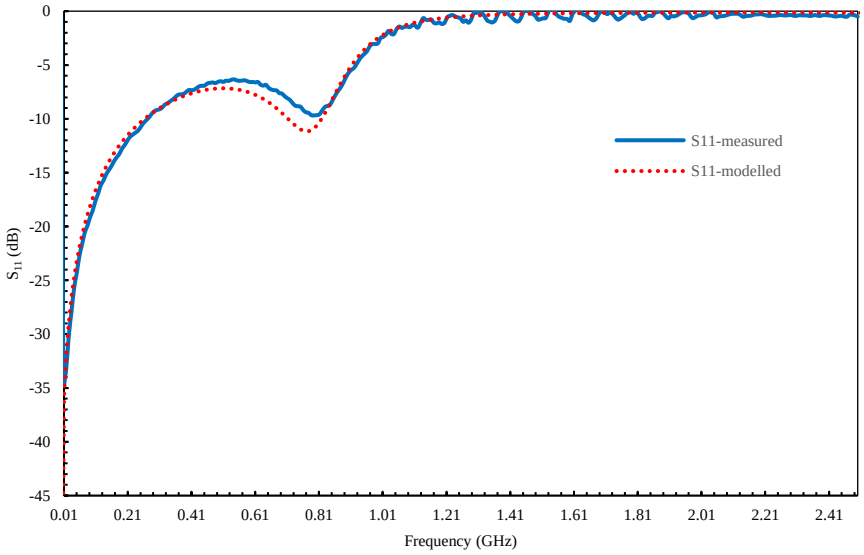

Figure 5-25. Measured and modelled S_{11} responses of Butterworth lowpass microstrip filter (3p)

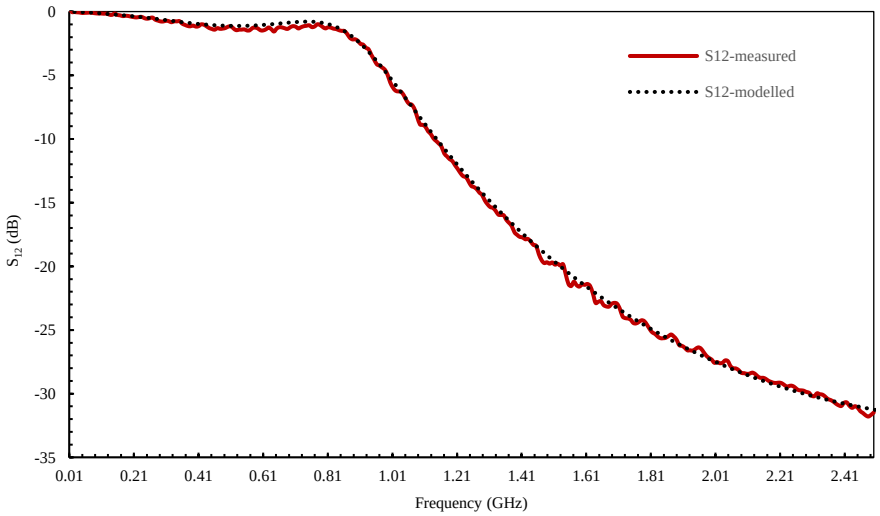

Figure 5-26. Measured and modelled S_{12} responses of Butterworth lowpass microstrip filter (3p)

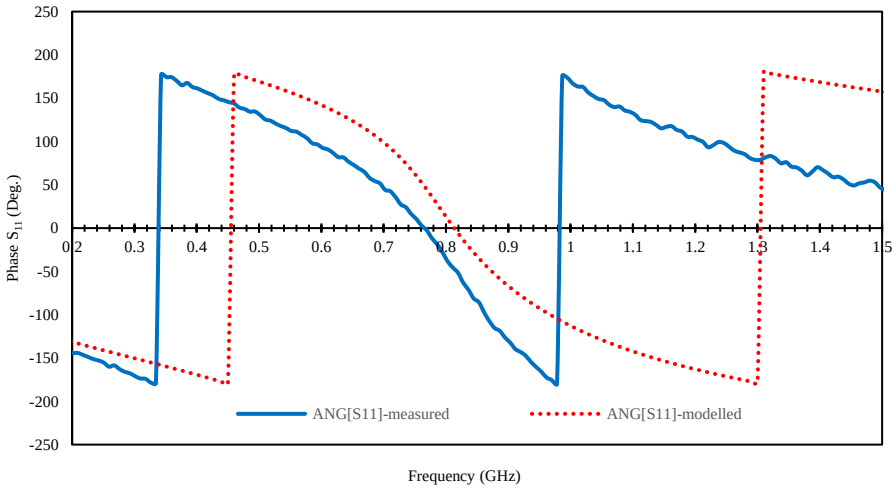

Figure 5-27. Measured and modelled S_{11} phase diagram of Butterworth lowpass microstrip filter (3p)

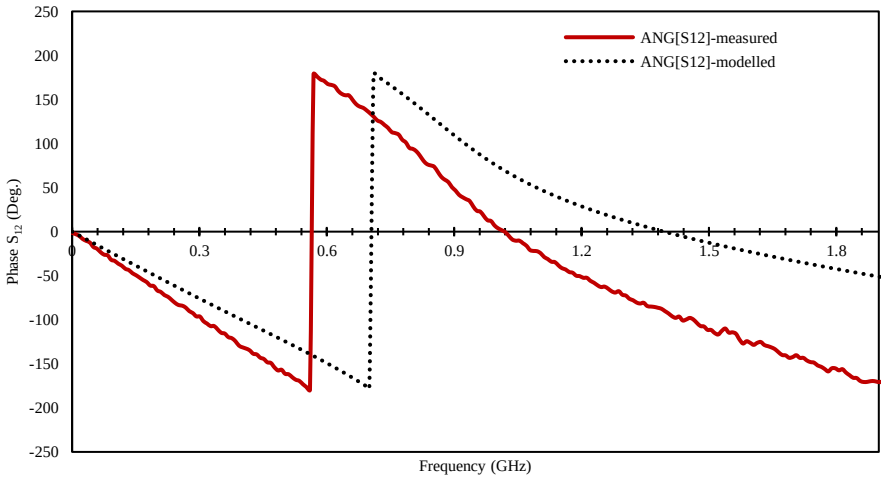

Figure 5-28. Measured and modelled S_{12} phase diagram of Butterworth lowpass microstrip filter (3p)

5.8.4 Chebyshev lowpass microstrip filter (4q)

This microstrip filter is first to fixture in a jig before measurement, analysed by Rohde & Schwarz ZVL analyser. Measuring parameters are; cut off frequency of lowpass microstrip filter is 1.47 GHz, ripples are -1dB, applied power is equal to -1dBm and spontaneous dB dynamic range is 80dB, impedance is 50 Ω for ports and cables. Measured data are shown in figures (5-29) to (5-32) as a comparison with modelled data of the device.

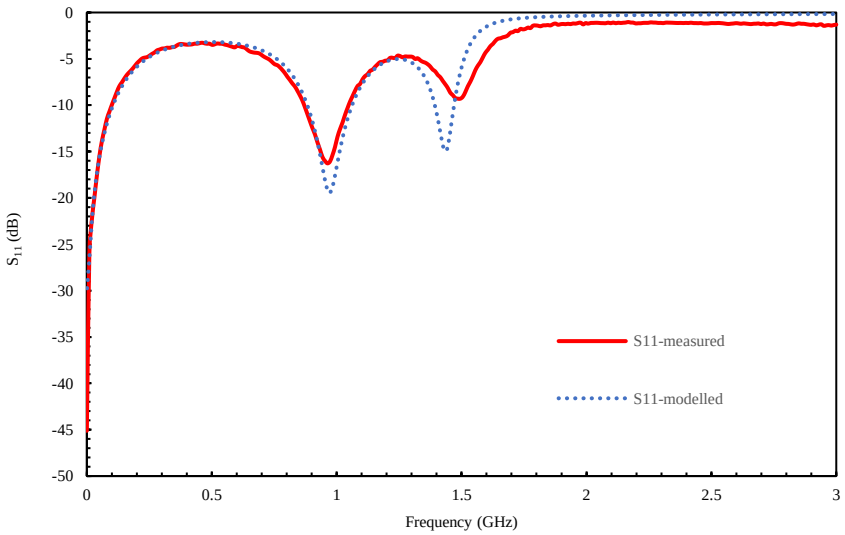

Figure 5-29. Measured and modelled S_{11} responses of Chebyshev lowpass microstrip filter (4q)

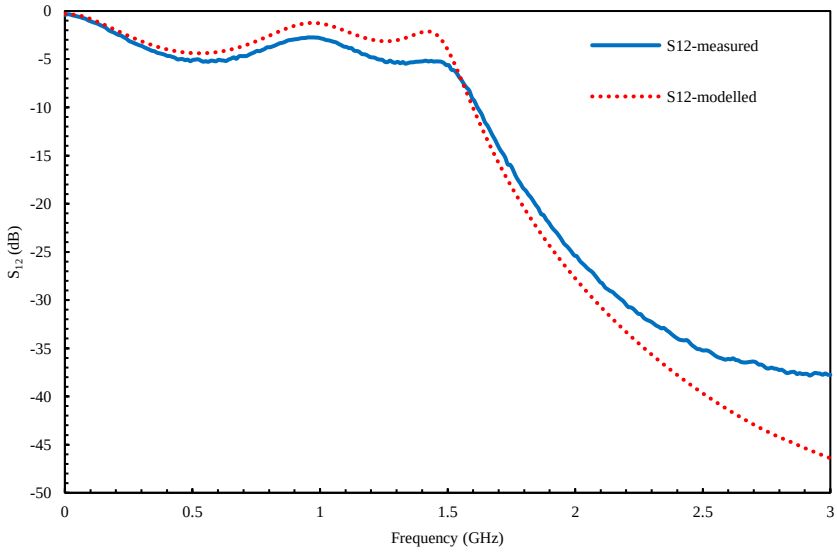

Figure 5-30. Measured and modelled S_{12} responses of Chebyshev lowpass microstrip filter (4q)

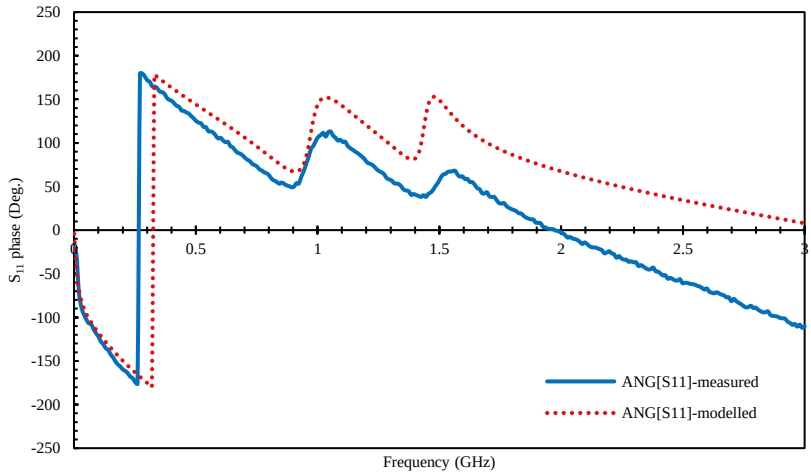

Figure 5-31. S_{11} phase diagram of Chebyshev lowpass microstrip filter on quartz (4p)

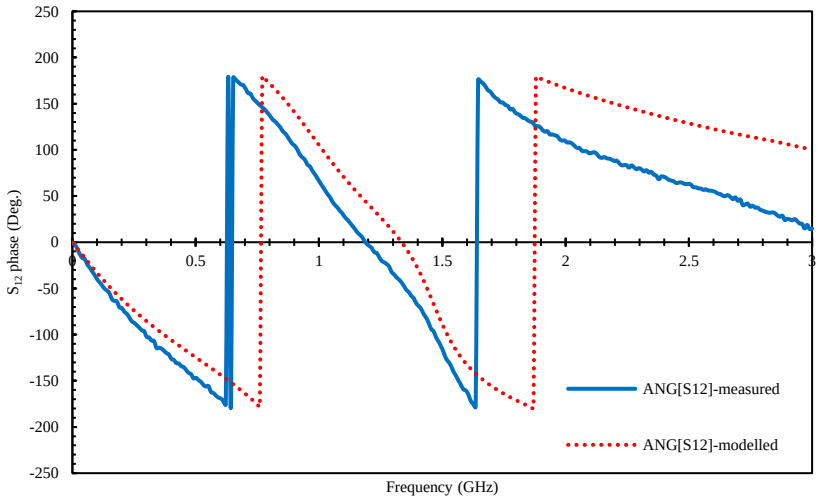

Figure 5-32. S_{12} phase diagram of Chebyshev lowpass microstrip filter on quartz (4p)

5.8.5 V-shaped Chebyshev bandpass microstrip filter (5q)

Rohde & Schwarz ZVL analyser characterised this device. Measurement configured according to device properties. Central frequency is 2 GHz, power is -1 dBm and spontaneous dB dynamic range, -1dB ripple, impedance is 50 Ω for ports and cables. Measured results compared to modelled results and showed in figures (5-33) to (5-36) respectively.

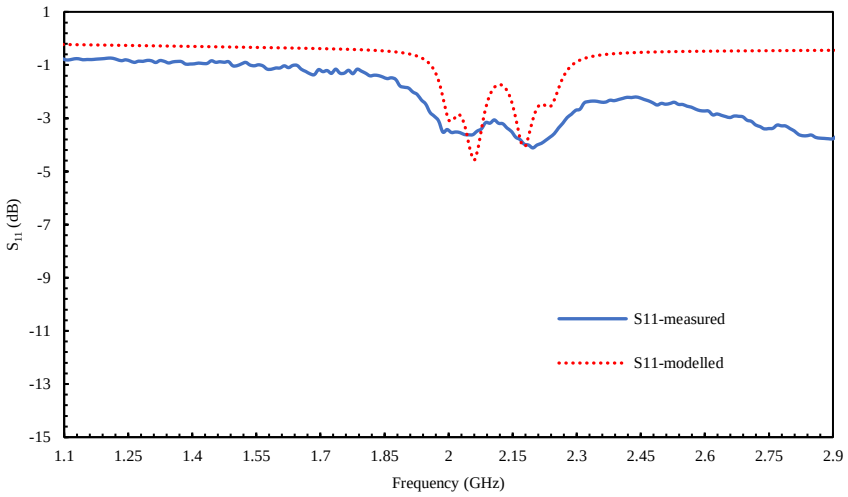

Figure 5-33. Measured and modelled S_{11} responses of V-shaped Chebyshev lowpass microstrip filter (5q)

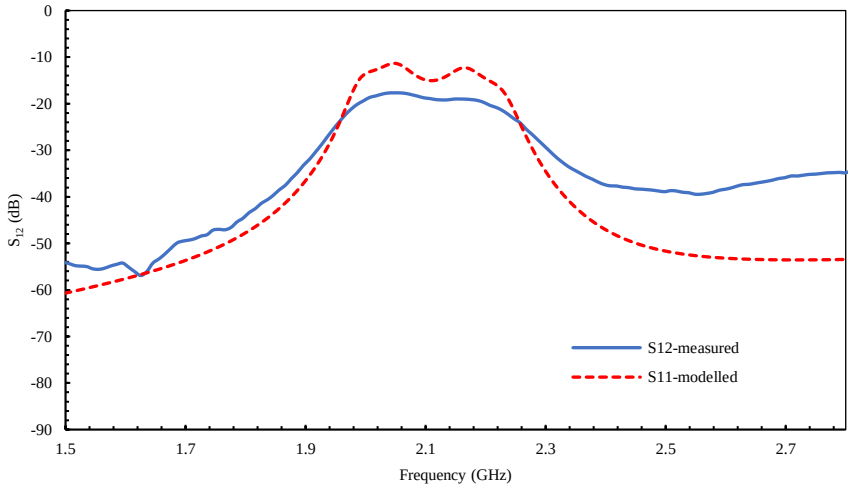

Figure 5-34. Measured and modelled S_{12} responses of V-shaped Chebyshev lowpass microstrip filter (5q)

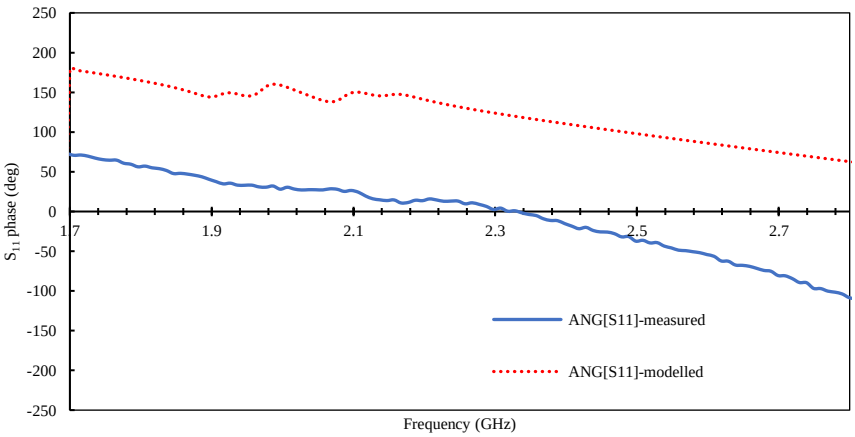

Figure 5-35. Measured and modelled S_{11} phase diagram of V-shaped Chebyshev bandpass microstrip filter (5q)

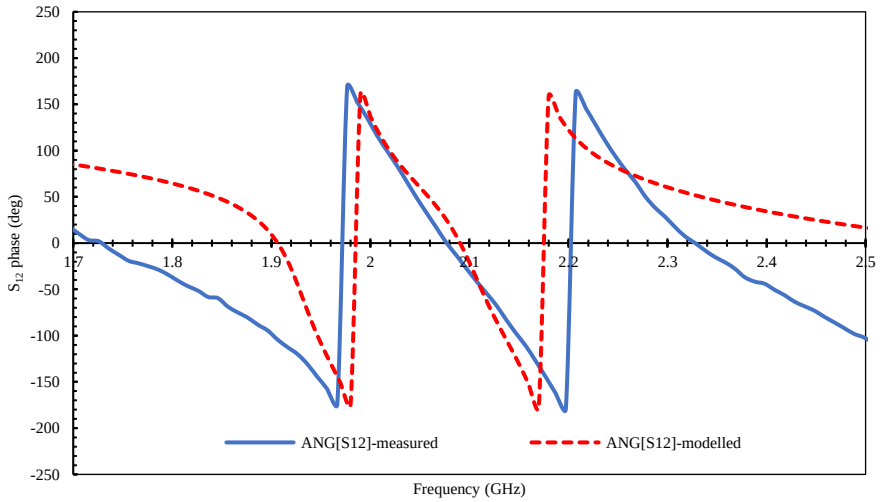

Figure 5-36. Measured and modelled S_{12} phase diagram of V-shaped Chebyshev bandpass microstrip filter (5q)

5.9 Reduced size microstrip filters analysis

5.9.1 Chebyshev bandpass microstrip filter (6q)

Fabricated reduced size bandpass microstrip filter is characterised by of Agilent PNA. Measurement setting configured according to device properties, and central frequency is 1.5 GHz, power is -17 dBm (0.02 mW), spontaneous dB dynamic range, -1dB ripple, impedance is 50 Ω for ports and cables, filter's parameters described in chapter 4 section 4.7.1. Nevertheless, bandpass microstrip filter has a short circuit defect due to a fabrication problem. One resonator has no space gap as shown in figure (5-37). Furthermore, it might be caused by the mishandling of shadow masks. Surface metal connectivity in the edge coupled affected filter performance by noticeable deformation. Deformed responses can be avoided by better fabrication. Therefore, an improved response shall occur. The measured response compared with modelled responses. Results are shown in figures (5-38) to (5-40). Reduced size versions of microstrip filter will serve the purpose of reducing the size ratio between the biosensor and investigated medical analytes.

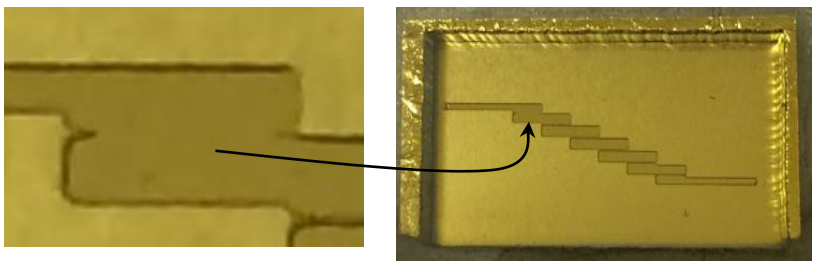

Figure 5-37. Short circuit deformation of reduced size edge coupled bandpass microstrip filter

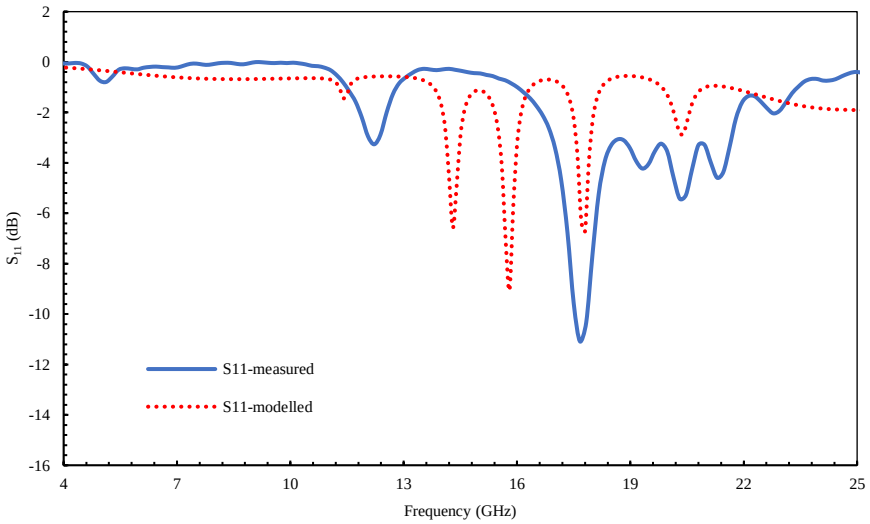

Figure 5-38. Measured and modelled S_{11} responses of reduced size Chebyshev lowpass microstrip filter on quartz (6q)

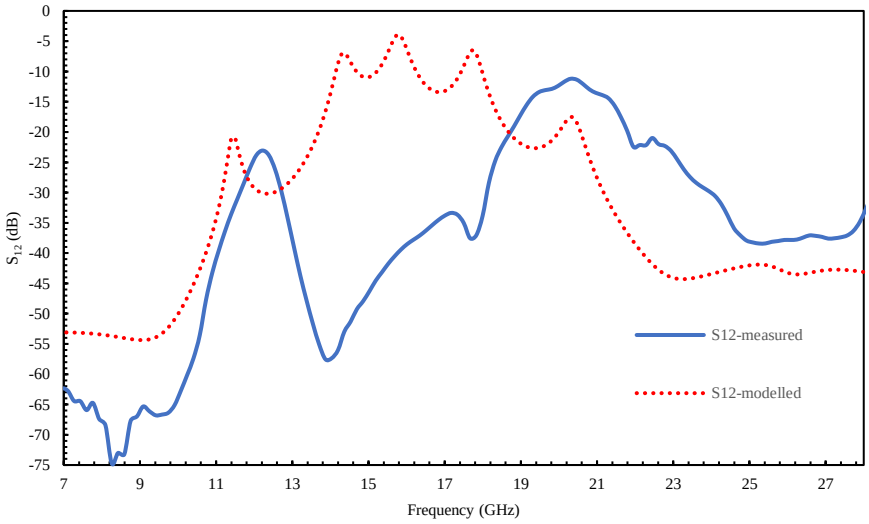

Figure 5-39. Measured and modelled S_{12} responses of reduced size Chebyshev bandpass microstrip filter on quartz (6q)

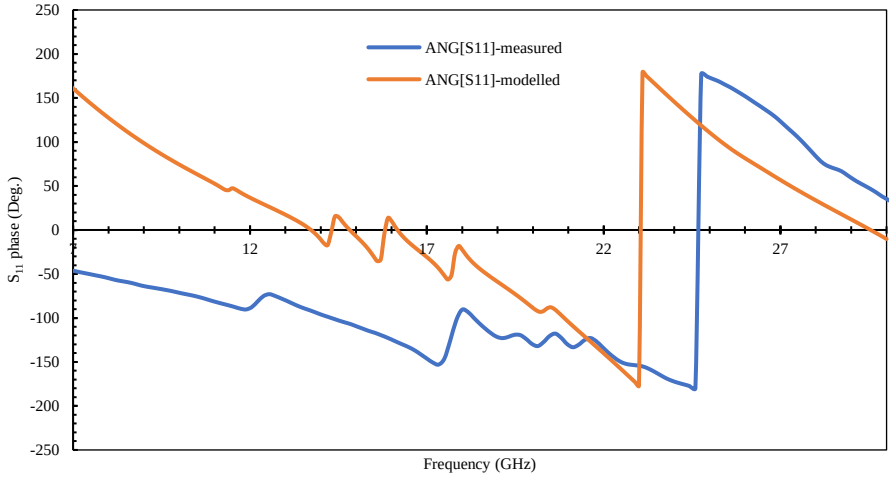

Figure 5-40. Measured and modelled S_{11} phase diagram of reduced size Chebyshev bandpass microstrip filter on quartz (6q)

5.9.2 Chebyshev lowpass microstrip filter (7q)

This device is analysed by Agilent PNA. The setting is; 26 GHz cut off frequency, ripples are equal to -1dB, applied power is equal to -17dBm and spontaneous dB dynamic range, impedance is 50 Ω for ports and cables. Measured and modelled scattering parameters response of reduced size Chebyshev lowpass microstrip filter shown in figures (5-41) and (5-42) compared to modelled data.

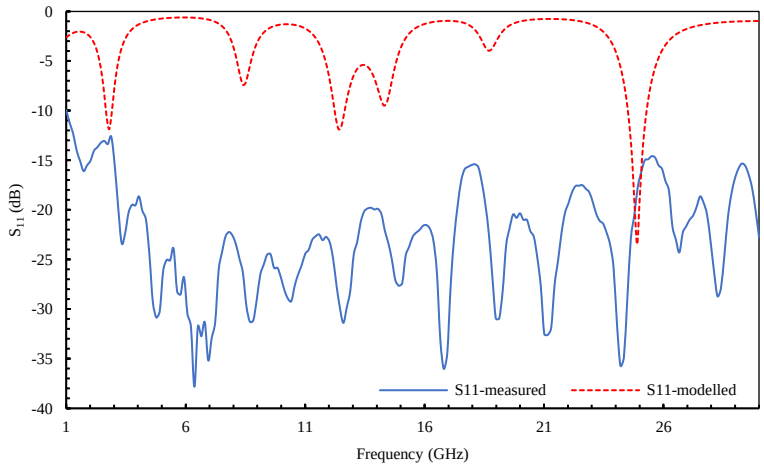

Figure 5-41. Measured and modelled S_{11} responses of reduced size Chebyshev lowpass microstrip filter on quartz (6q)

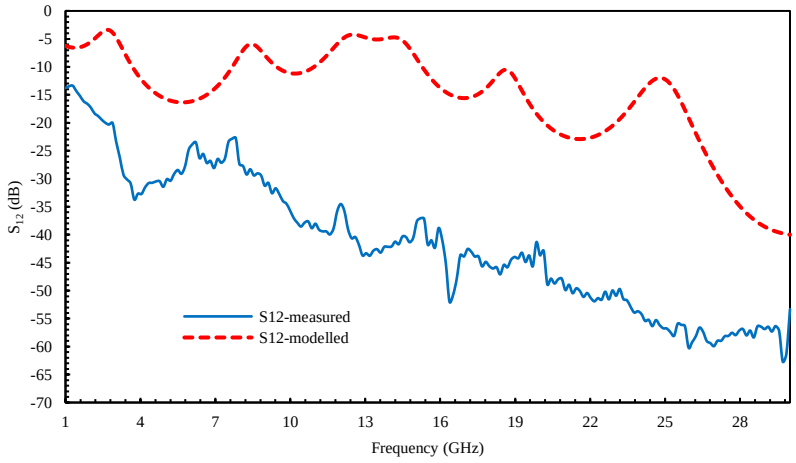

Figure 5-42. Measured and modelled S_{12} responses of reduced size Chebyshev lowpass microstrip filter on quartz (6q)

Agilent PNA might have error measurement as mentioned previously. Therefore, a portion of reflection coefficient S_{11} of this microstrip is investigated by Rhodes & Schwartz VNA within a band of 3 GHz, allowed frequency band is measured. Figure (5-43) showed the response of the microstrip filter at this range compared to modelled response. Result is showing the standard response of Chebyshev filter and the dip at 2.2 GHz as indicated by the curve in figure (5-41).

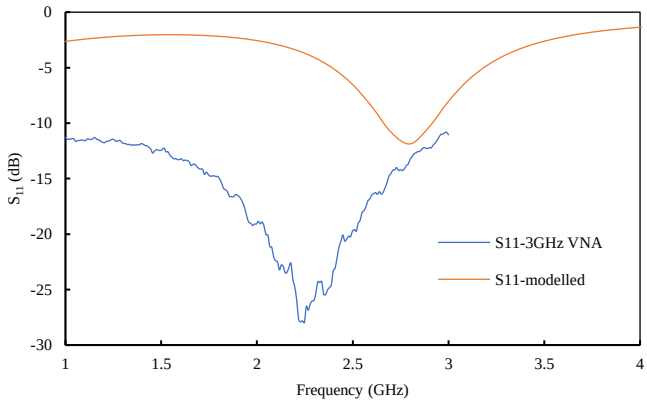

Figure 5-43. Reflection coefficient S_{11} of q6, measured by VNA of a 3GHz band and compared with a modelled

5.10 Connection repeatability examination

VNA consistency measurements of scattering coefficients are investigated. Moreover, stability measurement of VNA. Repeatability experiment is carried out by using Rohde and Schwartz VNA and connect-disconnect setup in different times to measure stability. Results are shown in figure (5-44). Devices showed very good stability occurrence over-repetition of the measurements. Rohde & Schwarz network analyser is calibrated and connected to the previously measured bandpass microstrip filter to achieve this experiment. Reflection coefficient S_{11} is used to show repeatability because all other results of scattering parameters are showing similar results.

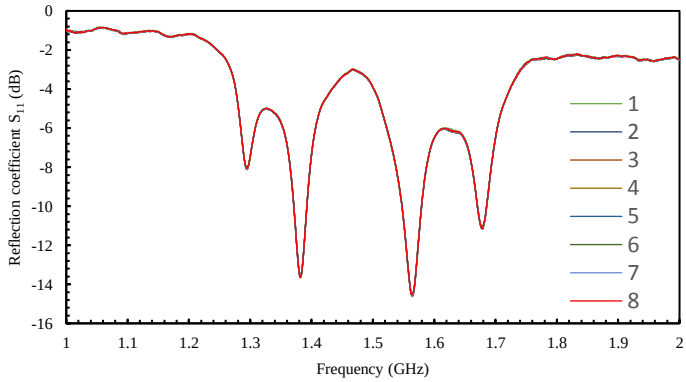

Figure 5-44. Repeatability of eight (connect-disconnect) experiments for reflection coefficient S_{11}

Examining connection repeatability showed the accuracy of the VNA measurements over a proposed frequency band. As well as cables and ports. VNA performed the same responses for several experiments. Acquired data are measured and collected at the same environmental considerations for VNA and device under test. Stability of VNA and microstrip devices is approved and can be used to further experiments and applications. In another hand, investigated connection repeatability provided information about the mechanical alignment setup and the consideration needed to handle microstrip devices and their connectors. Special care is regarded managing the microstrip filters on quartz and reduced size microstrip versions due to their agility as they are made on 100 µm thick quartz substrate.

5.11 Measurement evaluation of fabricated microstrip filters

Two ports network of microstrip filters is experimentally expressed by scattering parameters of reflected and transmitted waves. Components of S-matrix are enough to characterise and justify microstrip filters. Resultant data are collected, plotted and compared with modelled patterns. Microstrip filters 1p, 2p and 3p on FR-4 substrate showed good verification results. Their scattering coefficients analysis is in a good match with the modelled analysis of proposed filters. Microstrip filters made on 1mm height quartz substrate showed good results for the lowpass microstrip filter 5q. Data from the experiment are in good match with modelled data. V-shaped 4q bandpass microstrip filter results are good too. Despite the difficulty of design and fabrication process limitations of the mask, both devices retain their designated responses. The V-shaped filter is expected to offer more matched results, that can be explained by laser machined mask used in the evaporation process of the microstrip filter. An original design is modified to fit laser machine limit, an adjusted gap between microstrips increased space width. As a result, the coupling is reduced and might cause a possible power loss of the transmitted wave. Therefore, reducing the efficiency of the travelling wave and microstrip filter performance.

In terms of reduced size microstrip filters, in a higher frequency. Increased operational frequency will reduce microstrip dimensions. Microstrip filters converted to very small sizes. Therefore, dimensional accuracy and alignment of the microstrip filters become difficult to achieve. Misalignment of the microstrip and SMA connectors can be a source to an interface reflection, affecting electrical measurement to have incorrect values. Reduced size microstrip filters showed operational accepted responses with shaped design factors. They showed an acceptable match with their modelled designs, despite fabrication defect and measurement error caused by connection adaptor and old VNA machine. Defects can be due to different error sources. For example, miniature size and manual soldering have an impact on transmitted and

reflected waves of the filter in the port's region. Therefore, weak connectivity and voids may occur. Besides, the quality of the solder might affect the performance of wave transmission. Alignment of the microstrips in their jigs may affect signal integrity at the ports, and grounding also could have similar problems of welding. Therefore, it can reduce performance. Finally, characterised microstrip filters are operating correctly. Evaluation and analysis of collected data demonstrated the operation of microstrip filters according to their design criteria, regardless of fabrication and measurements difficulties. Practical data are compatible with the theoretical design calculations. The matched results of the proposed microstrip filters allowed further purposes to the health care applications.

5.12 Microchannel and microfluidic

Regarding biosensor realisation, a microfluidic is required to carry biological materials under test. Microstrip biosensor is prepared by integrated microfluidic or microchamber on selected regions of an uncovered top layer of the golden plane surface. Several microchamber designs and models are implemented. Microfluidic and microchamber fabrication is a complex process and typically expensive. Also, integrate microfluidic with microstrip in an appropriate alignment, and retain the fluid path from blockage with no deformation in the structures of microfluidic, due to bonding procedure is a practical challenge. In this research, cost-effective and straightforward microchamber is proposed and fabricated, the first microfluidic design made for bandpass microstrip filter (1q). Microfluidic is functioning to charge biochemical solutions to a specific region on the microstrip surface and discharge them after measurements.

Henceforward, the position of a microchannel is specified according to current density patterns of microstrips filters, demonstrated in chapter three of modelling. Microfluidic design and dimensions are compatible with the microstrip filter's selected sensitive region. For example, resonator inner space gap of bandpass edge coupled filter, it is calculated according to filter's dimensions to fit on the 500 µm width gap in the middle of a resonator. Channels made of acrylic of height 3mm. Channel has a fluid path of 500 µm width and depth equal to 1mm, and the path is not totally confiding inside the cell. Therefore, it is engraved inside the cell by laser and integrated with filter's surface to enable direct contact between fluid and filter's surface. The central part of the channel will completely cover the space between edge coupled microstrips. This configuration will allow samples under test to lay directly inside the filter's gap and cover the edges of gold strips allow direct exposure of the fluid to electromagnetic fields, while the channel is holding them during the test. Channel has two terminal holes. Inlet hole to charge solutions and outlet one to discharge solutions. Acrylic machined by Laser tool model: HPC Laser I. S4060. Laser machine operational parameters are

shown in the table (5-3). Microchamber capacity is equal to few microliters as shown in figure (5-45).

Table 5-2. Power and Speed setting of the Laser machine

Job	*Speed (mm/s)*	*Power % (kW)*
Engrave	300	80
Cut	8	98

Fluid path moves directly to the main channel over the filter's gap which is in the middle region. Flexible tube connection adaptors connected to the inlet and outlet holes.

5.13 Adhesion methods

In order to integrate microfluidics with microstrip filters, an interfacial force is required to hold them together by means of adhesion. Microfluidic channel will be attached to filter's surface by proper glue to guaranty the confined channel path will be capable of holding the solutions carrying the samples with no leak out of the channel. Liquid glue used to support the adaptors connection with the inlet and outlet opening's tip of the channels.

5.13.1 Adhesive

Selected glue is adhesive to plastics, solvent free, and have excellent chemical resistance. Also, it is waterproof. Epoxy resin is convenient to glue the microfluidic channel with the PCB device. Through apply it directly to microstrip surface and microfluidic, creating bonding between them with a minimum amount of externally applied force. Joined parts left several minutes in room temperature for curing. However, inspection results showed few problems related to microchannel maintenance after the joining process. These problems are due to the liquid nature of glue. Although, a limited amount of glue is applied and equally distributed over surfaces to ensure it is on the desired portions only. Concurrently, glue partially blocked the fluid path, and bubbles generated forming hard sectors. Also, liquid glue might cover the sensitive regions and prevent samples from reaching them. This condition caused an inevitable problem of sideslip of liquid glue inside the channel. Liquid glue has low resistance to flaw due to its low viscosity. This situation raised due to squeezing forces of pressure from microchannel weight during the gluing process and before glue solidify.

5.13.2 Remedy and possible solutions

To monitor the sideslip problem, trace and investigate liquid glue behaviour, a little amount of silver paint is mixed with the glue to make it visible and traceable. This method showed affected

regions inside the channel. These regions are filled with glue and blocked as shown in figure (5-45). Unaffected path showed by red trace.

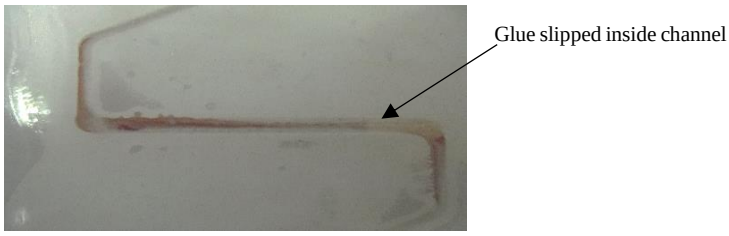

Figure 5-45. Affected regions showed in grey. Red colour indicates unaffected regions.

The first solution is to control glue balanced distribution around the fluid path. Besides, control the pressure over the cell to be towards the outer sides. Therefore, enforcing glue to moves toward outer sides and not concentrate around the fluid path and sideslip. Nevertheless, glue sideslip occurred at edges. Removable materials are tested aiming to prevent glue from sideslip inside channels, by filling the path during the adhesion process and can be removed later. Photoresist and water-soluble paste are utilised as a shield, suitable solvent and water applied to remove the solid materials after the adhesive process. Visual inspection is conducted to remove residual fillers. This protective method showed good result against sideslip of glue. Results are shown in figure (5-46). Liquid red dye injected to microfluidic to examine the path.

Although this method succeeded to stop glue sideslip inside fluid path, it is difficult to implement. Also, removing material from the inside path is time consumption. Moreover, it is difficult to fill and glue very thin microchannels. Adhesion process is improved by removable materials, control glue amount, control of pressure on the channel, and equal distribution of glue on the surface.

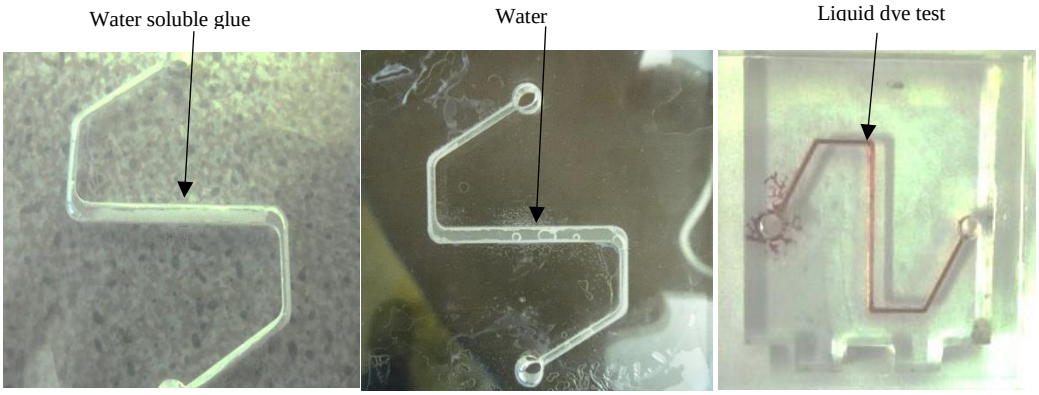

Figure 5-46. Removable filling material test, before and after the adhesion process

5.13.3 Pressure sensitive double coated adhesive tape

Although using glue to mount the microfluidic on the PCB filter is achieved, it is still unpractical and having difficulties of repeatability and complexity. Another adhesion method is proposed, it uses double-sided adhesive tape. Adhesive tape does not require a solvent or any additional material and cleaning. A tape is applied to mount microchamber and microfluidic to the microstrip surface. Sideslip problem is avoided even under high pressing pressure, and it provides a robust and immediate bond. Boundaries of channels can be easily specified by laser engraving and cutting machine, give it perfect fits because the tape is clear and can apply to microfluidic before machining with liner on. The laser can operate on a taped surface directly, more precisely cut and engraved with a precise shape. This method is successfully tested, contrary to liquid glue, no necessary curing time and mechanical support. Double-sided tape has enough strength to reserve bonded surfaces. Adhesive tape provides a uniform flat adhesive layer. The tape consists of a pressure sensitive adhesive acrylic foam core, coated on both sides by backing ribbon and liner. Tape thickness is 260 µm and width equal to 25mm (data provided by a supplier). It offered robust and fast adhesion and solidified instantaneously. Joined parts can be used immediately, which facilitates joining microfluidic to microstrip with perfect overlapping. Boundaries of channels can be easily specified by laser giving them complete fit and fastening. Edges of lined tape in the boundaries of the machined area are heated by the laser beam and melted down in location and solidify instantaneously, forming proper sealing around microfluidic channel edges. Handling time is reduced with high precision; light manual pressing applied on joined surfaces with rubbing to complete and reinforce the bonded contact. This method is cheap, reliable, and quick for microfluidic channels adhesion. Enabling highly uniform cross-sectional dimensions along the microfluidic channels and proper adhesion between different surfaces. Sophisticated designs and minor attribute size can be achieved depending on spot diameter and power of the laser. Moreover, the tape has good resistance to the chemicals and liquids in biochemical protocols. Realised biosensor by this method can be used directly [140, 141]. Double-sided adhesive tape considered to be used in further research steps.

5.14 Biosensor assembly

5.14.1 Microfluidic assembly

Microfluidic channel supplied by two adaptors fitted inside the two 2.5 mm radius holes to input and output. Adaptor one is used as an inlet to feed biological materials under test into the channel, therefore, charging biosensor with new biological material, second one used as an outlet to drain tested materials from the device after finishing the test. These adaptors are

straight barbed connectors of 3mm I.D shown in figure (5-47), (supplied by TCS micropumps, UK, product number is TC S701, made of Acetyl material). Connector accepts 2.4 mm radius tubes.

Figure 5-47, barbed straight connector.

Flexible silicone bore tube of 2.4mm radius (3/32") used to transports liquids to and from the microfluidic channel during the test. The tube is chemical resistant, had a wide range of working temperature and highly flexible. Tube wall thickness is 0.75mm. This bore tube is from adaptors supplier (product number is TC S602).

Tubes fitted securely to the adaptors of the microfluidic channel. The connection is strong enough to hold the tubes with the adaptors under the pressure of fluid injection into the channel and discharging from after test. Microfluidic channel is shown in figure (5-48).

The completed microfluidic channel had been installed on the PCB surface of the microstrip filter (1p) to complete the biosensor. Biosensor connected to outlet vessel to collect tested biological material. A schematic diagram of microfluidic fabrication and biosensor assembly is illustrated in figure (5-49).

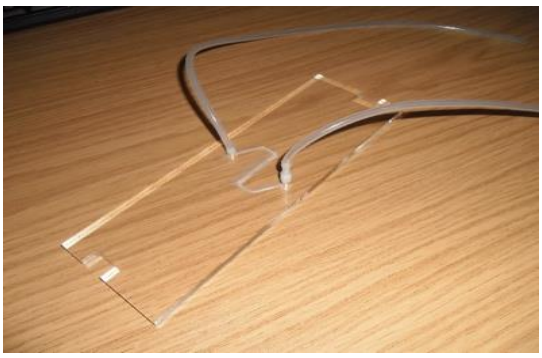

Figure 5-48. Realised microfluidic with adaptors and tubes.

Concerning biosensor integration with microfluidics, formerly made polymeric microfluidic is connected to the printed circuit board surface of microstrip filter (1p) directly by double-sided tape adhesion. The microfluidic position is selected depending on the current

density pattern. Therefore, high density of electromagnetic fields leading to a likelihood of more sensitive regions to react with biological materials. The electromagnetic field can be disturbed by dielectric change produced by loaded biological samples. Experimental inspection is made to identify the most sensitive surface regions. Droplets of nano-pure water are used on the surface to check reaction and sensitivity by measuring signal response change. The most sensitive surface area identified on the edges of microstrips. Volumes of targeted biomolecules solutions are small in comparison to microstrip's size. Only one unique part of the microstrip surface will be used in biosensing process. Microfluidic and microchamber are designed to expose the sensitive area with biochemical materials. An assembled biosensor is shown schematically in figure (5-49). Samples solutions feed from a container to microfluidic by a micro-pump. Input tube is connected to micro-pump to pump samples solution and flow control. Output tube connected to drain container.

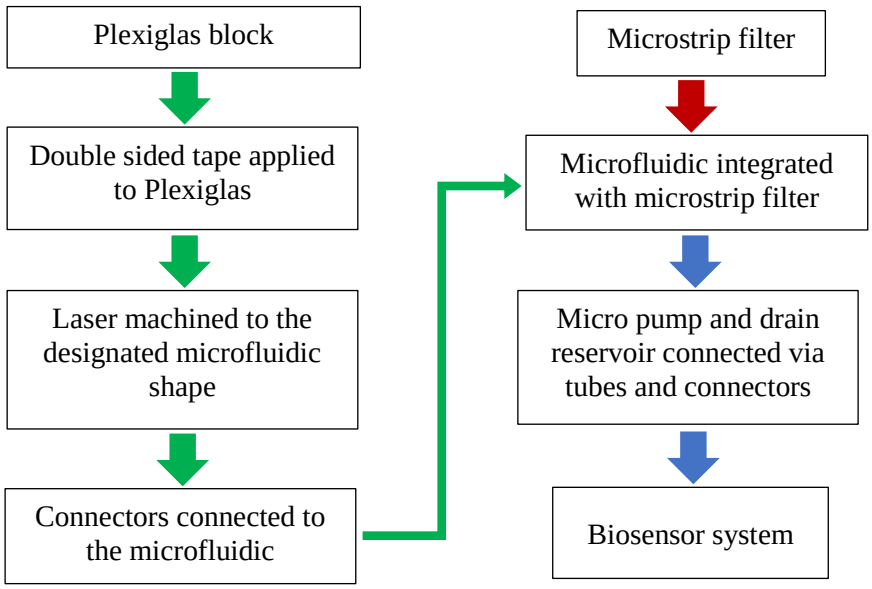

Figure 5-49. Schematic diagram illustrating biosensor assembly steps, green colour refers to the design and fabrication of microfluidic, red colour refers to microstrip filter integration with microfluidic and blue colour refers to biosensor assembly.

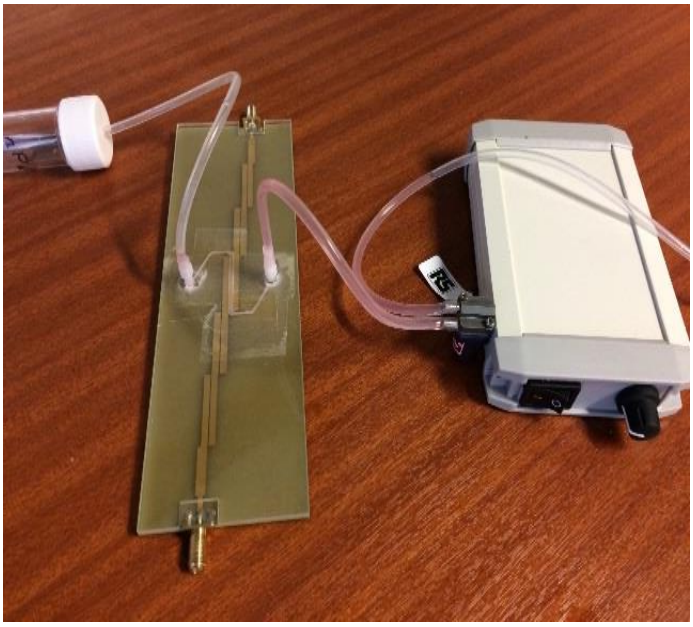

Figure 5-50. Assembled proposed biosensor
based on bandpass microstrip filter.

5.15 Microchamber

Regarding the biological experiment, a microchamber is used to input and carry biological materials, besides, allowing the surface cleaning of biosensor and reusability. Hence, microfluidic is not applicable due to cleaning scheme. Cleaning by radio frequency plasma and oxygen chamber requires direct surface exposure to reach biochemically treated surfaces. Unbinding attached molecules and chemicals from the surface, to allow straightforwardness of test repeatability and microstrip biosensor reusability. Opened microchamber is designed and fabricated to fit test and cleaning proposes of the microstrip surfaces. Several appropriate individual designs are fabricated to each microstrip biosensor depending on geometry and current density patterns. Therefore, guarantee the coverage of sensitive regions on the microstrips that has high electromagnetic fields density. For biosensor based on bandpass edge coupled microstrip filter (1p). The body of the microchannel is elongated in order to cover the whole surface of the microstrip filter. Microchamber made this way to protect other surface parts of the edge-coupled microstrip filter from influence the test because of their sensitivity. Also, preserves them for future use.

Regarding biosensor assembly, four new types of biosensor created depending on two ports planar surface geometry of microstrip filters, the short length of microstrip filters and their millimetre dimensions. Permitted low volumes of biological samples and nano-concentrations

analytes to be tested. First proposed biosensor is based on edge coupled bandpass microstrip filter (1p). Microchamber integrated with the microstrip filter specifically on the selected sensitive region. Microstrip filters are integrated with microchamber via double coated tape. A sensitive region is selected over two parts separated physically by a gap space and coupled electromagnetically to each other. Microchamber is placed to cover the gap area of the coupling region between the microstrip parts and microstrips edges. Loaded materials are uniformly distributed over microchamber channels over uniform microstrip parts and gap between them. Three more microstrip biosensor are assembled, produced biosensors based on lowpass microstrip filters. Microchamber designed to cover the edges of one capacitive part only. Edges regions are rich in field lines that can be disturbed by created biological cells and tissues.

The architecture of biosensor and microchamber is made to custom only one part of the microstrips track. Through testing the reflection coefficient S_{11} and S_{22} of microstrip filter based biosensors, it is found that the regions close to port one of microstrip filters have high current density. Therefore, high sensitivity to added materials. Besides, reflected wave would influence and change its response in this position. They are enhancing good sensing feature. Focusing on sensitive regions only enabled small microchamber size. Minimum volumes of samples are feasible, boosting measurement accuracy by reducing noises and signal loss of large liquor volumes. Different sizes, volumes and capacities of microfluidic chambers are designed and fabricated. Volumes range from 4 µl up to 35 µl, subsequently, microchamber designed to ensure the best coverage on microstrips sensitive regions. Therefore, biomedical materials affect the microstrips surface, edges and sides. Different configurations are submitted to reach maximum bio-sensitivity, and minimum used fluid of analytes, these biosensor configurations are shown in figure (5-50).

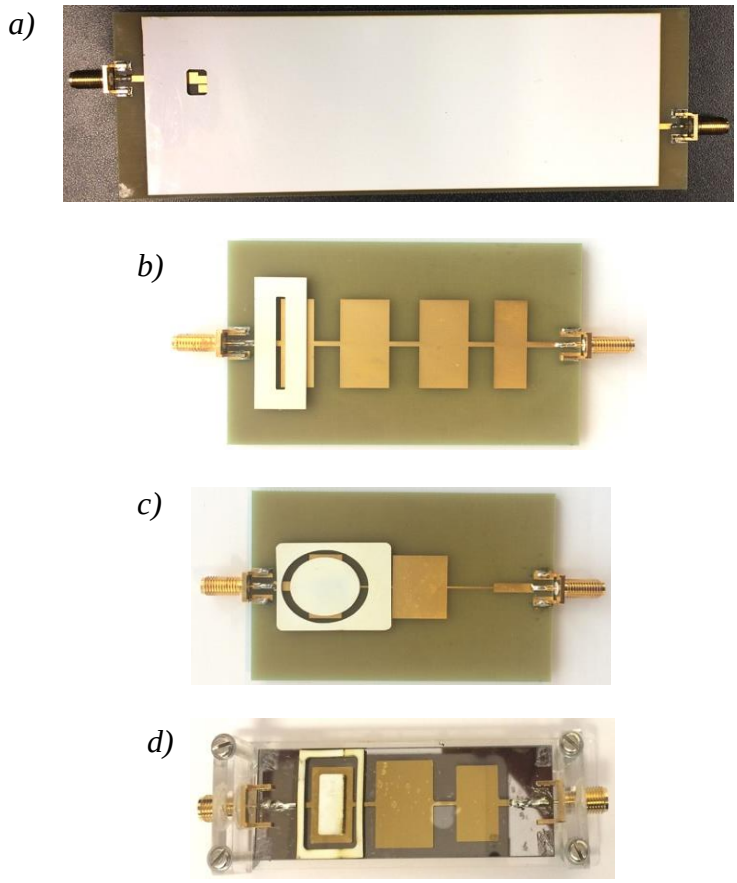

Figure 5-51. Biosensors based on microstrip filters integrated with microchambers in different architecture targeting maximum sensitivity and minimum sample volume. a) biosensor based on (1p), b) biosensor based on (2p), c) biosensor based on (3p), d) biosensor based on (4q) fixed on jig

5.16 Summary of fabrication and biosensor assembly chapter

The fabrication processes of microstrip filters, microfluidics, microchambers and assembly of biosensors are expressed in this chapter. In terms of biosensor assembly, previously designed and analysed microstrip filters in chapter three and four respectively are fabricated and integrated with microfluidics and microchambers. Hence, biosensors produced and verified. In this chapter, fabrication of microstrip filters and biosensors assembly introduced in detail. Two methods are used to manufacture microstrip filters, and these methods are printed circuit board (PCB) technology and clean room evaporation technique. Three types of microstrip filters are manufactured by PCB technology on FR-4 dielectric substrate. They are bandpass and low pass microstrip filters characterised by Chebyshev response and lowpass microstrip filter characterised by Butterworth response. Four devices are fabricated by a clean room evaporation

method on a quartz substrate; they are lowpass, V-shaped bandpass and reduced size microstrip filters. These fabricated devices are tested and validated by VNAs. The result of VNA measurements showed that the microstrip filters are operating correctly according to the design parameters except for two devices. Performing VNA verification for reduced size microstrip filters showed inconsistent results with modelled designs. This problem can be due to metal mask defects, therefore, evaporation defects. Besides, high-frequency VNA was an out of date machine and has some problems such as old cables that affected the measurements.

Microfluidics is designed, manufactured and conjoined with microstrip filters. A new method was utilised to join microfluidics and microchambers with microstrip filters surfaces. Different adequate configurations of microchambers made to each microstrip filter according to surface geometry of each filter, microfluidics and microchambers designed to cover specific regions only to enhance the sensitivity of the biosensors. Sensitive regions are on the edges of microstrips where high field's density is predicted. Assembled biosensors will be tested biomedically to verify their detection functionality and selectivity against targeted biological samples. PSA biomarkers represent the material under test in the biomedical experiment of microstrip based biosensor examination and will be explained in the next chapter.

Chapter 6: biochemical experiments for selected microstrip-based biosensors and data analysis

6.1. Introduction

This chapter demonstrates the biochemical test of the proposed new biosensor towards PSA detection. Prostate Specific Antigen (PSA) is a secondary protein particle and a biological marker. Prostate gland cells produce serine protease enzyme or a prostate-specific antigen protein. Serine protease of PSA function in the human body is to preserve seminal fluid liquefaction and generated by the prostate. Cancer cause PSA concentration increases above normal. It is worth mentioning. An elevated level of PSA concentrations may not indicate cancer; furthermore, it might indicate further abnormality of body functions. Although there is no specific threshold level for cancerous prostate concentration, levels are fluctuating. Higher and continuously increasing levels may refer to a potential risk of abnormality. In both cases detect and measure alternative levels of PSA is an essential criterion of medical diagnosis. Biological serum marker of PSA is a gauge of prostate cancer condition. Examination of it is concentration can diagnose cancerous prostate concentrations, repeatability of PSA levels test is vital in the diagnostic process.

Regarding biosensor examination, lab-based PSA detection protocol is selected for sensing functionality assessment, and scattering parameters are employed as biosensor functionality indicator, exclusively chosen are reflection coefficients S_{11} and S_{22}. Presence of fluids and analytes influence travelling wave and modify scattering parameters. Response change of reflection coefficient unveiled a reaction caused by biochemical protocols. Biosensors use these changes to detected different PSA concentrations. The resultant data were imported to Matlab and processed by a third and fifth order polynomial to find shifted points. Curve fitting is employed to calculate trend lines of the data.

6.2. Experimental protocol and Method

Regarding the biomedical experiment, PSA capture, detection and analysis are achieved. The biosensor is biologically activated, and its performance against bio-detection is verified. Two aspects of biochemical treatments applied to activate biosensor. It is functioning and immobilising of self-assembled monolayers on the gold surface of the biosensor. S-parameters change measured at each stage of a biochemical protocol. Primarily, functionalisation of the biosensor by antibodies provide necessary structure units to further biochemical reactions. Three layers included in the functioning process. They are crosslinkers, antibodies and surface blockers. The initial stage included cross-linkers attached directly to the gold surface and first

layer constructed. Afterwards, antibody proteins added and connected with a cross-linkers layer. Later, the blocking agent added. It used to shield and block non-functionalized regions to prevent their undesirable effects; functionalisation process provided a biosensor with PSA receptors. Detectability of functionalised biosensor towards targeted PSA analytes is evaluated. PSA implanted in different concentrations and constructed PSA layer on receptors. Nonetheless, a biochemical control process is applied to the biosensor. It involves the addition of PSA analytes to a biosensor holding cross-linkers only on its surface. Additionally, to assess biosensor over different PSA concentrations and reusability. The regeneration process tested by repeating detecting functionality of biosensor on several PSA concentrations. Different PSA concentrations are added, detected and chemically removed from one functionalised biosensor. One preserved receptors layer used for PSA concentrations. Data collected and analysed for all process. Biochemical protocols steps are shown in the table (6-1) and illustrated in figure (6-1) which is a schematic diagram of the biomedical experiment to examine biosensor detection functionality towards PSA selection, immobilisation and detection.

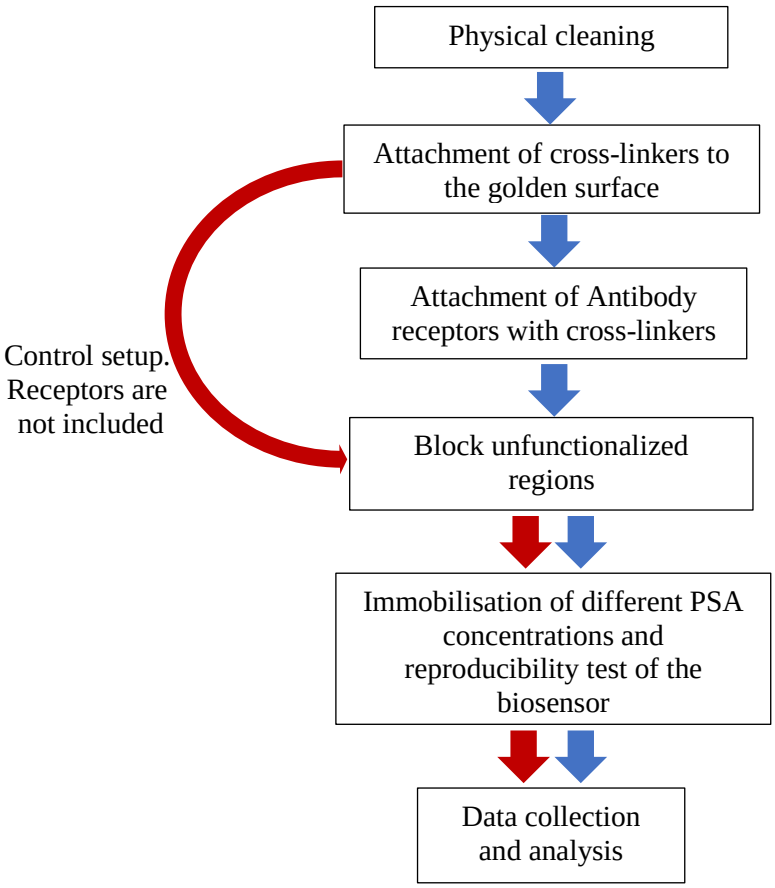

Figure 6-1. Schematic diagram illustrating experimental biochemical protocol.

Table 6-1. Biochemical protocols and method

Surface functionalisation			
No.	*Process*	*Repetition*	*Time (min)*
0	Air	1	1
1	2% Hellmanex II	1	15
2	dH_2O	5	2
3	DSP in DMSO	1	15
4	DMSO	1	1
5	dH_2O	5	2
6	Coating Ab in PBS	1	15
7	TBST	5	5
8	dH_2O	5	2
PSA immobilisation			
9	PBS-T	1	1
10	Blocking (PBS+2%BSA w/v)	1	5
11	PBS-T	5	2
12	Ag (Various PSA concs.)	1	10
13	PBS-T	5	2
PSA analyte removal			
14	Glycine/HCl	2	0.16
15	PBS-T	1	0.25

6.3. Physical cleaning

Biosensor went through a thoroughness cleaning process prior to the biomedical experiment. A process to remove any possible substantial contamination and retain surface cleanness. It is polished by slurry alumina powder mixed with deionised water. Next, the device washed by an ultrasonic bath filled with deionised water for ten minutes. The bath temperature is equal to 35^{o}C to remove alumina and any undesired material. After an ultrasonic bath, a flow of compressed nitrogen gas applied directly dry device. Biosensors cleaned by plasma machine and oxygen chamber after each biological experiment.

6.4. Biochemical protocol

Initial cleaning of the surface to prepare it to regeneration and control test, the biochemical sequence was expressed in figure (6-1). In terms of biochemical detection protocol, it is first utilised to test fabricated biosensor based on FR-4 PCB microstrip filters. Sequentially, applied

to biosensor on a quartz substrate. Change in reflected signal and frequency shift occurring due to perturbation from presented material under test represents the biosensor concept of detection. More specifically, measures biosensor response regarding input materials. Compare it to a standard biosensor response from standard buffer only before biochemical loading.

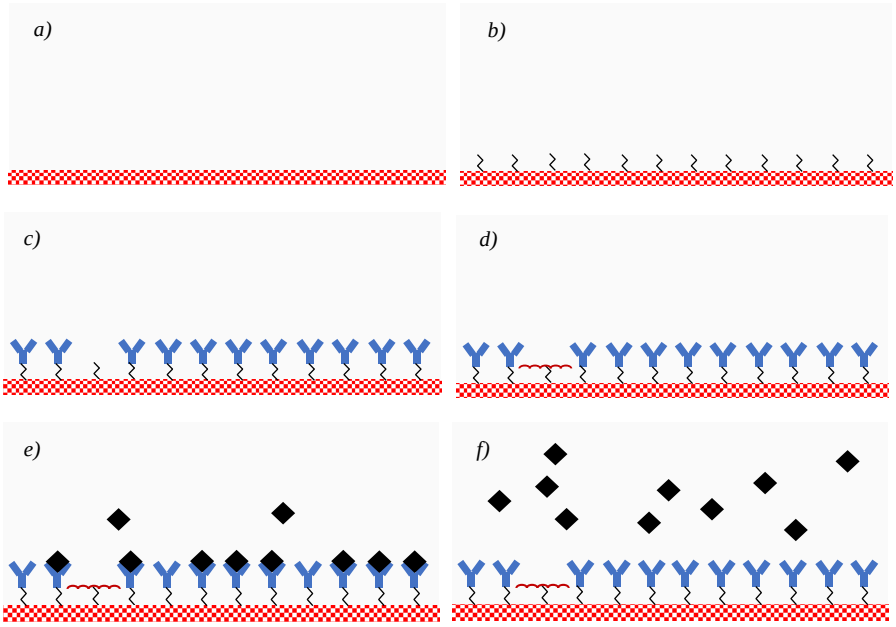

Figure 6-2. a) gold free surface, surface functioning by b) cross-linker, c) Anti-body, d) blocking layer, e) PSA immobilisation and analyte detection process, f) removing of PSA to apply different concentrations.

6.4.1. Chemical wash

Before biosensor functionalisation, Hellmanex II washes biosensor, step number 1 in the table (6-1). It is an effective aqueous solution of an alkaline liquid concentrate. Nano-Pure water dilutes Hellmanex II to an operational concentration of 2-vol %. Solution left inside microchamber for five minutes. Hellmanex removed, and microchamber washed five times by nano-pure water, step number 2 in the table (6-1).

6.4.2. Surface functionalization

Before the biochemical process start, a measurement data is collected from unloaded biosensor for comparison purposes. Nano-pure (np) water is a neutral solution for surface functionalising part. Microchamber rinsed five times by nano-pure water after Hellmanex II wash. Regarding baseline measurement and for comparison, a reference in liquid reading made of water occupied microfluidic chamber in the biosensor. Correspondingly, water used to rinse biosensor after

each biochemical functioning layer. Data collected after rinsing from water in a biosensor to measure the building of layers. Measured data of functioning compared to a reference measurement. Applied volumes are 4-35 µl depending on microstrip biosensor and microchamber configuration. The manual micropipette is used to feed biochemical fluids and buffers into the biosensor. Also, it is used to discharge biosensor by removing fluids and buffers. Water-based Phosphate Buffer Saline (PBS) solution used as carrying fluid for biological samples. Different buffers used in liquid measurements. Therefore, nano-pure water and buffers have two purposes, cleaning and in liquid measurement.

In terms of biosensor functionalisation, biomolecular interaction will be implemented on biosensor's surface. Chemical covalent bonding occurrence will influence biosensor. Biosensor showed good consistent results and reproducibility. Charging and discharging fluids into and from biosensor is achieved manually by micro-pipette.

6.4.3. Surface linkers (DSP Crosslinker)

Dithiobis (succinimidyl propionate) or DSP is a homobifunctional and amine-reactive cross-linker, step number 3 in the table (6-1). DSP crosslinkers are used to immobilise antibodies in the one-step crosslinking reaction. It possesses reactive group in both end spacer arm. DSP has a strong affinity to the gold surface. Linking between gold surface and DSP occur through chemisorption. Adsorption of DSP adsorbate by gold surface accompanied by a chemical reaction induced between gold and DSP creating chemical bonds at adsorbent gold surface. Disulphide linkage in DSP chemisorbs rapidly to gold surfaces, while active NHS groups on either end of DSP are reactive toward primary amine groups in proteins of antibody receptors. DSP embodies the infrastructure of a surface functionalised process.

DSP is the first chemical layer formed. DSP linkers are dissolved by appropriate volume of coating solution Dimethylsulfoxide (DMSO) and used directly. Microchamber filled with few microliters of DSP in DMSO by micropipette. They are forming reaction last fifteen minutes in room temperature. After that, microchamber rinsed with DMSO, later, five times wash by nano-pure water. Gold is activated with NHS groups. Therefore, the surface of a sensitive region is prepared primarily by DSP linkers. Washed up to remove the residual of the coating solution and unreacted DSP. VNA measurement is collected and compared with a free biosensor. A change occurred in reflected signal due to the presence of DSP linkers on the surface. The biosensor is promptly ready for a further step of antibody receptors.

6.4.4. Antibody Receptors protein

DSP linkers have a short lifetime. Therefore, the antibody coating stage is accomplished immediately after DSP linkers-gold association, figure (6-1-c). PSA antibody is a specific

ligand for PSA capture and can selectively bind with it. Receptor function is to catch PSA molecules. PSA antibody solution is added directly to the treated surface and incubated for time 15 minutes in room temperature, step number 6 in the table (6-1). Anti-bodies bonded with crosslinkers by a covalent chemical bond. Conjugation process took place during the specified time. Anti-bodies are connected directly to DSP linkers from their second reactive terminal. Biosensor showed signal modification detected by a vector network analyser. Change in surfaces layers indicated. Accordingly, after completion of receptors installation. A solution of anti-body discharged, and microfluidic chamber rinsed five times by TBS-Tween. Rinse to remove unconjugated proteins and by-products of cross-linkers. They are NHS leaving groups and unattached antibodies. Therefore, eliminating their undesirable influence on the measurement. Nevertheless, microfluidic chamber washed five times by nano-pure water. Measurement data collected in liquid at fifth water wash. Biosensor showed signal variation after the presence of antibodies.

6.4.5. Blocking by Bovine serum albumin

Realised receptors layer is accompanied by non-functionalized and inoperative groups of residual chemicals tied to surface. The blocking agent is used in order to prevent effects of these non-specific binding spots remaining parts. It is accomplished by a chemical obstructing process to terminate them, figure(6-1-d). For blocking purposes, a Bovine Serum Albumin (BSA) is added, step number 10 in the table (6-1). A stable form of BSA is dissolved in phosphate buffered Saline. Attachment of antibodies to treated surface is followed by the addition of a blocking agent of Bovine Serum Albumin. Furthermore, BSA blocking agent will not block receptors or affect the binding process. It has no affinity to a protein of interest. A diluted solution of BSA is left over for 5 minutes. BSA solution removed and followed by rinsing microfluidic chamber five times by PBS-Tween. Data collected during the fifth wash.

6.4.6. Immobilisation of Prostate Specific Antigen

The biosensor is prepared to capture and immobilise PSA molecules. Analytes are in free diffusing in PBS solution. They can reach receptors for binding and immobilise. Biochemical capture of PSA antigens by antibodies receptors is self-assembled multilayers process, step number 12 in the table (6-1). These layers form new surface morphology affect electromagnetic signals. Figure (6-1-e) showed PSA capture. PSA diluted in PBS buffer to different concentrations, and the minimum is 6.25 ng/ml. PSA solution added to a functionalised biosensor. PSA solution kept in a biosensor for 10 minutes in room temperature. PSA solution then removed. Five times wash by PBS-Tween is applied to the biosensor to remove non-immobilised PSA, steps 13 in the table (6-1). Reading is taken during fifth wash from fluid in

microchamber. The biosensor cleaned by radio frequency plasma plus oxygen chamber after each experiment.

Different concentrations of PSA have been immobilised. The biosensor first tested by a concentration of 2000 ng/ml. Biosensor showed good response change to PSA presence. Besides, perfect consistency and repeatability results exhibited by biosensor after several experiments. Biosensor response influenced by immobilised PSA. PSA immobilisation steps are shown in the table (6-1), steps 1-13.

6.4.7. Regeneration of PSA and calibration analysis

Regeneration process applied to the biosensor with six different nano concentrations of PSA solutions in order to perform a calibration analysis. Nevertheless, a regeneration process applied to biosensor using six different nano-concentrations of PSA, they are 6.125, 12.5, 25, 50, 75 and 100 ng/ml respectively. All utilised PSA concentrations are from one origin. The same sample is diluted to different concentrations by PBS only. Measurements are repeated four times, and an average of them is calculated. The analyte successfully removed, and ligand receptors are steadily reserved. Hereafter, sensor chip surface reused. Biosensor presented a constant pattern of responses over regeneration repeatability, figure (6-1-f).

The occurrence of distinctive response for each concentration measurement revealed biosensor ability to detect different nano-concentrations of PSA with a measurable change in both frequency and amplitude, and different concentrations have different dielectric constants and biosensor responses because electrical properties are depending on concentrations. Restore bio-sensing functionality realised correctly by a removal method using low pH buffer. Apply a low pH buffer will prompt Proteins to be positively charged and partially spread-out. Subsequently, binding sites counteract each other and disassociate similarly charged molecules. Biosensors are cleaned by low pH Glycine/HCl after each specific concentration test, a droplet of low pH Glycine is flushed into the microfluidic chamber for ten seconds followed by PBS-Tween cleanse for 15 seconds. Cleaning procedure repeated twice, the purpose of low pH Glycine/HCl addition is to change the charge of molecular interactions between PSA and antibody receptors from attractive forces to repulsive forces, leading to dissociation between PSA and antibody receptors. Therefore, end of covalent bindings between them releases PSA molecules. Accordingly, they can wash out, finally, chip surface and microfluidic chamber rinsed by a PBS buffer. Repeatability and consistency of regeneration process found to be satisfactory using the same device. Deterioration is not spotted on reprocessed biosensor over experiments repeatability. Therefore, the biosensor is stable and reusable. Purpose of cleaning practice after each concentration is to remove captured PSA molecules only. Nevertheless, preserving receptors antibodies and biosensor adequate detection environment. Furthermore,

maintenance ability of a functionalised surface to operating correctly. Reactive towards new PSA molecules and capture them directly after cleaning procedure. The regeneration process sequence is tabulated in steps 12-15, table (6-1), and regeneration part.

6.4.8. Biosensors non-functionalised

Biochemical control is realised from a part functionalised biosensor. Crosslinkers layer added, and the antibody layer is not added to placed crosslinkers. Subsequently, a blocking layer is added directly on a cross-linkers layer. A functionalised surface has only crosslinkers and no receptors to capture PSA molecules, figure1-g. No PSA should be immobilised on the surface, though, some molecules can react with other chemicals and connected to them, these portions can be neglected due to their insignificant influences. Chemical control performed over previous concentrations of PSA. Comparison of resulted measurements with standard biosensing data. Also, the same regeneration steps of PSA adding, removing and washing are applied in control experiments. Data are measured and collected instantaneously for all PSA concentrations. The control process sequence is showed in the table (6-1) of the control part. Response after each assembled biochemical layer compared with the previous layer, and a measurable change occurred after new steps.

6.5. Results of Lowpass Chebyshev based biosensor (2p)

Fabricated biosensor based on lowpass Chebyshev microstrip filter (2p) is tested first to investigate biochemical protocol. Results showed proper functionality and good trend regarding PSA detection. Hence, this biosensor tested on one concentration only equal to 2000ng/ml of PSA biomarker. Biosensor showed measurable response changes in functionalisation stage as shown in figure (6-2), and PSA analyte detection stage. Measured response at each stage of detection is shown in the table (6-2). Figure (6-3) showing PSA detection point.

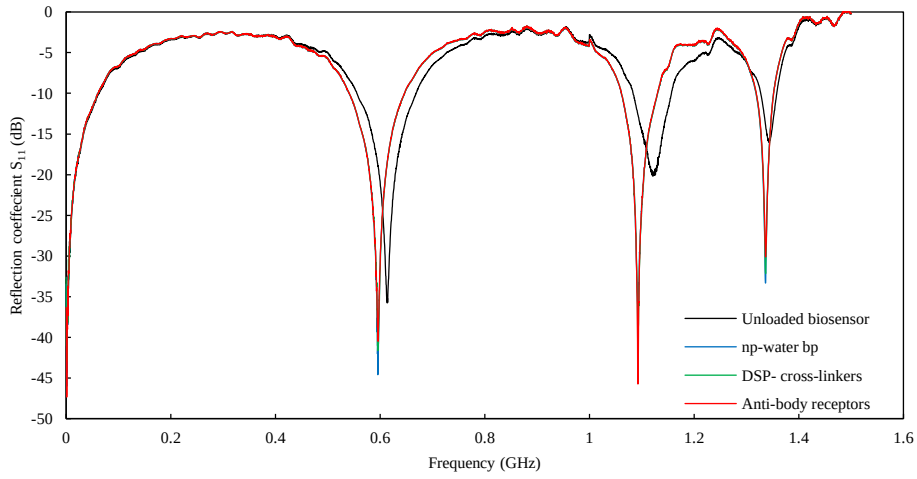

Figure 6-3. S_{11} responses of biosensor based on Chebyshev microstrip lowpass filter to functionalisation process.

Table 6-2. Measured points of PSA detection stages

Stage	*Frequency (GHz)*	*S_{11} (dB)*
base point	0.6087	-44.52
blocking point	0.6084	-44.57
PSA detection point	0.6087	-48.70

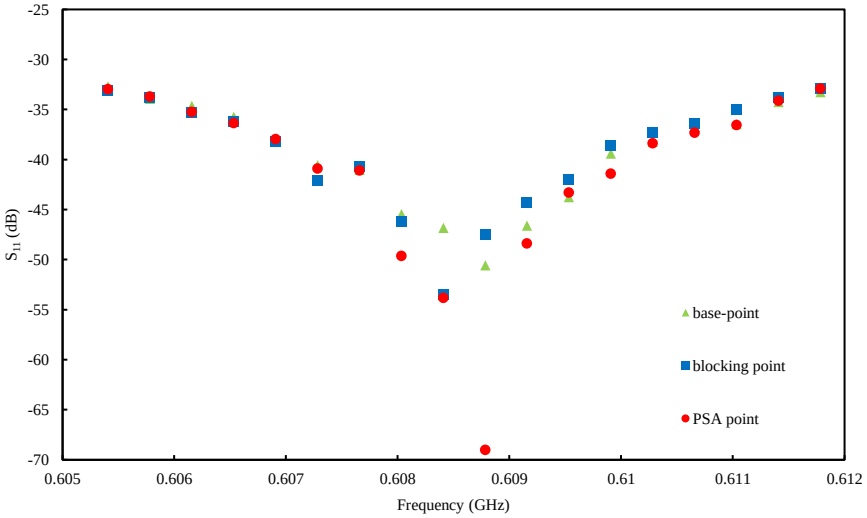

Figure 6-4. Resultant S_{11} scattering parameter for 2000ng/ml of PSA capture, blocking and measurement base point at 0.6 -0.612 GHz.

Characteristic dips in S_{11} parameter all demonstrated both an amplitude and frequency shift due to the functionalisation process. Moreover, Biosensor sensitivity towards PSA detection has been assessed. 2000ng/ml concentration of PSA is immobilised on a functionalized surface, captured by antibodies within 5-minute time. PSA presents lead to a surface change effect. Therefore, a signal change occurred in S_{11}. Results are shown in figure (6-4), curve fitting. PSA immobilisation showed the response to change of approximate 4.18 dB from blocking and base point of measurement. Measured frequency shift approximate value is 0.22760 MHz from base point measurement. Biosensor expressed on one high concentration and showed the technology is feasible. Results are proof of direct radio frequency detection principle.

6.6. Results of biosensor based on bandpass microstrip filter (1p)

The biosensor has three different responses to each added biochemical layer of functionalisation. Measurements are in the liquid. Nano-pure water (np-water) is measurements neutral fluid. New response pattern has a minimum dip occurred due to loaded np-water. Data collected at each characteristic surface layer realisation. Base-point referenced to other measured layers of cross-linkers and antibodies. Basepoint from unloaded free surface

biosensor measurement of amplitude and frequency. Although biosensor reserved new pattern response over newly added layers. It showed a definite shift in amplitude and frequency connected to each added biochemical layer. Responses compared to the reading of np-water base point. Dip amplitude and frequency are increased over addition. Biosensor indicated good sensitivity and recognition to biochemical changes during functionalisation.

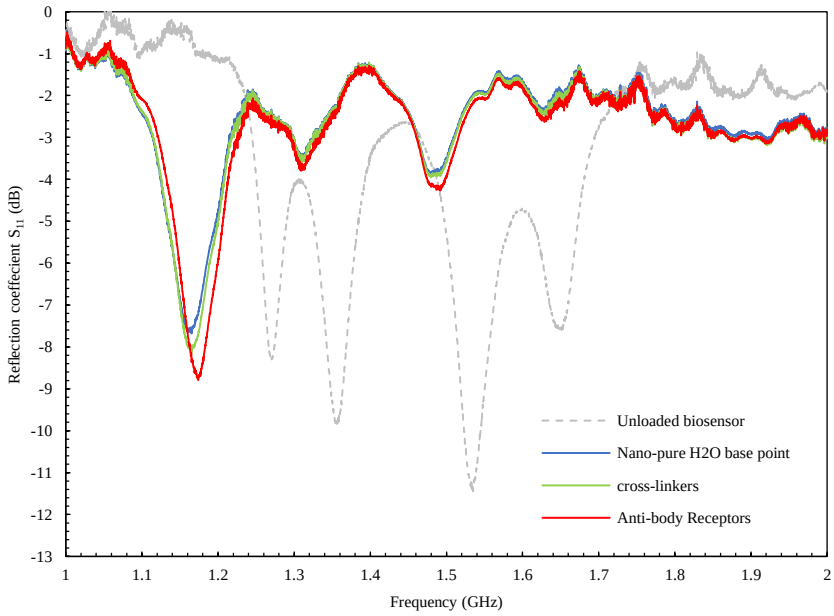

Figure 6-5. S_{11} response of surface functionalisation of biosensor based on PCB bandpass microstrip filter by DSP crosslinkers and antibody receptors to prepare it for detection

Results are shown in figure (6-5). Therefore, response change refers to succeed preparation of biosensor's surface by immobilised antibody receptors. Data analysis revealed values of frequency shift after anti-body is equal to 9.77802 MHz. Amplitude altered by 0.7 dB from cross-linkers values. Besides, 11.8 MHz and 1dB respectively from the np-water base point of an unloaded biosensor, table (6-3).

Table 6-3. Measured amplitude and frequency shifts of a functionalised biosensor

Stage	*Frequency shift (MHz)*	*S_{11} (dB)*
Nano-pure water	08.64	-7.617
DSP cross-linkers	11.80	-8.038
Anti-body receptors	09.78	-8.713

The biosensor is functionalised, results shown in figure (6-5) and prepared to be tested towards immobilisation of PSA molecules from different concentrations. A biosensor is utilised to test six different PSA concentrations. They are 6.125 ng/ml up to 100 ng/ml. Regeneration procedure is used to perform successive detection over altered concentrations. Four subsequent experiments are made to test regeneration process, started by immobilising a concentration of PSA equal to 6.125 ng/ml, tested and removed by regeneration process, followed by 12.5, 25, 50, 75 and 100 ng/ml of PSA. A zero concentration of PSA is used for comparison purpose. Results of regeneration showed a good detection ability of proposed biosensor, biosensor can distinguish and sense these different concentrations by using unchanged individually functionalised surface in a single experiment, four experiments of regeneration are performed, average data are shown in table (6-4), figures (6-6), (6-7), (6-8) and (6-9) showing analysed data of regeneration and control processes.

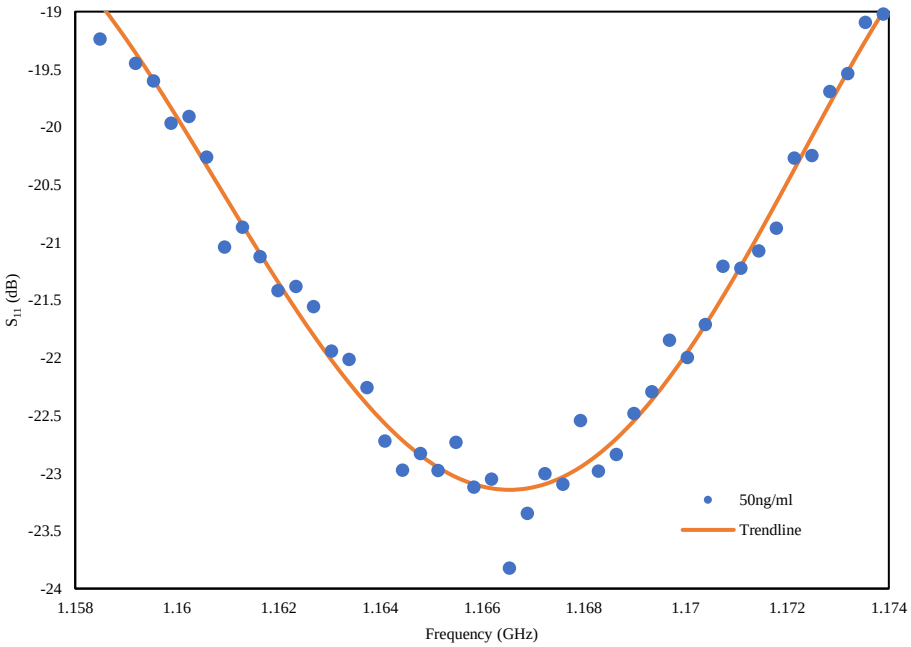

Figure 6-6. S_{11} curve fitting of 50ng/ml of PSA concentration in regeneration

Curve fitting of 50ng/ml concentration of PSA shown in figure (6-6), trend line showed in red, minimum point of the trendline is approximately equal to – 23.3 dB. Results above are an example of regeneration process data analysis.

Table 6-4. PSA immobilisation data of concentration, frequency and amplitude.

Conc. (ng/ml)	*Frequency (GHz)*	*S_{11} (dB)*
0	1.161	-20.87
6.25	1.155	-21.20
12.5	1.157	-21.60
25	1.164	-22.62
50	1.166	-23.23
75	1.166	-23.60
100	1.166	-24.31

Control results showed the reliability of the functionalised surface of the biosensor. Control biosensor reached saturation after 25 ng/ml of PSA keeping the same level of response over increased concentrations, figure (6-6) and table (6-5).

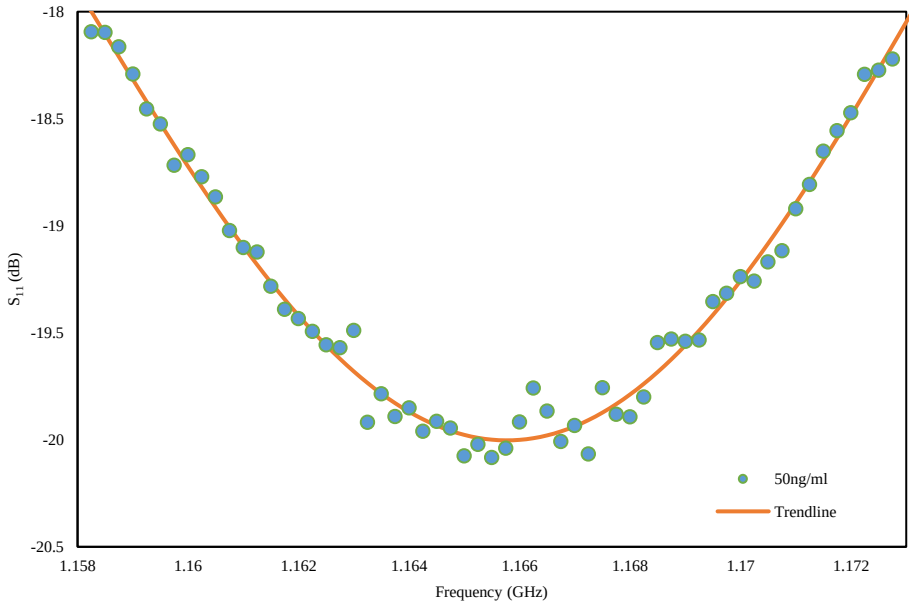

Figure 6-7. S_{11} curve fitting of 50ng/ml of PSA concentration in control process

An example of the control process showed in figure (6-7) belongs to 50ng/ml of PSA concentration. Fitted curve dip is approximately equal to -20 dB.

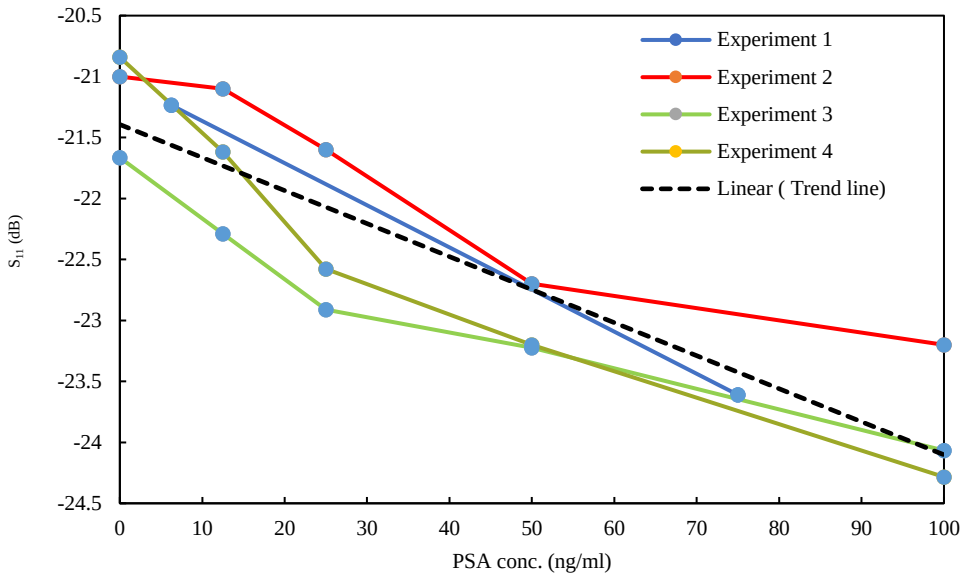

Figure 6-8. Reflection coefficient S_{11} values vs concentration, showing the linear trend of biosensor to PSA regeneration

There is an odd point in plot figure (6-8) at zero concentration. This pattern repeated in all biological experiments of biosensor based on bandpass microstrip filter. However, a linear change found between S_{11} and concentration change. This phenomenon needs further investigation. Notably, the addition of minimum concentration is enough to change the behaviour of the biosensor to a different shape.

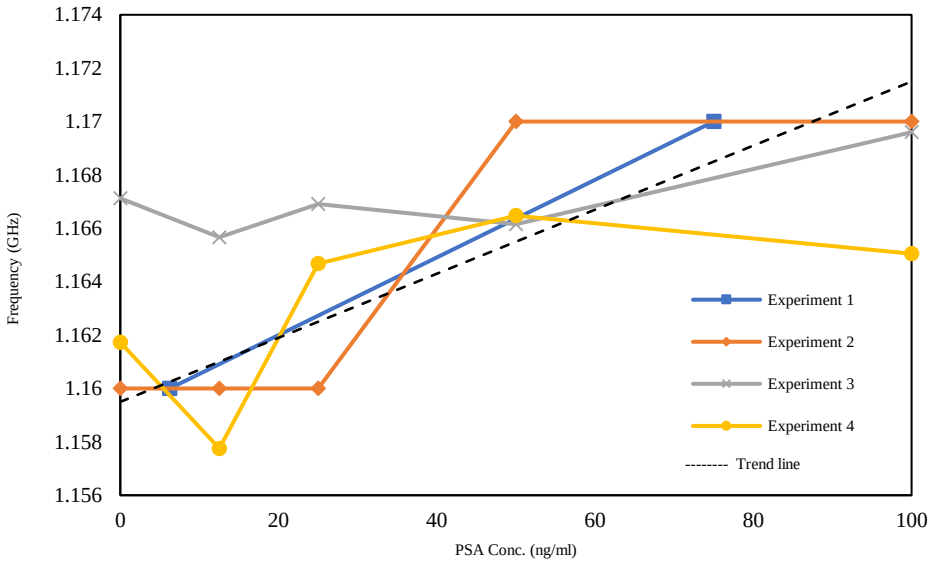

Figure 6-9. PSA regeneration, frequencies with concentration, linear trend of biosensor

Figure (6-9) showed a frequency change depending on PSA concentration change, according to this observation, no regular model obtained for frequency. However, a linear trend between frequency and concentration increment can be noticed as shown in the table (6-5). Further investigation is required to verify and define the relationship between frequency and analyte concentration.

Table 6-5. Resultant control surface, data of frequency, S_{11} and PSA concentrations

Conc. ng/ml	*Frequency (GHz)*	*S_{11}(dB)*
0	1.1546	-17.64
6.25	1.1561	-18.21
12.5	1.1624	-18.83
25	1.1636	-19.36
50	1.1656	-20.01
75	1.1655	-20.11
100	1.1656	-20.03

Biosensor showed response change signature of 3dB/100ng/ml. The frequency trend of approximate 10 MHz of first 20 ng/ml, which then sensed level over 20ng/ml. Potentially, it is better to use this biosensor to low concentrations. Further investigation for the consistency might be conducted in future. Block is shown relatively ineffective, that can be due to surface morphology. Gold micro-roughness caused blocking agent not to attach perfectly over the surface. Surface roughness caused the random distribution to BSA and activity loss. Therefore, potential non-specific binding occurred. Also, it might be due to golden surface roughness. Better fabrication in future might reduce the problem.

6.7. Results of biosensor based on Butterworth lowpass microstrip filter (3p)

Functionalised biosensor based on Butterworth lowpass microstrip filter is showed in figure (6-10), functionalised results of three different layers. Three dips at 0.706, 0.7033 and 0.711 GHz represent two added layers and np-water base point respectively.

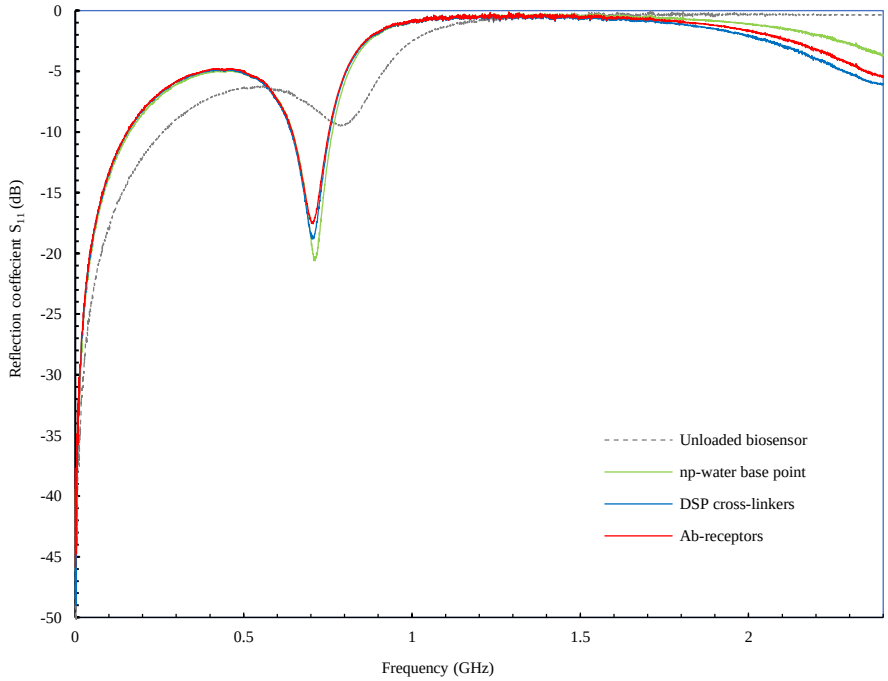

Figure 6-10. S_{11} of the functionalised biosensor of lowpass microstrip filter, functionalised vs unloaded biosensor's surface.

Addition of biochemical layers showed changes frequency and amplitude; biosensor showed different values of responses against different biochemical additions as illustrated in figure (6-11). Control measurement has experimented on lowpass biosensor. Results showed biosensor ability to differentiate among several nano concentrations of PSA biomarkers. Table (6-6) is showing analysed data of calculated non-functionalised. Calculated changes of frequency and amplitude due to different concentrations shown in figures (6-11) and (6-12). Biosensor showed a regular tendency towards detection of PSA nano-concentrations.

Table 6-6. Control data of lowpass Butterworth PCB biosensor.

conc. (ng/ml)	*Frequency (GHz)*	*S_{11} (dB)*
6.125	0.7559	-30.66
12.5	0.7558	-31.07
25	0.7562	-32.07
50	0.7553	-33.36
75	0.7548	-34.34
100	0.7544	-35.23

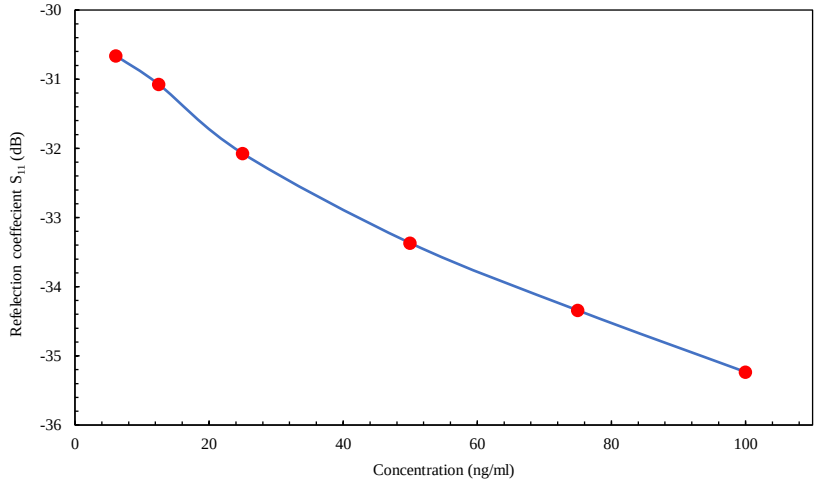

Figure 6-11. Analysed data of reflection coefficient S_{11} of several PSA concentrations from biosensor based on Butterworth lowpass microstrip filter

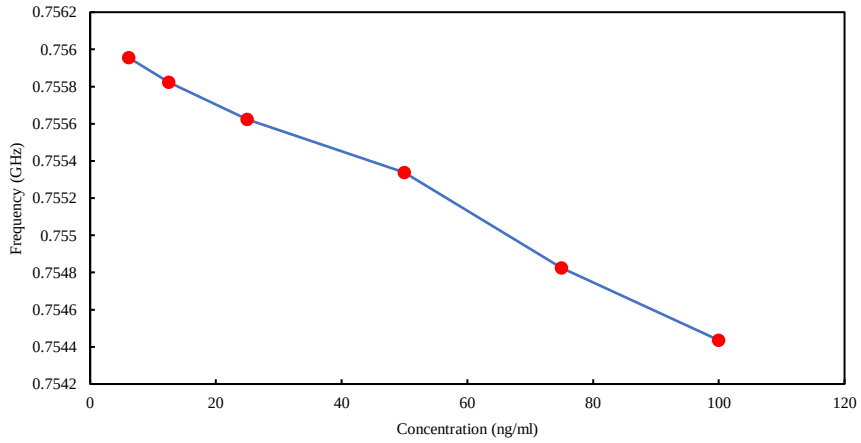

Figure 6-12. Analysed data of reflection coefficient S_{11} of several PSA concentrations from biosensor based on Butterworth lowpass microstrip filter

This biosensor showed a good responsive reaction to the material under test. Amplitude and frequency both changed. Frequency shift is 1Mhz/ 100ng/ml. Attenuation change is 1 dB. Limited time prevent further investigation of the biosensor.

6.8. Biosensor of lowpass microstrip filter on quartz (4q)

One of the fabricated biosensors on a quartz substrate and has an operational frequency up to 3 GHz tested. Four different nano-concentrations of PSA applied. They are 12.5, 25, 50 and 100 ng/ml. Biosensor showed promising detection reliability. Functioning and immobilising procedures are the same as previous biosensors on PCB. Data collected in real-time and at room temperature. The regeneration process is successfully applied to this biosensor. Measured and analysed data confirmed the detection ability of such biosensor.

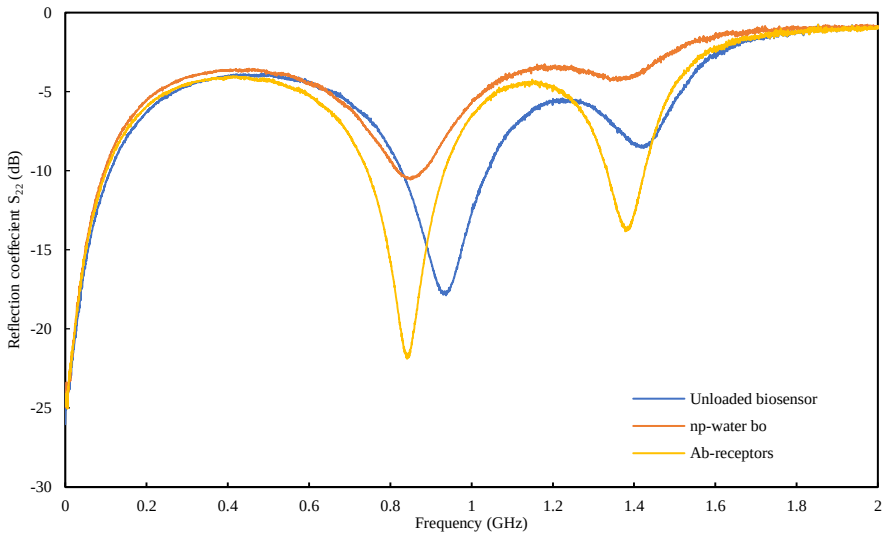

Figure 6-13. S_{22} of the Functioned biosensor of a quartz substrate, three different curves showed three stages of surface function of biosensor.

Biosensor based on quartz microstrip filter is functioned and prepared to biosensing test of PSA immobilisation. Functioning results are shown in figure (6-13). The biosensor tested over four PSA concentration, and they are 12.5, 25, 50 and 100 ng/ml. It is found that for this biosensor, it is better to use reflection coefficient S_{22} rather than S_{11}. Hence, S_{22} is more sensitive to the biochemical treatment of the surface. PSA capture is shown in figure (6-14). Signal changes from S_{22} are collected and analysed. Results are shown in the table (6-7). Despite changes detected, these changes of immobilised PSA are insignificant as previous devices. It might be related to gold layer thickness and distribution in comparison with microchamber height. Therefore, fluid height and loss from it.

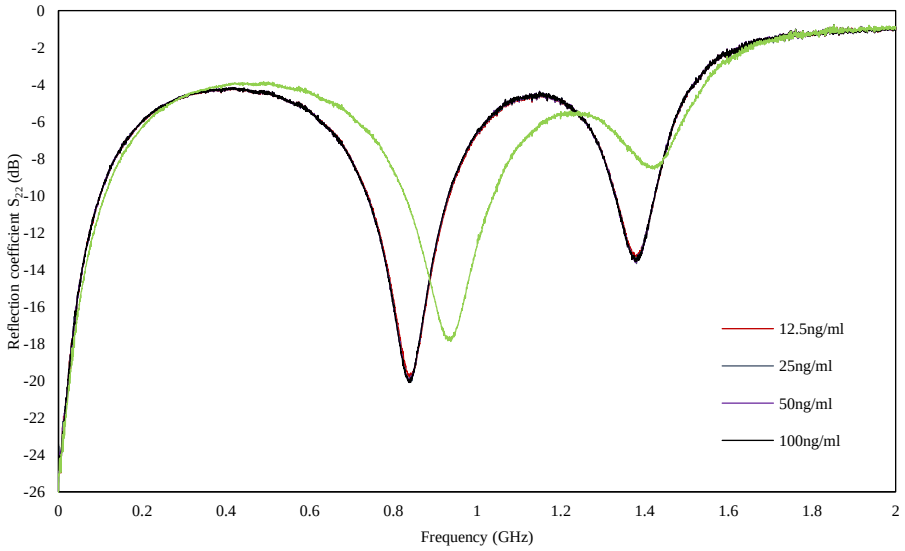

Figure 6-14. S_{22} signal changes due to four different PSA concentrations loaded to biosensor on quartz substrate.

Table 6-7. Control results of biosensor on quartz substrate (4q).

Conc. (ng/ml)	*Frequency (GHz)*	*Reflection coefficient S_{22} (dB)*
12	0.8403	-19.76
25	0.8384	-19.99
50	0.8380	-19.98
100	0.8381	-20.02

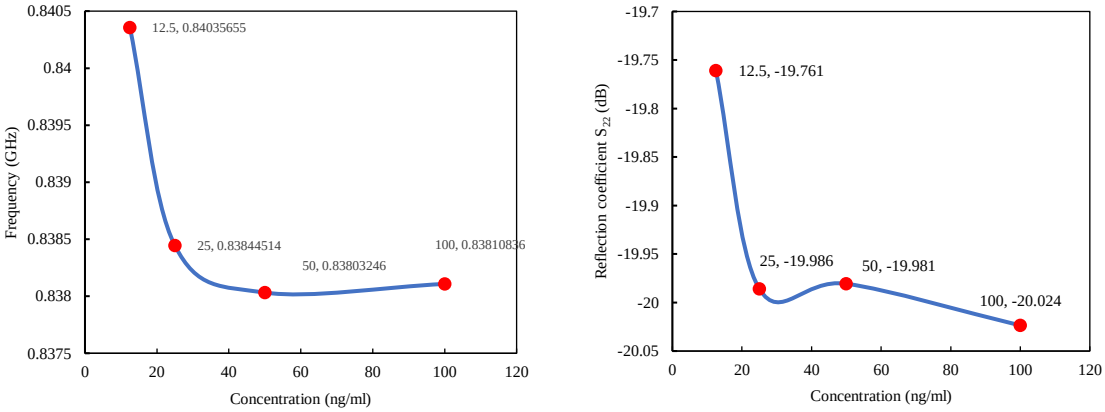

Figure 6-15. Comparisons between analysed data of control, frequency and amplitude changes vs concentrations loaded.

Biosensor showed that adding concentrations of analytes over 50 ng/ml drive biosensor to approach saturation state. Figure (6-15) showing the relationship between concentrations and frequency, as well as attenuation. Nevertheless, biosensor showed detection trend over low concentrations lower than 50ng/ml. Moreover, biosensor differentiated among different concentrations of analytes at this point. The saturation point is reached after 50ng/ml due to a thin surface of microstrips. Narrow field pack passing through the microchamber region and low applied power. Losses disruptive the signal. Biosensor showed little response variation due to smaller geometry and nano-thickness of a functionalised surface. Although, low skin depth might be a reason of weak response due to charges dispersion.

6.9. Bio-detection variables and responses

Regarding response indicator for all manufactured biosensors, scattering matrix identification used to characterise biosensors and their detection ability of measurements. One scattering parameter can be used to measure the biosensor response. Scattering parameters change their standard behaviour and express different response due to added materials. Nevertheless, for

biosensor based on (1p), (2p), and (3p) microstrip filters, reflection coefficient S_{11} is found to offer best responsive reaction due to the selected position of microchamber and biological samples nature. Microchamber is close to port one of microstrip filter. Whereas, for biosensor based on microstrip filter (4q) reflection coefficient S_{22} identified to be the best change measuring indicator. Fabricated biosensor systems are using a frequency-domain (FD) microwave measurement scheme. Hence, continues wave applied by the biosensing system on the test samples. Therefore, wave scattering parameters provide good measurement criteria. Proposed biosensors aimed at utilising reaction of non-labelled biomolecules under test with applied microwave at a high radio frequency in the biological medium.

6.9.1. Surface geometry

Structure of microstrip based biosensor is sensitive to mini factors changes. Small surface change stimulates significant electrical change due to the affected characteristic impedance. Added biochemical layers have changed edges geometry and dimensions of microstrips regarding constant influences of buffer fluids. Crosslinkers, receptors and PSA layers have definite nano-thickness, average from 3-50 nm. Their constructed biochemical layers have different electrical properties. Therefore, different mediums for travelling wave to passing through and reflected from them. Modify field lines coupling between microstrip resonators and a ground layer. Also, coupling between microstrips around gaps. Electromagnetic waves affected by mediums change. Moreover, propagation modes will have a specific change depending on properties of added materials. The thickness of layers influence propagation mode. Electromagnetic waves losses in microstrip filter can occur from dissipation of dielectric loss and conductance. Radiation can be neglected due to its minor value [142].

6.9.2. Interfaces impedance and Buffer influence

Presence of biochemical layers and fluids perturbed electromagnetic fields in sensitive regions. Provoke biosensor response pattern alternation. Constructed biochemical layers of functionalised biosensor produce an interface impedance. Condensed charges on the skin of microstrip affect reflection signal response. Therefore, interface impedance is altered due to immobilised biochemical layers of receptors and PSA. Electrical properties of deposited biomolecules yielded a change in medium electrical properties. The charge density of interface can partially disturb impedance at sensitive regions. Consequently, disturb passing signals. Furthermore, Buffer solutions disturb the electrical properties of the medium of the travelling wave. Reorienting dipoles of tissues absorb microwave energy of oscillating electric fields and emit it as dissipated heat. For biomolecules content, changing outward signal from inward one according to tissue nature and relative permittivity. Wave's energy is absorbed and scattered by

different biosensor's mediums. On the other hand, supportive fluids of biomolecules and analytes are mostly aqueous saline solutions. Electromagnetic wave suffers losses when propagating through these saline solutions, their significant volumes and coverage of a wide surface area of the biosensor. Henceforth, to enhance clarity of biosensor signal change. Few microliters of samples are utilised to fill a compact size microchamber over a limited surface area. The impact produced by a fluid is static and stable inside microchamber. After that, reduced signal losses and improved biosensor responses measurement. Some of the previous researches of biosensors based on a coplanar transmission line to detect biological cells and tissues. They utilised scattering parameters to indicate responses change, compared with this research.

A comparison of the results of this thesis and state of the art research of biomolecules detection showed that this research obtained good results of a change in frequency shift and amplitude changes. Table (6-7) refers to research by Y. Kim et al. [81]. C. Dalmay et al. [143]. L. Zhang et al. [73] and K. Jaruwongrungsee et al. [71].

Table 6-8. Comparison of some published studies and this study

Name	*Amplitude (dB)*	*Frequency (MHz)*	*Tested material*
Y. Kim et al.	0.80	---	Glucose oxidase (GOx)
C. Dalmay et al.	---	10	HaCaT
L.Y. Zhang et al.	0.32	40	SW620 cell
K. Jaruwongrungsee et al.	---	6.5	IgG
This study	1.50	11	PSA biomarker

Comparison results showed that this biosensor achieved amplitude change more than the others in 0.7 dB and frequency shift is 1 MHz larger for PSA detection.

6.10. Summary of Biochemical verification chapter

Biomedical test of biosensors is detailed in this chapter. Four microstrip based-biosensors have been designed and manufactured as shown in chapter 5. In terms of biological functionality, these biosensors were tested by biochemical experiments to evaluate their biological detectability. An experimental protocol to immobilise and detect different concentrations of PSA analytes is applied to these biosensors. Moreover, selectivity and reproducibility were investigated and validated. The PSA detection protocol consists of two stages, they are surface functionalisation and capturing of PSA analytes. Cross-linkers and antibodies were added to a

functionalised biosensor. The functionalised biosensors were then used to capture and immobilise different concentrations of PSA.

It was found out that the bandpass microstrip filter-based biosensor has bio-sensitivity higher than the other devices. The reason behind that is the separated microstrips and the fields between them, electrical fields travel from microstrip to another passing through a material under test and suffer dramatic change and this process strongly impacted biosensor response.

Comparison between tested biosensors revealed that all of them showed high response change due to the functionalisation process. However, they showed different responses to PSA immobilisation and detection. Lowpass microstrip filter on quartz-based biosensor showed a saturation trend for concentration above 50 ng/ml. This saturation could be due to thin microstrip layer which has a thickness equal to 350 nm, also small area exposure to analytes depending on micro-chambers design. Microstrip filter on FR-4 based biosensors showed a stable trend of responses towards increased concentrations of analyte. The higher thickness of microstrip filters might cause this steady trend. Further investigation needed to analyse biosensor behaviour and uncover the reasons for it is different responses.

Before the biochemical test, a biosensor was washed and dried. The unloaded biosensor measurement was taken at this level. In order to a functionalised biosensor, a chemical layer of cross-linkers was attached to the gold surface, to prepare it for the next step. After that, an antibody bio-receptors layer is added and connected to the linkers because they cannot attach directly to the golden surface. An antibody interacts, select, and catch targeted analyte. A biochemical blocking agent was added to block non-functional regions and prevent their undesirable effects. The biosensor is now biochemically functionalised towards selective immobilisation of PSA biomarkers. Different nano-concentration of PSA were utilised in the biochemical experiments. Biosensors showed LOD equal to 6.125 ng/ml of immobilised PSA.

However, biosensors recognised different concentrations of PSA. Several concentration levels were tested. Biosensing ability to detect several concentrations is critical in PSA detection and monitoring as mentioned early in chapter 1.

The Data of the biosensor’s responses calibrated according to PSA concentrations, data were imported to Matlab for analysis and curve fitting. The analysed data showed potential healthcare application of the designed biosensor.

Chapter 7. Conclusions and future work

7.1. Introduction

This chapter starts by summarising the outline of the thesis and giving brief conclusions of the previous chapters. The limitation of the research introduced as well as recommendations of the further work are also highlighted, and future work is recommended. Thesis distribution is addressed including published, contributed and planned publications.

Several problems and factors were included in cancerous diseases diagnosis and monitoring. Therefore, the research trend of biosensors is overgrowing since it started years ago to enhance diagnosis and treatment. Despite the fact of medical progress and different biosensing methods including radio frequency-based biosensors being studied, uncomplicated and practical diagnostic tools are not available commercially. From this point, a hypothesis to design new biosensor based on existing technology of microstrip filter is introduced and realised in this thesis. This biosensor features simplicity and other required properties such as cost-effective production. The produced biosensor consists of a microstrip filter and microfluidics. Regarding biosensor fabrication, microfluidic is integrated with microstrip filter to carry liquids of biological materials under test.

This thesis used microstrip filter-based biosensor to approach possible solutions to previously mentioned problems. Microstrip filters featured simple geometry of transmission line. Moreover, a low range of operating frequency less than 3 GHz used. Miniaturised and disposable versions of biosensor were created. The produced biosensor targeted PSA analyte detection in different concentrations.

Biosensor realisation starts with microstrip filters design through modelling and fabrication. Regarding design, several parameters and their values were considered, such as operational frequencies. Microstrip filters design was successfully modified to fit biosensor functionality. Five different microstrip filters designed, plus two reduced size microstrip filters which designed towards achieving a miniaturised biosensor. In order to realise the targeted biosensor, the fabricated microstrip filters were integrated with microfluidics.

Biosensor functionalised by self-assembled biochemical layers of receptors provided analytes capturing surface and created biosensor selectivity. Measurements were achieved by means of scattering parameters of the travelling electromagnetic waves. This results in a signal change that is induced by analyte immobilisation, it was found that this signal change is proportional to the concentration of immobilised analytes. Minimum tested PSA concentration is 6.125 ng/ml, and 500 ng/ml is maximum concentration. Biochemical tests supported the assumption of microstrip biosensor functionality. Label-free detection of a Prostate Specific

Antigen was implemented, where the PSA molecules were immobilised on a functionalized surface populated with antibodies receptors. Frequency shift and signal attenuation occurred due to immobilised analytes. One biochemical protocol was employed to test all fabricated biosensors.

7.2. Conclusions

7.2.1. Biosensors research

Biosensors research was reviewed, and evaluation of limitations and advantages was expressed. The resultant is that, although reasonable progress has been realised, biosensors field are still inside research laboratories only. On the other hand, radio frequency biosensor is a new trend and showed unique properties in healthcare applications. RF biosensing by using active components can enhance passive RF based biosensors.

7.2.2. Radio frequency-based biosensor types

Radio frequency-based biosensors are majorly focused on coplanar waveguides with operational frequencies that are as high up to 45 GHz. Split ring resonator and hairpin resonators in the form of stepped impedance resonator are used, and other electrical components enhance some of them. Regarding utilisation, they are applied to detect different biomolecules and glucose levels. However, no published research about using low-frequency microstrip filter based biosensor regarding PSA analyte detection. Nevertheless, this is the first time PSA is tested and detected by radio frequency-based biosensor.

7.2.3. Defining the research problem

The scientific motivation, problems, and aim of this work was defined to find a solution to a medical issue by radio frequency biosensor. Additionally, it expressed the significant contribution for the utilisation of radio frequency microstrip filter of lower than 3 GHz frequency as a biosensor to detect PSA biomarkers.

7.2.4. Building the biosensor

Modelling investigations of the microstrip filters, the currents patterns were extracted in order to recognise the current rich area because they are appropriate for biosensing. Although some microstrip dimensions were adjusted, the microstrip filters are verified, it is found that changing these dimensions has no impact on the microstrip filter's response.

Two methods were used to manufacture microstrip filters; a printed circuit board (PCB) and clean room evaporation. Lowpass, V-shaped bandpass and reduced size microstrip filters were fabricated on a quartz substrate by clean room method. VNAs was used to test and validate the fabricated devices. The result of VNA measurements showed that the microstrip filters were

operating correctly according to design parameters except for reduced size microstrip filters. The validity of them discussed and problems defined.

A new method was invented to attach microfluidics and microchambers to microstrip surfaces. Microfluidics and microchambers designed to cover specific regions only to enhance the sensitivity of the biosensors. A unique adequate geometry of microchamber was made for each microstrip filter to exploit the regions on the edges of microstrips where high fields densities are found.

7.2.5. Testing the biosensor

The biomedical test of the assembled biosensors is presented to verify their detection functionality and selectivity against targeted biological samples. Four microstrip based-biosensors were tested by biochemical experiments to evaluate their biological detectability. Experimental protocol for the selection and detection of the immobilise PSA analytes was executed here as well. The selectivity and reproducibility were investigated and validated. The detection protocol consists of surface functionalisation to create selectivity and capturing of PSA analytes. Cross-linkers and antibodies used to functionalise the Biosensor.

In this research, it is found out that the proposed biosensors can detect different nano-concentration of PSA analytes. The results of biosensing showed LOD equal to 6.125 ng/ml of PSA. However, the biosensors recognised different concentrations level s of PSA.

The resultant data were discussed and analysed. The data also imported to Matlab for analysis and curve fitting. The analysed data showed potential healthcare application of the proposed biosensor. This Biosensors response calibrated according to PSA concentrations.

7.3. Outcome and limitations

Seven microstrip filters were produced, two of them were reduced size microstrip filters with microstrip thickness equal to 350 nm towards miniaturised biosensor. All microstrip filters designs were modelled and analysed to be fabricated. The fabrication schemes were planned and implemented by two approaches, printed circuit board on FR-4 dielectric substrate and clean room evaporation on quartz dielectric substrate. The Fabricated microstrip filters were tested and verified by VNA measurements. The flat top of the microstrip surface enabled the integration of microfluidics and microchambers on it. Microfluidics made by laser machining. Double-Sided sticky tape was employed to integrate microfluidics with microstrip filters. Consequently, an appropriate form of the biosensor was completed and examined.

A bio-sensing function of the fabricated biosensors is experimentally tested. The function of the proposed biosensor is to select, capture and sense the targeted biomolecules. The results were discussed and analysed thoroughly. The outcomes showed that the biosensors could select

and detect targeted analytes. It is important to know that the right position of microfluidic and volume of used solutions are essential factors in biosensing measurements.

In this thesis, utilising microstrip filter as a biosensor proved to be feasible within frequency range less than 3 GHz. Therefore, biosensors created successfully detected the targeted biomolecules with high selectivity. A detectable change observed with each biochemical change. Moreover, a measurable change occurred from different analyte concentrations. The devices showed different behaviour against different biochemical sample concentration.

Manufacturing defects and other sources of errors reduced the signal change clarity. More so, it is found that the volume of liquids affects signal change, reduced volumes improved signal change clarity, as well as the soldering of SMA connectors, might affect the signals. The results indicated the biosensing capability of the proposed biosensor despite the defects and limitations of manufacturing and measurement devices. The proposed device showed a good trend towards biosensing functionality.

Collected data from biosensor for the verification of results showed the possible feasibility of radio frequency biosensing and healthcare applications.

7.4. Future work

7.4.1. Biosensor optimisation

The microstrip filters and biosensor design need to be optimised to improve sensitivity towards sensing of less than 1 ng/ml PSA concentration. Different algorithms can be used for microstrip optimisation, for example, Genetic Algorithms (GA). Equivalent model of a transmission line can be used in the modelling process while having in mind that bandwidth and scattering parameters influence the cost function. In the same manner, the sensitivity of biosensor can be optimised according to microstrip design. Therefore, optimisation of biosensor design and architecture is possible by Taguchi method. Improve surface quality and flatness will promote the biosensor sensitivity, this can be done by a very flat substrate and thin microstrip layer (few nano-thick).

Size reduction is another recommended work of the optimisation process. Reduced biosensor size will reduce the sample volume.

New materials can be applied such as graphene to study their functionality. Improve surface quality and fabrication to make it more amenable to biochemical processes, leading to a more successful bio-detection.

Nanotechnology was applied to investigate the feasibility of self-functionalised surfaces by built-in capture mechanism. A self-functionalised surface was Prepared to enable the

biosensor to work directly. The integration of biomaterials with selected surface regions to create a self-functionalised biosensor is investigated, the reason is to prevent the preparation and modification of the biochemical process, therefore, providing a direct test induction. Finally, microstrip based sensor can be tested as an industrial sensor with different materials.

7.4.2. Experimental investigations and modelling

The Biosensor detection level is less than 10 ng/ml concentration. Future investigation is the aim to detect 1 ng/ml or less concentration of analytes, as well as to evaluate a lower limit of detection. Determine the maximum sensitivity of the biosensor by defining a measurement limit of change in concentration for a targeted analyte. Furthermore, Different type of biomolecules can be applied.

The analysis of field interaction with biological materials can provide more information about biomolecule's behaviour and their electrical properties. The deduced information was then used to model and simulate biomolecules under fields. This, therefore, promotes microstrip biosensor design and properties towards improved biosensing. Modelling use finite element method and HFSS Ansys software in different conditions.

The collected data of the biosensor responses due to the presence of a biological analyte can be used to model responsive behaviour of the sensor. The Analyse data might provide the guide to the possible synthesis of new design, as well as biological molecules behaviour. Biosensor models will provide more information about biosensing performance and bio-cells behaviour under electromagnetic fields and how they react. Moreover, this investigation can be used to find possible new industrial applications of the sensor such as remote detection of metal defects and cracks.

7.4.3. Commercialisation of microstrip-based sensor

Since the microstrip-based biosensor design was realised, therefore, commercialisation plans are essential. Final design requirements, properties, challenges, costs, a timeline of production and risks identification; all these factors should be addressed in the commercialisation process. Some of the desired biosensor properties are; ability to measure in different conditions, disinfected, disposable, ease of integration, consume low power, safe and easy to use.

Providing commercial plan will prompt sensor research. Therefore, considering different applications with the efforts towards the final form of microwave-based sensors. Finally, a microstrip-based sensor can be employed in industry, for example, gas sensing.

Dissemination

Parts of the work accomplished throughout the time of conducting the research have been presented in two international conferences:

- High frequency biosensor based on a side coupled microstrip band pass filter (May 2017, Reva Del Garda, Italy)
- High radio frequency biosensor for a nano-concentration detection of the label free Prostate Specific Antigen cancerous cells (June 2017, Tampere, Finland)

Biosensor based on lowpass microstrip filter that characterised by Chebyshev response was made into a paper published in the proceedings of joint Conference of the European Medical and Biological Engineering Conference (EMBEC) and the Nordic-Baltic Conference on Biomedical Engineering and Medical Physics (NBC), Tampere, Finland, June 2017 [144].

References

1. Halpern, J.A., et al., *Prognostic Significance of Digital Rectal Examination and Prostate Specific Antigen in the Prostate, Lung, Colorectal and Ovarian (PLCO) Cancer Screening Arm.* The Journal of Urology. **197**(2): p. 363-368.
2. Mehrotra, P., *Biosensors and their applications – A review.* Journal of Oral Biology and Craniofacial Research, 2016. **6**(2): p. 153-159.
3. Perret, E., *Radio Frequency Identification and Sensors : from RFID to Chipless RFID*. 2014, London: ISTE-Wiley.
4. Tofighi, M.-R., et al., *Principles and applications of RF/microwave in healthcare and biosensing*. 2017: Amsterdam ; Boston : Elsevier/AP, Academic Press is an imprint of Elsevier.
5. Vander Vorst, A., et al., *RF/Microwave Interaction with Biological Tissues.* Medical Physics, 2007. **34**(2).
6. Chien, J.C., *Advanced High-Frequency Measurement Techniques for Electrical and Biological Characterization in CMOS.* 2015.
7. Rejinold, N.S., R. Jayakumar, and Y.-C. Kim, *Radio frequency responsive nano-biomaterials for cancer therapy.* Journal of Controlled Release, 2015. **204**: p. 85-97.
8. Zakharov, A., S. Rozenko, and N. Zakharova, *Microstrip bandpass filters on substrates with high permittivities.* Journal of Communications Technology and Electronics, 2012. **57**(3): p. 342-351.
9. Xu, J., et al., *Compact Microstrip Filter With Third-Order Quasi-Elliptic Bandpass Response.* Access, IEEE, 2018. **6**: p. 63375-63381.
10. Xiaolin Fan, P.D. and P.D. Laforge, *Design of a chebyshev microstrip filter using the reflected group delay method and the aggressive space mapping technique*. 2015. p. 1-4.
11. Xiao, F., H. Gong, and Y. Zhang, *Optimal design of third-order microstrip bandpass filters by direct synthesis technique (DST.* International Journal of Circuit Theory and Applications, 2018. **46**(10): p. 1827-1837.
12. Sen, C., et al., *An Alternate Circuit for Narrow-Bandpass Elliptic Microstrip Filter Design.* Microwave and Wireless Components Letters, IEEE, 2017. **27**(7): p. 624-626.
13. Rajput, A., K. Patel, and A. Birwal, *Compact microstrip low pass filter design using U-shaped folded high-impedance line.* Microwave and Optical Technology Letters, 2018. **60**(7): p. 1812-1815.
14. Peng, Y. and W.X. Zhang, *Compact sub-wavelength microstrip band-reject filter based on inter-digital capacitance loaded loop resonators.* Microwave and Optical Technology Letters, 2010. **52**(1): p. 166-169.
15. Peng, Y. and W.-X. Zhang, *MICROSTRIP BAND-REJECT FILTER BASED ON INTER-DIGITAL CAPACITANCE LOADED LOOP RESONATORS.* Progress In Electromagnetics Research Letters, 2009. **8**: p. 93-103.
16. Mo, J., et al., *High-selectivity microstrip bandpass filters using stub-loaded resonators.* Optik - International Journal for Light and Electron Optics, 2015. **126**(21): p. 2844-2847.
17. Mezaal, Y.S., J.K. Ali, and H.T. Eyyuboglu, *Miniaturised microstrip bandpass filters based on Moore fractal geometry.* International Journal of Electronics, 2015. **102**(8): p. 1306-1319.
18. Maharjan, R. and N.-Y. Kim, *Microstrip Bandpass Filters Using Window Hairpin Resonator and T-Feeder Coupling Lines.* Arabian Journal for Science and Engineering, 2014. **39**(5): p. 3989-3997.
19. Kong, W., et al., *Optimization design of fragment-type microstrip filter using boundary-based filtering operator.* IEICE Electronics Express, 2018. **15**(15): p. 20180499-20180499.

20. Kant, R. and N. Gupta, *Design and implementation of inverse legendre microstrip filter.* Microwave and Optical Technology Letters, 2017. **59**(1): p. 69-73.
21. Inclan-Sanchez, L., et al., *New EBG-filter design in inverted microstrip gap waveguide technology*. 2017. p. 1663-1664.
22. Gorur, A.K., et al., *Dual-mode dual-band microstrip bandstop filter design with independently tunable center frequencies.* Microwave and Optical Technology Letters, 2017. **59**(10): p. 2542-2547.
23. Fallahzadeh, S., A. Akbarzadeh, and M. Tayarani, *Spurious Response Suppression in Microstrip Bandpass Filters Using Defected Microstrip Structures.* Electromagnetics, 2012. **32**(7): p. 389-400.
24. Chakravorty, P. and D. Mandal, *Microstrip bandpass filter design using split-path method and optimized curvature corrections.* International Journal of Numerical Modelling: Electronic Networks, Devices and Fields, 2016. **29**(3): p. 520-529.
25. Cai, C., et al., *A New Approach to Design Microstrip Wideband Balun Bandpass Filter.* Microwave and Wireless Components Letters, IEEE, 2016. **26**(2): p. 116-118.
26. Avinash, K.G. and I.S. Rao, *Highly Selective Dual-Mode Microstrip Bandpass Filters Using Triangular Patch Resonators.* Advanced Electromagnetics, 2017. **6**(1): p. 77-84.
27. Zougagh, M. and Á. Ríos, *Micro-electromechanical sensors in the analytical field.* The Analyst, 2009. **134**(7): p. 1274-1290.
28. Alodhayb, A., et al., *A 16-microcantilever array sensing system for the rapid and simultaneous detection of analyte.* Sensors & Actuators: B. Chemical, 2016. **237**(C): p. 459-469.
29. Huang, L.-S., et al., *Detection of the antiepileptic drug phenytoin using a single free-standing piezoresistive microcantilever for therapeutic drug monitoring.* Biosensors and Bioelectronics, 2014. **59**(1): p. 233-238.
30. Kim, H.H., et al., *Highly sensitive microcantilever biosensors with enhanced sensitivity for detection of human papilloma virus infection.* Sensors & Actuators: B. Chemical, 2015. **221**(C): p. 1372-1383.
31. Chen, Y., et al., *Bio/chemical detection in liquid with self-sensing Pr-Oxi-Lever (piezo-resistive SiO 2 cantilever) sensors.* Microelectronic Engineering, 2010. **87**(12): p. 2468-2474.
32. Wu, G., et al., *Bioassay of prostate-specific antigen (PSA) using microcantilevers.* Nature Biotechnology, 2001. **19**(9): p. 856-60.
33. Kirstein, K.U., et al., *Cantilever-Based Biosensors in CMOS Technology.* 2007.
34. Huang, Y.-J., et al., *A CMOS Cantilever-Based Label-Free DNA SoC With Improved Sensitivity for Hepatitis B Virus Detection.* IEEE Transactions on Biomedical Circuits and Systems, 2013. **7**(6): p. 820-831.
35. Bausells, J., *Piezoresistive cantilevers for nanomechanical sensing.* Microelectronic Engineering, 2015. **145**(C): p. 9-20.
36. Maduraiveeran, G., M. Sasidharan, and V. Ganesan, *Electrochemical sensor and biosensor platforms based on advanced nanomaterials for biological and biomedical applications.* Biosensors and Bioelectronics, 2018. **103**: p. 113-129.
37. Uniyal, S. and R.K. Sharma, *Technological advancement in electrochemical biosensor based detection of Organophosphate pesticide chlorpyrifos in the environment: A review of status and prospects.* Biosensors and Bioelectronics, 2018. **116**: p. 37-50.
38. Naderi Asrami, P., et al., *A novel impedimetric glucose biosensor based on immobilized glucose oxidase on a CuO-Chitosan nanobiocomposite modified FTO electrode.* International Journal of Biological Macromolecules, 2018. **118**(Pt A): p. 649-660.
39. Chung, Y.-K., et al., *An electrical biosensor for the detection of circulating tumor cells.* Biosensors and Bioelectronics, 2011. **26**(5): p. 2520-2526.
40. Luo, X. and J.J. Davis, *Electrical biosensors and the label free detection of protein disease biomarkers.* Chemical Society Reviews, 2013. **42**(13): p. 5944-5962.

41. Li, J., et al., *Red blood cells aggregability measurement of coagulating blood in extracorporeal circulation system with multiple-frequency electrical impedance spectroscopy.* Biosensors and Bioelectronics, 2018. **112**: p. 79-85.
42. Pihikova, D., et al., *Aberrant sialylation of a prostate-specific antigen: Electrochemical label-free glycoprofiling in prostate cancer serum samples.* Analytica Chimica Acta, 2016. **934**: p. 72-79.
43. Kaur, G., M. Tomar, and V. Gupta, *Development of a microfluidic electrochemical biosensor: Prospect for point-of-care cholesterol monitoring.* Sensors & Actuators: B. Chemical, 2018. **261**: p. 460-466.
44. Suresh, L., et al., *Development of an electrochemical immunosensor based on gold nanoparticles incorporated chitosan biopolymer nanocomposite film for the detection of prostate cancer using PSA as biomarker.* Enzyme and Microbial Technology, 2018. **112**: p. 43-51.
45. Hu, F., et al., *An electrochemical biosensor for sensitive detection of microRNAs based on target-recycled non-enzymatic amplification.* Sensors & Actuators: B. Chemical, 2018. **271**: p. 15-23.
46. Qi, H., et al., *Isothermal exponential amplification techniques: From basic principles to applications in electrochemical biosensors.* Biosensors and Bioelectronics, 2018. **110**: p. 207-217.
47. Shin, K.S., et al., *Sensitivity Enhancement of Bead-based Electrochemical Impedance Spectroscopy (BEIS) biosensor by electric field-focusing in microwells.* Biosensors and Bioelectronics, 2016. **85**: p. 16-24.
48. Jiang, Y., et al., *Silver nanoparticles modified two-dimensional transition metal carbides as nanocarriers to fabricate acetycholinesterase-based electrochemical biosensor.* Chemical Engineering Journal, 2018. **339**: p. 547-556.
49. Keiser, G., *Biophotonics : concepts to applications*. 2016: Singapore : Springer.
50. Espina Palanco, M., et al., *Optical Biosensors to Explore Biological Systems*. 2016. p. 638a-639a.
51. Carrascosa, L.G., C.S. Huertas, and L.M. Lechuga, *Prospects of optical biosensors for emerging label-free RNA analysis.* Trends in Analytical Chemistry, 2016. **80**(C): p. 177-189.
52. Sansone, L., et al., *Label-free optical biosensing at femtomolar detection limit.* Sensors & Actuators: B. Chemical, 2018. **255**(P1): p. 1097-1104.
53. Farkas, E., et al., *Label-free optical biosensor for real-time monitoring the cytotoxicity of xenobiotics: A proof of principle study on glyphosate.* Journal of Hazardous Materials, 2018. **351**: p. 80-89.
54. Khansili, N., G. Rattu, and P.M. Krishna, *Label-free optical biosensors for food and biological sensor applications.* Sensors & Actuators: B. Chemical, 2018. **265**: p. 35-49.
55. Yoo, S.M. and S.Y. Lee, *Optical Biosensors for the Detection of Pathogenic Microorganisms.* Trends in Biotechnology, 2016. **34**(1): p. 7-25.
56. Wang, Q. and W.-M. Zhao, *Optical methods of antibiotic residues detections: A comprehensive review.* Sensors & Actuators: B. Chemical, 2018. **269**: p. 238-256.
57. Santangelo, M.F., et al., *SiPM as miniaturised optical biosensor for DNA-microarray applications.* Sensing and Bio-Sensing Research, 2015. **6**(C): p. 95-98.
58. Hornyak, R., M. Lewis, and B. Sankaranarayan, *Radio frequency identification–enabled capabilities in a healthcare context: An exploratory study.* Health Informatics Journal, 2016. **22**(3): p. 562-578.
59. Rosen, A., M.A. Stuchly, and A. Vander Vorst, *Applications of RF/microwaves in medicine.* Microwave Theory and Techniques, IEEE Transactions on, 2002. **50**(3): p. 963-974.

60. Gudkov, A.G., et al., *Prospects for Application of Radio-Frequency Identification Technology with Passive Tags in Invasive Biosensor Systems.* Biomedical Engineering, 2015. **49**(2): p. 98-101.
61. Stuchly, M.A., et al., *Dielectric properties of animal tissues in vivo at radio and microwave frequencies: Comparison between species.* Physics in Medicine and Biology, 1982. **27**(7): p. 927-936.
62. Garcia-Banos, B., et al., *Enhancement of Sensitivity of Microwave Planar Sensors With EBG Structures.* IEEE Sensors Journal, 2006. **6**(6): p. 1518-1522.
63. Costanzo, S., *Non-Invasive Microwave Sensors for Biomedical Applications: New Design Perspectives.* Radioengineering, 2017. **26**(2): p. 406-410.
64. Guha, S., F.I. Jamal, and C. Wenger, *A Review on Passive and Integrated Near-Field Microwave Biosensors.* Biosensors, 2017. **7**(4).
65. Liu, C.-F., M.-H. Wang, and L.-S. Jang, *Microfluidics-based hairpin resonator biosensor for biological cell detection.* Sensors & Actuators: B. Chemical, 2018. **263**: p. 129-136.
66. Nerguizian, V., et al., *Characterization of several cancer cell lines at microwave frequencies.* Measurement, 2017. **109**: p. 354-358.
67. Hanai, T., K. Asami, and N. Koizumi, *Dielectric Theory of Concentrated Suspensions of Shell-Spheres in Particular Reference to the Analysis of Biological Cell Suspensions*. Vol. 57. 1979.
68. Ji, J.-H., et al., *Fundamental monomeric biomaterial diagnostics by radio frequency signal analysis.* Biosensors and Bioelectronics, 2016. **82**: p. 255-261.
69. Wellenzohn, M. and M. Brandl, *A Theoretical Design of a Biosensor Device Based on Split Ring Resonators for Operation in the Microwave Regime.* Procedia Engineering, 2015. **120**: p. 865-869.
70. Sberveglieri, G., et al., *EUROSENSORS 2014, the 28th European Conference on Solid-State TransducersDevelopment of High Frequency Microfluidic Biosensors for Intracellular Analysis.* Procedia Engineering, 2014. **87**: p. 54-57.
71. Jaruwongrungsee, K., et al., *Microfluidic-based Split-Ring-Resonator Sensor for Real-time and Label-free Biosensing.* Procedia Engineering, 2015. **120**: p. 163-166.
72. Chen, Y.-F., et al., *40 GHz RF biosensor based on microwave coplanar waveguide transmission line for cancer cells (HepG2) dielectric characterization.* Biosensors and Bioelectronics, 2014. **61**(C): p. 417-421.
73. Zhang, L.Y., et al., *Discrimination of colorectal cancer cell lines using microwave biosensors.* Sensors & Actuators: A. Physical, 2014. **216**: p. 405-416.
74. Lee, H.-J., et al., *A planar split-ring resonator-based microwave biosensor for label-free detection of biomolecules.* Sensors and Actuators B: Chemical, 2012. **169**: p. 26-31.
75. Dalmay, C., et al., *On-Chip Biosensors Based on Microwave Detection for Cell Scale Investigations*, in *Biomedical Engineering Systems and Technologies: International Joint Conference, BIOSTEC 2009 Porto, Portugal, January 14-17, 2009, Revised Selected Papers*, A. Fred, J. Filipe, and H. Gamboa, Editors. 2010, Springer Berlin Heidelberg: Berlin, Heidelberg. p. 51-63.
76. Dalmay, C., et al., *Label-free RF biosensors for human cell dielectric spectroscopy.* International Journal of Microwave and Wireless Technologies, 2009. **1**(Special Issue 06): p. 497-504.
77. Dalmay, C., et al., *Ultra sensitive biosensor based on impedance spectroscopy at microwave frequencies for cell scale analysis.* Sensors & Actuators: A. Physical, 2010. **162**(2): p. 189-197.
78. Grenier, K., et al. *New broadband and contact less RF / microfluidic sensor dedicated to bioengineering*. in *Microwave Symposium Digest, 2009. MTT '09. IEEE MTT-S International*. 2009.

79. Sanghyun Seo, T., et al., *High frequency wideband permittivity measurements of biological substances using coplanar waveguides and application to cell suspensions*. 2008. p. 915-918.
80. Chien, J.H., et al., *Protein detection using a radio frequency biosensor with amplified gold nanoparticles.* Applied Physics Letters, 2007. **91**(14).
81. Kim, Y.I., et al., *Biosensors for label free detection based on RF and MEMS technology.* Sensors and Actuators B: Chemical, 2006. **119**(2): p. 592-599.
82. Jinhu, Z., et al., *High sensitive biosensor based on aSRR and high-impedance microstrip line*. 2013. p. 234-237.
83. Deshours, F., et al., *Improved microwave biosensor for non-invasive dielectric characterization of biological tissues.* Microelectronics Journal, 2018.
84. Zarifi, M.H. and M. Daneshmand, *Liquid sensing in aquatic environment using high quality planar microwave resonator.* Sensors & Actuators: B. Chemical, 2016. **225**: p. 517-521.
85. Nikolic-Jaric, M., et al., *Microwave frequency sensor for detection of biological cells in microfluidic channels.* Biomicrofluidics, 2009. **3**(3): p. 034103.
86. Yang, C.-H., et al., *Development of a multilayered polymeric DNA biosensor using radio frequency technology with gold and magnetic nanoparticles.* Biosensors & bioelectronics, 2012. **31**(1): p. 349.
87. Harnsoongnoen, S., et al., *Planar microwave sensor for detection and discrimination of aqueous organic and inorganic solutions.* Sensors & Actuators: B. Chemical, 2018. **271**: p. 300-305.
88. Wang, L., *Early Diagnosis of Breast Cancer.* Sensors (Basel, Switzerland), 2017. **17**(7).
89. Abedeen, Z. and P. Agarwal, *Microwave sensing technique based label-free and real-time planar glucose analyzer fabricated on FR4.* Sensors & Actuators: A. Physical, 2018. **279**: p. 132-139.
90. Harnsoongnoen, S. and A. Wanthong, *Coplanar Waveguide Transmission Line Loaded With Electric-LC Resonator for Determination of Glucose Concentration Sensing.* Sensors Journal, IEEE, 2017. **17**(6): p. 1635-1640.
91. Camli, B., et al., *A Microwave Ring Resonator Based Glucose Sensor*. Procedia Engineering, 2016. **168**: p. 465-468.
92. Kim, N.Y., et al., *A reusable robust radio frequency biosensor using microwave resonator by integrated passive device technology for quantitative detection of glucose level.* Biosensors and Bioelectronics, 2015. **67**: p. 687-693.
93. Park, H., et al., *Radio frequency based label-free detection of glucose.* Biosensors and Bioelectronics, 2014. **54**: p. 141-145.
94. Mason, A., et al., *A resonant co-planar sensor at microwave frequencies for biomedical applications.* Sensors & Actuators: A. Physical, 2013. **202**: p. 170-175.
95. Li, L. and D. Uttamchandani, *A Microwave Dielectric Biosensor Based on Suspended Distributed MEMS Transmission Lines.* Sensors Journal, IEEE, 2009. **9**(12): p. 1825-1830.
96. Roelvink, J., S. Trabelsi, and S.O. Nelson, *A Planar Transmission-Line Sensor for Measuring the Microwave Permittivity of Liquid and Semisolid Biological Materials.* Instrumentation and Measurement, IEEE Transactions on, 2013. **62**(11): p. 2974-2982.
97. Hamzah, H., J. Lees, and A. Porch, *Split ring resonator with optimised sensitivity for microfluidic sensing.* Sensors & Actuators: A. Physical, 2018. **276**: p. 1-10.
98. Choi, J.H., et al., *A novel Au-nanoparticle biosensor for the rapid and simple detection of PSA using a sequence-specific peptide cleavage reaction.* Biosensors and Bioelectronics, 2013. **49**(C): p. 415-419.
99. Najeeb, M.A., et al., *A novel classification of prostate specific antigen (PSA) biosensors based on transducing elements.* Talanta, 2017. **168**(C): p. 52-61.

100. Lee, H.-J., J.-H. Lee, and H.-I. Jung, *A symmetric metamaterial element-based RF biosensor for rapid and label-free detection.* Applied Physics Letters, 2011. **99**(16).
101. Khan, Y., et al., *Gold nano disks arrays for localized surface plasmon resonance based detection of PSA cancer marker.* Sensors & Actuators: B. Chemical, 2018. **255**(P2): p. 1298-1307.
102. Presnova, G., et al., *Biosensor based on a silicon nanowire field-effect transistor functionalized by gold nanoparticles for the highly sensitive determination of prostate specific antigen.* Biosensors and Bioelectronics, 2017. **88**(C): p. 283-289.
103. Su, L., et al., *Detection of cancer biomarkers by piezoelectric biosensor using PZT ceramic resonator as the transducer.* Biosensors & bioelectronics, 2013. **46**: p. 155.
104. Lee, H.-J. and J.-G. Yook, *Recent research trends of radio-frequency biosensors for biomolecular detection.* Biosensors and Bioelectronics, 2014. **61**: p. 448-459.
105. Collin, R.E., *Foundations for microwave engineering*. 2nd ed.. ed. 2001, New York: New York : IEEE Press.
106. Grigoriev, A.D., *Microwave Electronics*, ed. V.A. Ivanov, S.I. Molokovsky, and SpringerLink. 2018: Cham : Springer International Publishing : Imprint: Springer.
107. Fooks, E.H., *Microwave engineering using microstrip circuits*, ed. R.A. Zakarevičius. 1990, New York: New York : Prentice Hall.
108. Bayliss, C.R., *Transmission and distribution electrical engineering*. 4th ed. / C.R. Bayliss, B.J. Hardy.. ed, ed. B.J. Hardy. 2012, Oxford: Oxford : Elsevier Newnes.
109. Mansour, G., et al., *DESIGN OF FILTERING MICROSTRIP ANTENNA USING FILTER SYNTHESIS APPROACH.* Progress In Electromagnetics Research, 2014. **145**: p. 59-67.
110. Gorbunova, A. and Y. Kuznetsov, *Equivalent circuit synthesis for microstrip structures design and optimisation*. 2011. p. 1-4.
111. Wadell, B.C., *Transmission line design handbook*. 1991, Boston: Boston : Artech House.
112. Rebeiz, G.M., *RF MEMS : theory, design, and technology*. 2003, Hoboken, NJ: Hoboken, NJ : J. Wiley.
113. Cornetta, G., et al., *Wireless radio-frequency standards and system design advanced techniques*. 2012, Hershey, Pa.: Hershey, Pa. : IGI Global 701 E. Chocolate Avenue, Hershey, Pennsylvania, 17033, USA.
114. Maloratsky, L.G., *Passive RF & microwave integrated circuits*. 2004, Amsterdam
Bosto: Amsterdam
Bosto : Elsevier/Newnes.
115. Howe, H., *Stripline circuit design*. 1974, Dedham, Mass.: Dedham, Mass., Artech House.
116. Edwards, T.C., *Foundations for microstrip circuit design*. 2nd ed.. ed. 1991, Chichester, West Sussex, England
New York: Chichester, West Sussex, England
New York : Wiley.
117. Pozar, D.M., *Microwave engineering*. 2012: Fourth edition. Hoboken, NJ : Wiley, [2012] ©2012.
118. Edwards, T.C., *Foundations of interconnect and microstrip design*. 3rd ed.. ed, ed. M.B. Steer and T.C. Edwards. 2000, Chichester: Chichester : John Wiley.
119. Hong, J.-S., *Microstrip filters for RF/microwave applications*, ed. M.J. Lancaster and C. Ebooks. 2001, Chichester: Chichester : Wiley.
120. Balasenthilmurugan, L., et al., *Design and Implementation of a Microstrip Band-Stop Filter for Microwave Applications.* Procedia Engineering, 2012. **38**(C): p. 1346-1351.
121. Roussy, M.G., *Foundations and industrial applications of microwave and radio frequency fields : physical and chemical processes*, ed. J.A. Pearce. 1995, Chichester, W. Sussex, England: Chichester, W. Sussex, England : Wiley.

122. *Microwave solid state circuit design*. 2nd ed.. ed, ed. I.J. Bahl and P. Bhartia. 2003, New York: New York : J. Wiley.
123. al, M.V.e., *Contact Killing and Antimicrobial Properties of Copper.* Journal of Applied Microbiology, 2018. **124**: p. 1032–1046.
124. Stine, K.J., *Enzyme Immobilization on Nanoporous Gold: A Review.* Biochemistry Insights, 2017. **10**.
125. Mazzuferi, M., et al., *The Biocompatibility of Materials Used in Printed Circuit Board Technologies with Respect to Primary Neuronal and K562 Cells.* Biomaterials, 2010. **vol. 31**: p. 1045–1054.
126. Wong, K.-L., *Design of nonplanar microstrip antennas and transmission lines*. 1999, New York: New York : Wiley.
127. Mehdizadeh, M., *Microwave/RF applicators and probes for material heating, sensing, and plasma generation a design guide*. 2009, Norwich, N.Y. : Oxford: Norwich, N.Y. : William Andrew
Oxford : Elsevier Science distributor.
128. Bowick, C., *RF circuit design*. 2nd ed.. ed, ed. J. Blyler and C.J. Ajluni. 2008, Amsterdam
Boston: Amsterdam
Boston : Newnes/Elsevier.
129. Glover, I.A., S.R. Pennock, and P.R. Shepherd, *Microwave devices, circuits and subsystems for communications engineering*. 2005, Chichester: Chichester : Wiley.
130. Zaiki, A., *Microwave systems design*. 2013: Singapore : Springer.
131. Aryan, N.P., *Design and modeling of inductors, capacitors and coplanar waveguides at tens of GHz frequencies*. 2015: Cham : Springer.
132. Ma, B., A. Chousseaud, and S. Toutain, *A new design of compact planar microstrip filter*. 2009. p. 690-693.
133. Ghaderi, A., A. Golestanifar, and F. Shama, *Design of a compact microstrip tunable dual-band bandpass filter.* AEUE - International Journal of Electronics and Communications, 2017. **82**: p. 391-396.
134. Chen, C.-Y. and C.-C. Lin, *THE DESIGN AND FABRICATION OF A HIGHLY COMPACT MICROSTRIP DUAL-BAND BANDPASS FILTER.* Progress In Electromagnetics Research, 2011. **112**: p. 299-307.
135. Weber, R.J., and Ieee Microwave Theory and Techniques Society, *Introduction to Microwave Circuits : Radio Frequency and Design Applications.* 2001, New York: IEEE.
136. Wu, Y., et al., *A Simple Microstrip Bandpass Filter with Analytical Design Theory and Sharp Skirt Selectivity.* Journal of Electromagnetic Waves and Applications, 2011. **25**(8-9): p. 1253-1263.
137. Chen, L.-F., *Microwave electronics : measurement and materials characterisation*, ed. V.K. Varadan. 2004, New York
Chichester: New York
Chichester : Wiley.
138. Birta, L.G.a.G.A., *Modelling and Simulation.* 2013, London: Springer.
139. Bala, B.K.B.K., et al., *System Dynamics Modelling and Simulation*. 2017, Springer Singapore: Springer.
140. Bernasconi, A., et al., *Experiments on the Combined Use of a Double-Sided Pressure-Sensitive Tape and an Epoxy Adhesive to Reduce Handling Time.* Journal of Adhesion Science and Technology, 2018. **32**(15): p. 1687–1699.
141. Khashayar, P., et al, *Rapid Prototyping of Microfluidic Chips Using Laser-Cut Double-Sided Tape for Electrochemical Biosensors.* ournal of the Brazilian Society of Mechanical Sciences and Engineering, 2017. **39**(5): p. 1469–1477.

142. Mark, S.S., and Springerlink (Online Service), . *Bioconjugation Protocols Strategies and Methods.* 2011, Totowa, NJ: Humana Press.
143. Dalmay, C., et al. *Label free biosensors for human cell characterization using radio and microwave frequencies*. in *Microwave Symposium Digest, 2008 IEEE MTT-S International*. 2008.
144. Ashelaish, H., J. Hedley, and N. Keegan. *High radio frequency biosensor for a nano-concentration detection of the label free Prostate Specific Antigen cancerous cells*. 2018. Singapore: Springer Singapore.